MECHANISMS OF MODULATION OF

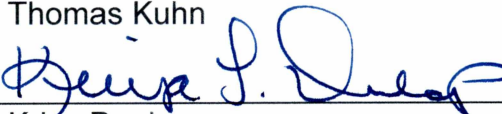# NICOTINIC ACETYLCHOLINE RECEPTORS
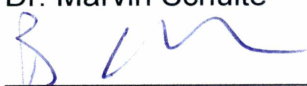
By

Arianna Lynn Demmerly
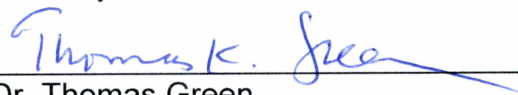
RECOMMENDED:

Dr. Thomas Kuhn

Dr. Kriya Dunlap

Dr. Marvin Schulte
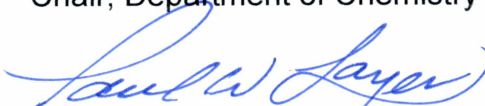
Dr. Brian Edmonds
Advisory Committee Chair

Dr. Thomas Green
Chair, Department of Chemistry
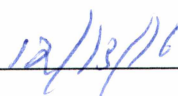
APPROVED:

Dr. Paul Layer
Dean, College of Natural Science and Mathematics

Dr. Michael Castellini
Dean of the Graduate School

Date 12/13/16

MECHANISMS OF MODULATION OF

NICOTINIC ACETYLCHOLINE RECEPTORS

A

Dissertation

Presented to the Faculty

of the University of Alaska Fairbanks

in Partial Fulfillment of the Requirements

for the Degree of

Doctor of Philosophy

By

Arianna L. Demmerly, B.S.

Fairbanks, AK

December 2016

Abstract

Inappropriate expression of nicotinic acetylcholine receptors in the central nervous system is associated with nicotine addiction, Alzheimer's disease, Parkinson's disease and other disorders. Modulators (drugs) have the potential to restore circuit properties that arise from inappropriate expression of nicotinic receptor's. Compounds that interact with allosteric sites have a distinct advantage over agonists and partial agonists, in that, they retain normal activation patterns by allowing binding of the endogenous ligand. Positive allosteric modulators boost the receptors ability to respond to agonist. Studies of these modulators constitute a first step toward the identification and development of better compounds that minimize signaling errors at cholinergic synapses. We have used single molecule methods to investigate the action of a novel positive allosteric modulator, desformylflustrabromine (dFBr), on nicotinic receptors. Our studies were focused on the $\alpha 4\beta 2$ subtype of nicotinic receptors in the brain. These receptors exist in two forms with low sensitivity ($\alpha 4_3\beta 2_2$) or, alternatively, high sensitivity ($\alpha 4_2\beta 2_3$) to agonist. Our experiments allowed us to develop detailed gating models for high and low sensitivity receptors, as well as gain new insights regarding the mechanisms that underlie potentiation by allosteric modulators. We found that dFBr potentiates low sensitivity receptors by destabilizing desensitized states of the receptor. In contrast, potentiation of high sensitivity receptors arises from a synchronization of openings following an application of agonist due to an increase in the opening rate. Based on our results we now have a better understanding of the advantages of dFBr on high and low sensitivity receptors.

Table of Contents

Page

List of Figures

Chapter 1. Overview and Research Aims

Chapter 2. Destabilization of Desensitized states of Low Sensitivity Nicotinic
Acetylcholine Receptors.

Chapter 3: Synchronization of High Sensitivity $\alpha 4\beta 2$ Nicotinic Acetylcholine Receptors

List of Tables

Acknowledgements

I would first and foremost like to thank my family and friends for their never ending support in my endeavors. My friends, with the many coffee and lunch dates to go over papers or just talk about life, allowed me to truly enjoy my graduate school experience. My family, who bought me numerous plane tickets just to see them for a holiday. Out of everyone I miss my father the most, he always encouraged me to always see everything to completion. I know he would be proud of me if he were around today, and I will always cherish his memory.

I would like to thank my advisor, Brian Edmonds for his expertise and knowledge in single molecule techniques. I have learned a great deal while under his guidance and I am glad we had the ability to work together. I would also like to thank all of my mentors and committee members, for their support throughout my graduate studies. Last, but not least I am thankful to those who have helped me in the lab as well as those who provided materials, Spencer Hirt, Savanna Chesworth, and Max Hesser-Knoll. They helped me with so many laboratory tasks and maintenance, while Dr. Marvin Schulte and Dr. Joe Steinbach supplied cells and cDNA for my research. I would have had a much harder time without their involvement.

I also would like to thank the little things in life, like my fiancé Craig for his support and my cats Tesla and Korra for their constant snuggles, as well as California Napa Valley. Two crucial graduate school items, cute, soft and fluffy animals, and of course, lots of wine.

Chapter 1: Overview and Research Aims

1.1 Background

1.1.1 General Overview of Synaptic Transmission

At chemical synapses, invasion of the axon terminal by the action potential results in opening of voltage gated calcium channels and calcium influx. Elevated levels of calcium ions trigger fusion of synaptic vesicles that contain neurotransmitter with the presynaptic membrane. Neurotransmitter is released into the synaptic cleft and diffuses a short distance (~30 nm) where it binds to postsynaptic receptors. Binding of neurotransmitter biases the receptor to open, allowing cations to enter the post synaptic cell. If a threshold is reached in the membrane potential, then an action potential is produced. Activation of excitatory receptors leads to cation influx resulting in depolarization of the postsynaptic membrane (Albuquerque et al., 2009).

Neurotransmitter receptors affect signals that are sent from one neuron to another and therefore harbor an opportunity for intervention by drugs. Inappropriate expression of nicotinic receptors in cholinergic systems is associated with diseases and disorders such as nicotine addiction and Alzheimer's disease. Nicotine addiction is a complex disorder, but upregulation and consequent overexpression of nicotinic receptors in the brain is a primary contributing factor in the reinforcing nature of nicotine addiction (Fenster et al., 1999; Buisson and Bertrand, 2001). While nicotine addiction is thought to occur by an overexpression of receptors, the loss of cholinergic receptors is likely to contribute to cognitive decline in Alzheimer's disease and other

1

neurodegenerative disorders. Alzheimer's disease emerges when there is underexpression of nicotinic receptors in the brain, with cell loss and loss of receptors being correlated to a loss of cognitive abilities in patients with the disease (Nordberg and Winblad, 1986). If there are too few receptors on postsynaptic cells, then signals are too weak, and neurons are unable to effectively communicate. If too many receptors are present and are overexpressed, then the resulting signals can become too strong. In scenarios where circuits are not working properly due to over- or underexpression of nicotinic receptors, then a strategy is needed to alter receptor responsiveness.

Two competing strategies for correcting errors in cholinergic signaling include the use of partial agonists or positive allosteric modulators. While partial agonists (Coe et al., 2005) are one strategy for modulation of nicotinic receptors, they an improper choice due to competition with acetylcholine for binding. Continuous exposure of receptors to agonist and partial agonists can produce receptor desensitization, resulting in receptors being unavailable for further activation. Alternatively, a compound that interacts with allosteric sites can be utilized for correcting cholinergic signals, allowing retention of the normal activation pattern of the endogenous agonist. Positive allosteric modulators are compounds that are unable to or produce little receptor activation on their own, and instead boost the receptors ability to respond to agonist. These compounds have a potential advantage in not only preventing drug induced desensitization, but also by restoring normal levels of acetylcholine activity, yielding better functional outcomes compared to partial agonists.

Given that inappropriate expression $\alpha4\beta2$ receptors are associated with a variety of CNS disorders an effective therapeutic intervention would require a library of allosteric modulators with unique functional properties. Selective positive allosteric modulators are important in the development of compounds with specific functional properties. Studying the mechanism of action for positive allosteric modulators helps cultivate an understanding of the effects a drug has on a cholinergic synapse. Establishing a model constitutes a first step toward the development and identification of better compounds that can correct errors in cholinergic signaling. In this thesis we investigated the action of a particular modulator called dFBr. A long term goal of these studies is to facilitate the directed development of new and better compounds.

1.1.2 Characteristics of α4β2 Receptors

In mammals, neuronal nAChRs are transmembrane proteins with a pentameric arrangement of subunits arranged around a central pore. Neuronal nAChRs are formed from a collection of nine α ($\alpha2$-$\alpha7$,$\alpha9$,$\alpha10$), and three β ($\beta2$-$\beta4$) subunits (Changeux, 2010). The major nAChRs within the brain are homomeric receptor composed of $\alpha7$ subunits and heteromeric receptors composed of $\alpha4$ and $\beta2$ subunits (Khiroug et al., 2004; Moore and McCarthy, 1995). The heteromeric receptors can assemble in alternate forms alternate forms, low sensitivity (LS) receptors consisting of three alpha and two beta subunits ($\alpha4_3\beta2_2$) that bind ACh and nicotine with low affinity (EC_{50} ~100 μM), and high sensitivity (HS) receptors consisting of two alpha and three beta subunits ($\alpha4_2\beta2_3$) that bind ACh and nicotine with high-affinity (EC_{50} ~1μM) (Nelson et al., 2003;

Khiroug et al., 2004; Buisson et al., 1996). High sensitivity receptors require a relatively low concentration of agonist in order to produce a half maximal response, (low EC_{50}). Low sensitivity receptors require higher concentrations in order to elicit a half maximal response. Isolated $\alpha4\beta2$ receptors display two distinct conductance's, ~20 pS for the HS subtype and ~30 pS for the LS subtype (Charnet et al., 1992; Buisson et al., 1996; Li and Steinbach, 2010).

Most work on the physiological properties of $\alpha4\beta2$ nAChRs has been done in oocytes and HEK 293 cells. When equivalent amounts of $\alpha4$ and $\beta2$ cDNAs are injected into oocytes, both HS and LS receptors are expressed in equivalent amounts, whereas in HEK293 cells the receptors predominantly assemble as the LS subtype, comprising 80% of the receptor population (Harpsøe et al., 2011). Using HEK293 cells is an advantage, in that, it allows us to compare our single-channel data to whole-cell data that has been previously obtained from studies utilizing this cell line. This allows us to determine whether our models are supported by whole-cell data.

nAChRs binds agonists such as the endogenous agonist ACh or exogenous agonist nicotine (Changeux, 2010). In the absence of agonist, nAChRs are in a closed, nonconductive state. Binding of ACh leads to channel opening and cation influx, however, in the continued presence of agonist receptors become unresponsive. This phenomenon is called desensitization. If agonist is removed when receptors are mostly open, then receptors have the chance to close (deactivate) allowing them to be available to immediately reopen upon exposure to agonist. In contrast, when receptors are exposed to extended periods of elevated levels of agonist then receptors are not

4

immediately available for reactivation due to being desensitized. Once desensitized receptors require time to return to a resting state.

Nicotinic receptors play interesting and unusual roles within functional circuits, with some being activated quickly, while others are slower. In classical transmission the concentration profile is fast, in this situation it is unlikely that nAChRs will desensitize. If the concentration profile is fast then receptors will open for a short time, ACh will unbind and the receptors will close. In volume transmission model, agonist could remain elevated for extended periods. In this scenario diffusion of acetylcholine through extracellular fluid would activate extrasynaptic nAChRs (Agnati et al., 1995). Delaying transmitter removal gives receptors the opportunity to enter desensitized states.

While the precise functional roles of nAChRs in cholinergic transmission are unclear, reduction in the total number of available nicotinic receptors has been linked to a wide variety of neurodegenerative disorders and diseases including: schizophrenia, Parkinson's disease, autism, Alzheimer's disease, and PTSD (Breese et al., 2000; Terry et al., 2015; Dome et al., 2010; Hajos and Rogers, 2010; Dani and Bertrand, 2007). Alzheimer's is a catastrophic disease accompanied by a loss of cholinergic cells within the brain, and reduced expression levels of $\alpha 4$ and $\alpha 7$ containing nAChRs (Martin-Ruiz et al., 1999; Guan et al., 2000; Whitehouse and Au, 1986; Marutle et al., 1999).

1.1.3 Diseases Associated with Cholinergic Transmission

1.1.3.1 Alzheimer's Disease

Alzheimer's disease (AD) is a neurodegenerative disorder with patients eventually showing a loss in cognition and control of daily activity over time. β-amyloid (Aβ) is an important factor in the initiation and promotion of AD, and soluble $A\beta_{42}$ oligomers are currently thought to be the primary cause of the disorder. Investigations into the role of Aβ in AD patients show significant reductions in the number of nAChRs (37 to 57%) (Marutle et al., 1999). The degree of high affinity nicotinic agonist binding in the temporal cortex is correlated to the severity of AD, with a deficiency of high affinity nAChR binding sites linked to a loss of cognitive abilities (Wevers et al., 1999; Martin-Ruiz et al., 1999; Guan et al., 2000; Whitehouse and Au, 1986; Nordberg and Winblad, 1986).

A possible treatment option for alleviating the symptoms in AD patients is to elevate the concentration of ACh within the brain by using compounds that inhibit acetylcholinesterase (ChE) (Christner et al., 2003; Paterson and Nordberg, 2000). Galantamine is a ChE inhibitor that also interacts directly with nAChRs. While ChEs like galantamine improve cognitive function, the numerous peripheral and central nervous system side effects commonly associated with ChE compounds outweighs their benefits (Christner et al., 2003). These side effects coupled with ChEs being unable to prevent or reverse the progression of AD, means other options may be more suitable to address nAChR dysfunction in the disease. Additional treatment options include the development of selective nAChR agonists, partial agonists or positive allosteric

modulators (PAMs). The agonist nicotine has been shown to be beneficial for many neurodegenerative disorders including AD, but the addictive properties of nicotine make this compound unsuitable as a treatment option (Levin and Rezvani, 2000; Rusted and Warburton, 1992; Jones et al., 1992). The partial agonist varenicline has recently been shown to disrupt the action between fibrillary Aβ and α7 nAChRs, due to a possible overlap in binding sites (Ni et al., 2013). While there is interest in agonists and partial agonists as a potential treatment option for individuals with AD, these choices offer little in the area of selectivity (Pandya and Yakel, 2011). Compounds such as PAMs are better suited for boosting nAChR function in disorders such as AD due to their ability to interact with a site distinct from ACh, thus potentially yielding better functional outcomes. Desformylflustrabromine is a PAM for the α4β2 receptors (Sala et al., 2005) has promise as a future therapeutic option in the treatment of AD. Along with the compounds observed potentiation on α4β2 receptors, it has an additional unique property of being able to interfere with the inhibitory action of A$\beta_{1\text{-}42}$ withα4β2 receptors (Pandya and Yakel, 2011).

1.1.3.2 Nicotine Addiction

Tobacco use and nicotine addiction are serious risk factors in the development of cancer, heart and respiratory diseases. Over 6 million deaths each year are a result of tobacco use, 5 million of those deaths are the result of direct tobacco use and over 600,000 deaths due to secondhand smoke (World Health Organization, 2015). The primary compound responsible for strong addiction to smoking is nicotine.

Nicotine is an effective nicotinic receptor agonist that displays relatively high affinity for nAChRs, exhibiting an EC_{50} between 2-14 µM (Buisson et al., 1996; Buisson and Bertrand, 2001; Paradiso and Steinbach, 2003). Nicotine addiction is thought to be the result of profound desensitization, triggering upregulation of $\alpha4\beta2$ receptors. In $\alpha4\beta2$ nAChRs ACh and nicotine are similar with regards to how fast desensitization develops, but receptors stay desensitized for longer in the presence of nicotine (Paradiso and Steinbach, 2003). nAChRs are able to increase their expression (upregulation) when chronically exposed to nicotine, the receptor exhibiting the greatest upregulation being $\alpha4\beta2$. The underlying mechanism for upregulation is not agreed upon, however, it is universally thought that upregulation of high affinity receptors is a main contributing factor in the reinforcing nature in nicotine addiction (Staley, 2006; Buisson and Bertrand, 2001; Fenster et al., 1999).

Nicotine can influence the mesocorticolimbic dopamine system (MDS), a dopaminergic pathway that leads from the ventral tegmental area (VTA) to the nucleus accumbens (NAcc) and limbic systems, the primary reward system of the brain. Figure 1.1 is a visual guide to interactions of some neurons in the VTA and where various subtypes of nAChRs are presumed to be located. Nicotine's influence leads to increased levels of extracellular dopamine in the ventral striatum and pre-frontal cortex. Although the MDS is composed of many sections, nAChR's expressed on dopaminergic cells and inputs into these cells contribute to the rewarding effects of nicotine (Dome et al., 2010; Mansvelder et al., 2002, 2007). Nicotine administration into the VTA results in an increase in dopamine release into the NAcc. This increase is due to the activation of $\alpha4\beta2$ receptors on dopaminergic and GABAergic cells, and $\alpha7$ nAChRs on

8

glutamatergic nerve terminals. Exposing $\alpha4\beta2$ receptors on the GABAergic and dopaminergic terminals to nicotine causes receptors to undergo rapid desensitization (Dome et al., 2010; Mansvelder and McGehee, 2000). While $\alpha4\beta2$ receptors are heavily affected by nicotine, the concentration is not high enough to desensitize $\alpha7$ nAChRs on glutamatergic inputs into the VTA. Thus, nicotine can activate the glutamatergic nerve endings, further triggering the dopaminergic cells of the VTA. Dopaminergic neurons are under tonic inhibitory control by $GABA_A$ and removal of this inhibition leads to increased activity of dopaminergic neurons, which in turn leads to an increase in dopamine release in the NAcc (Dome et al., 2010; Mansvelder et al., 2007; Mansvelder and McGehee, 2000; Mansvelder et al., 2002).

The primary contributor for the pleasurable effects of nicotine is the desensitization of $\alpha4\beta2$ receptors, leading to disinhibition of dopaminergic neurons within the VTA. Once nicotine dependence has developed it requires nicotine reinforcement and is difficult to quit. The only smoking cessation treatments currently available are varenicline and nicotine replacement therapies. Other compounds have the potential to be useful, such as cytisine, bupropion, NS9283 and dFBr (Mohamed et al., 2015). While varenicline and cytisine have been found to be as effective as nicotine replacement therapies for nicotine addiction, very little research has been done on the effectiveness of PAMs. Whether these compounds will disrupt nicotine specific desensitization and aid in smoking cessation remains to be seen, with more research in this area being required.

1.1.4 Positive Allosteric Modulators of α4β2 Receptors

The benefit of PAMs is that they occupy binding sites distinct from that of acetylcholine, thereby altering the receptors responsiveness to the endogenous ligand. PAMs have the ability to increase the probability of channel opening, while potentially decreasing the agonists potential for receptor desensitization (Williams et al., 2011; Pandya and Yakel, 2011; Hajos and Rogers, 2010). PAMs demonstrate a wide variety of modulatory actions on α4β2 receptors and can potentiate maximal amplitude responses differently. NS206 and dFBr are PAMs that affect both forms of α4β2 nAChRs. However, both potentiate max amplitude responses in a different manner. NS206 is thought to increase efficacy by an increase of the mean open time of the receptor for both stoichiometries, whereas our single channel analysis of dFBr found that it potentiation occurs by destabilizing desensitized states for the LS subtype, and increasing mean open time for the HS subtype (Olsen et al., 2013). PAMs cannot produce receptor activation on their own and can affect ligand gated ion channel function in a couple of ways, by either influencing channel conductance or by altering channel gating. (Williams et al., 2011; Pandya and Yakel, 2011; Hajos and Rogers, 2010).

A PAM can increase the apparent affinity (potency) on the receptor for agonist, while simultaneously not increasing the maximal response amplitude (efficacy). A modulator can be a PAM, having an effect on one of those properties while simultaneously not affecting the other. Several PAM's of α4β2 nAChRs currently exist

and affect the channel in a variety of ways. Some are selective for one subtype of $\alpha4\beta2$, while others affect both subtypes differently.

1.1.4.1 NS9283

Preclinical studies have shown that NS9283 shows promise in the treatment of cognitive disorders (Timmermann et al., 2012; Lee et al., 2011). NS9283 is a PAM that selectively increases ACh potency for the LS subtype of nAChRs. It is thought to exert potentiation predominantly through reduction in the rate of deactivation of the receptor with the mechanism of action bearing resemblance to that of benzodiazepines at the GABAA receptor. With ultra-short applications of high concentrations of (1 mM) ACh, current decay is substantially slower with NS9283 (Grupe et al., 2013). The PAM does not have an effect on desensitization produced by ACh and was incapable of reactivating desensitized receptors (Grupe et al., 2013). The mechanism of NS9283 is thought to not involve a decrease in macroscopic desensitization, but rather via slowing the rate at which the receptor deactivates. However, we have shown for simulations involving dFBr that the deactivation time course of LS receptors is not a simple reflection of channel closing, but also involves entry into desensitized states. Therefore, the mechanism of modulation for NS9283 could involve the destabilization of a desensitized state, resulting in what appears to be a slowing of deactivation. The presence of NS9283 in the synaptic cleft would prolong the agonist-bound receptor state and ultimately result in an increase in charge transfer. Other PAMs, like dFBr, exhibit potentiation via an increase in mean open time, as well as decreasing ACh-induced macroscopic desensitization (Sala et al., 2005; Weltzin and Schulte, 2010).

1.1.4.2 Desformylflustrabromine (dFBr)

Desformylflustrabromine is an indolic alkaloid isolated from the marine bryozoan Flustra foliacea and was identified as a selective PAM of $\alpha4\beta2$ nAChRs (Sala et al., 2005). dFBr has the ability to potentiate ACh-induced responses at concentration less than 10 µM and inhibit responses at concentrations greater than 10 µM. In the presence of dFBr, dose response curves show a decrease in the EC_{50} and an increase in the maximal response curve. dFBr exhibits an EC_{50} of 120 nM and IC_{50} of 150 µM, and the observed inhibition invoked by dFBr is thought to be due to the displacement of ACh binding (Kim et al., 2007). Rebound currents on washout of ACh/dFBr were seen, indicating the presence of open channel block. Rebound currents occur when the open channel blocker is released while agonist is still bound to the receptor (Kim et al., 2007).

Studies on the therapeutic potential of dFBr are still in their early stages, but a rat self-administration study showed that dFBr has qualities that would make it an ideal candidate for smoking cessation treatments. Pretreatment of dFBr, as well as treatment while rats were engaged in self administration, reduced long term nicotine self-administration behavior. It was also found that dFBr was present in cerebral spinal fluid at one third the concentration of that within the blood stream of administered rats. This provides evidence that dFBr crosses the blood brain barrier, but at one-third the concentration found in the bloodstream (Liu, 2013). Effective transit across the blood brain barrier is important if a compound is to be considered for smoking cessation therapies.

The in vitro effects of dFBr have been previously studied, but the mode by which dFBr selectively potentiates $\alpha4\beta2$ nAChRs remains to be determined. The existing single-channel information on the effects of dFBr are limited and the information that is available briefly demonstrates that dFBr increases the channel-opening probability. It is speculated that the effects of dFBr occur because of an increase in the rate constants designated for channel opening and closing (Sala et al., 2005). A complete understanding of the mechanism of modulation is unavailable for the individual receptor subtypes. Gaining an understanding of the mechanism would improve our understanding of the potential effects dFBr has on a cholinergic synapse as well as aid in the development of future allosteric modulators. The selectivity that dFBr demonstrates makes it a valuable asset for further investigation involving modulation of $\alpha4\beta2$ receptors.

1.1.5 Modeling

1.1.5.1 Classical Mechanisms

The earliest functional models for nAChR kinetics were made by del Castillo and Katz in 1957 and described the similarity between enzyme-substrate and receptor ligand interactions (Figure 1.2A) (Castillo and Katz, 1957). This model was further elaborated on by Katz and Theslaff in 1957 to account for desensitization and led to a cyclical like scheme (Figure 1.2B) (Katz and Thesleff, 1957). This cyclical scheme was expanded to include two open states, and is one of the more common mechanisms utilized for analyzing kinetic data (Edelstein et al., 1996).

In 1965, Monod-Wyman-Changeux (MWC) put forth an allosteric transitions theory in order to explain cooperative ligand binding observed in oligomeric proteins. This approach has had a large effect on the understanding of the cooperative interactions between hemoglobin and allosteric enzymes and has further been extended to neuronal transmembrane receptors. Allosteric theory has several components to it: (i) allosteric proteins are oligomers where the individual subunits are equivalent; (ii) each subunit contains a site for a ligand to bind to it; (iii) subunit conformations are restricted based on the interactions with the subunits around them; (iv) allosteric oligomers have access to two conformational states, O and C; (v) binding of ligand to one site alters the affinity of additional sites for ligand; (vi) molecular symmetry is conserved when an oligomer goes from one conformational state to another (Monod et al., 1965). Typical MWC model is shown in Figure 1.2C. Typical nAChR mechanisms, as shown in Figure 1.3A, give adequate fits with the fit often being improved by adding

14

an additional shut state following the open state, like a desensitized state. Our nicotinic HS and LS receptor mechanisms use the MWC model as a base.

1.1.5.2 Models Established for the HS and LS α4β2 Receptors

Determining the mechanisms of modulation for α4β2 nAChRs in the presence of dFBr is important for enhancing our understanding of the potential impact allosteric modulators could have on a cholinergic synapse. In this thesis we utilized single molecule methods to investigate the mechanism by which dFBr potentiates nAChRs. We provide the first understanding of the mechanism for the two α4β2 nicotinic receptor subtypes. We have developed full gating models that provide a fairly accurate representation of function for both forms of the receptor, LS (Figure 1.3B) and HS (Figure 1.3C). These models were used to perform simulations and determine the effects dFBr would have under a variety of agonist concentration profiles. The mechanisms of modulation are determinant on how the receptor subtypes are expressed within a system, with receptors changing their agonist concentration profile when they are modulated.

1.2 Research Aims

The focus of my research is establishing gating models for the HS and LS $\alpha4\beta2$ receptors and determining the mechanisms of modulation of the positive allosteric modulator dFBr. These goals were accomplished in two aims.

1.2.1 Aim 1: Establishment of Gating Models for the HS and LS $\alpha4\beta2$ Receptors

Before a modulators mechanism can be determined on a single channel level a baseline needs to be established. This is accomplished by determining gating models in agonist alone for each of the receptor subtypes. In Chapter 2, a 7 state gating model is established for the low sensitivity $\alpha4\beta2$ nAChRs under low concentrations of agonist ($\leq$1 μM ACh). The 7 state model contained two ligand binding reactions C1$\rightarrow$C2 and C2$\rightarrow$C3, two open states; a monoliganded state off of C2 (O1) and a diliganded state off of C3 (O2), as well as two desensitized states, one off of C3 (D1) and O2 (D2). In Chapter 3, the high sensitivity $\alpha4\beta2$ nAChRs required an 8 state model using data with concentrations ranging from 0.1 μM to 10 μM ACh for construction. The 8 state model contained two ligand binding reactions C1$\rightarrow$C2 and C2$\rightarrow$C3, mono and diliganded interconnected open states (O1 off C2 and O2 off of C3), and three desensitized states with two off of O2 (D1 and D2) and one off of C3 (D3).

1.2.2 Aim 2: Modulation of α4β2 nAChRs by dFBr in Low Concentrations of Agonist

Once baseline models have been established in the absence of modulator then the mechanism of modulation by dFBr for the LS and HS receptors can be elucidated. Analysis of the mechanisms for the LS and HS receptors revealed two distinct mechanisms of modulation for dFBr on these receptors. In the latter half of Chapter 2 the mechanism of modulation of dFBr on LS α4β2 receptors are discussed in detail, with dFBr exhibiting potentiation by destabilizing desensitized states. Chapter 2 also contains a discussion on slow solution exchange in oocytes and its contribution in peak responses. Some of the discrepancy between our data and oocyte data is due to the slow response profile in oocytes. In Chapter 3 the mechanism of modulation of dFBr on HS receptors is determined, where it is found that dFBr's effects are dependent upon the concentration of agonist. At low concentrations of agonist dFBr increases the mono-liganded open state lifetime, while at high concentrations an increase in the probability of entering the diliganded open state from the diliganded closed state is seen. Chapter 3 also contains a short discussion on the presence of HEPES and the effects the buffer may have on the HS data.

1.3 Hypothesis

1.3.1 dFBr Can Modulate α4β2 Receptors in Low Concentrations of Agonist

This hypothesis is based on the previous studies done by Weltzin et al and utilizes single-channel techniques (Weltzin and Schulte, 2010). This hypothesis addresses whether dFBr potentiates at low concentrations of agonist for the high and

low sensitivity $\alpha4\beta2$ nAChRs. We express human $\alpha4\beta2$ receptors in a mammalian cell line and use patch-clamp methods to record acetylcholine-evoked responses of HS or LS receptors in isolated patches of membrane. Unlike other methods, the single-channel methodology allows us to limit receptor heterogeneity as well as subject channels to a low concentrations of agonist. Utilizing this technique, we can gather long steady state recordings and develop a basic gating model for both stoichiometric forms of the receptor, which will be further used to determine dFBr's mechanism of modulation.

1.3.2 dFBr Modulates by Destabilizing Desensitized States for $\alpha4\beta2$ Receptors.

This hypothesis is an extension of the previous hypothesis and relies on the establishment of a basic gating model. The models generated will help determine the mechanism by which dFBr potentiates the high and low-sensitivity stoichiometric forms of the receptors. It is thought that the primary mode of potentiation exhibited by dFBr is through an increase in the open probability of the receptor. This can be achieved a few different ways, including: an increase in the rate of entry into the open state, leading to an increased probability of opening, or decreasing the rates out of the open states leading to an increase in mean open lifetime. However, an increase in open probability is not the only mechanism by which a potentiator can modulate a receptor. Our hypothesis is that dFBr's primary mode of action is by the destabilization of one or more desensitized states, leading to potentiation. The development of a model and elucidating the mechanism of modulation will help further the characterization and therapeutic benefits of dFBr, as well as future $\alpha4\beta2$ PAMs.
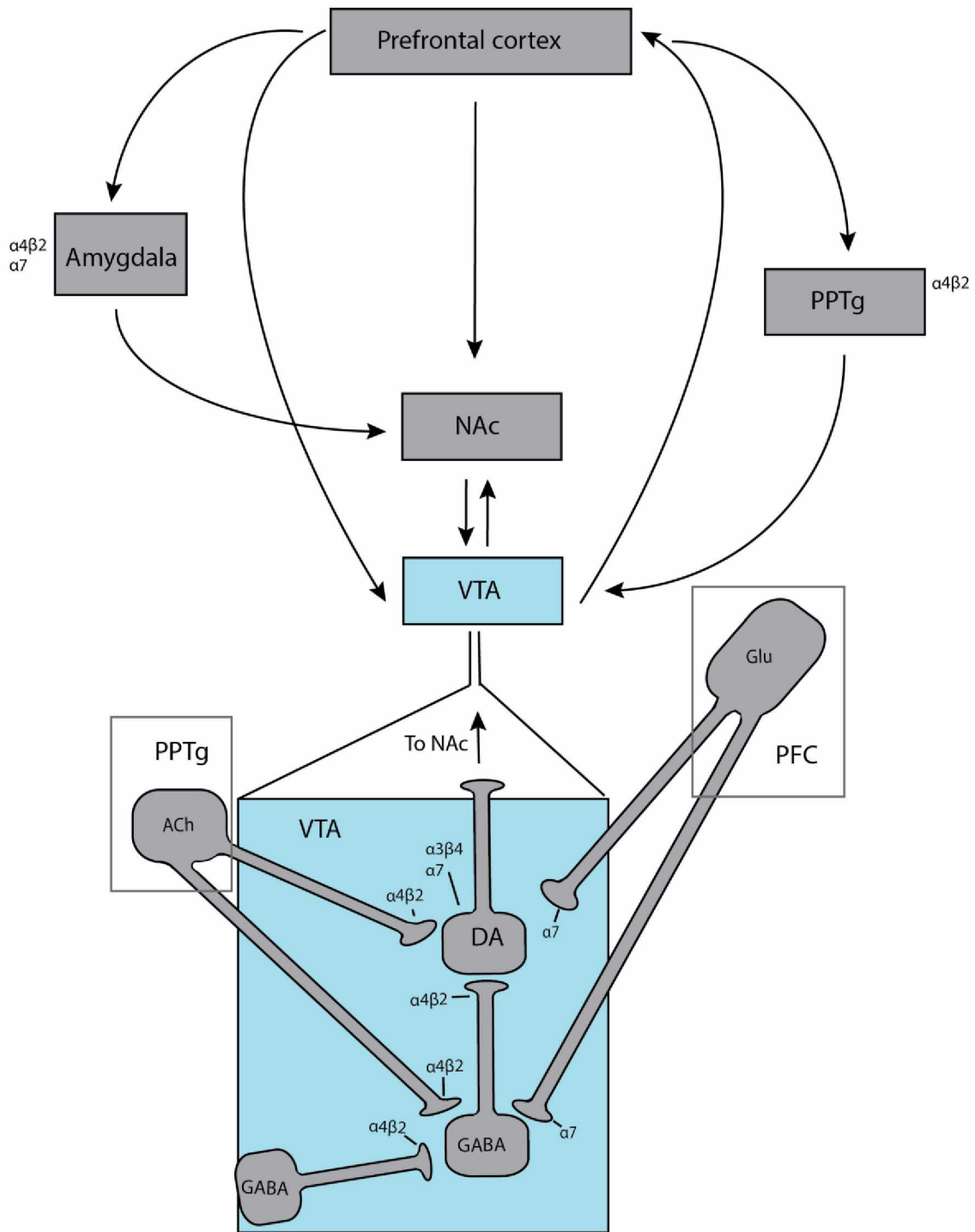
Figure 1.1: Interactions between VTA, NAcc and the Prefrontal Cortex. VTA: Ventral Tegmental Area, NAcc: Nucleus accumbens, PFC" prefrontal cortex, Glu: glutamatergic terminal, DA: Dopamingergic, GABA: GABAergic Nicotinic receptors found on these terminals are labeled, with lines for the specific area the nicotinic receptor is located.

A

$$A + R \rightleftharpoons AR \rightleftharpoons AR'$$

B

$$R + 2A \underset{k_{-1}}{\overset{2k_{+1}}{\rightleftharpoons}} AR + A \underset{2k_{-1}}{\overset{k_{+1}}{\rightleftharpoons}} A_2R \underset{\alpha}{\overset{\beta}{\rightleftharpoons}} A_2O$$

$$d_{-2} \updownarrow d_{+2} \qquad\qquad\qquad\qquad\qquad\qquad\qquad d_{-1} \updownarrow d_{+1}$$

$$D + 2A \underset{k_{-3}}{\overset{2k_{+3}}{\rightleftharpoons}} AD + A \underset{2k_{-3}}{\overset{k_{+3}}{\rightleftharpoons}} A_2D$$

C

$$R + 2A \underset{k_{-1}}{\overset{2k_{+1}}{\rightleftharpoons}} AR + A \underset{2k_{-1}}{\overset{k_{+1}}{\rightleftharpoons}} A_2R$$

$$\alpha_0 \updownarrow \beta_0 \qquad\qquad\qquad \alpha_1 \updownarrow \beta_1 \qquad\qquad\qquad \alpha_2 \updownarrow \beta_2$$

$$O + 2A \underset{k_{o-1}}{\overset{2k_{o+1}}{\rightleftharpoons}} AO + A \underset{2k_{o-1}}{\overset{k_{o+1}}{\rightleftharpoons}} A_2O$$
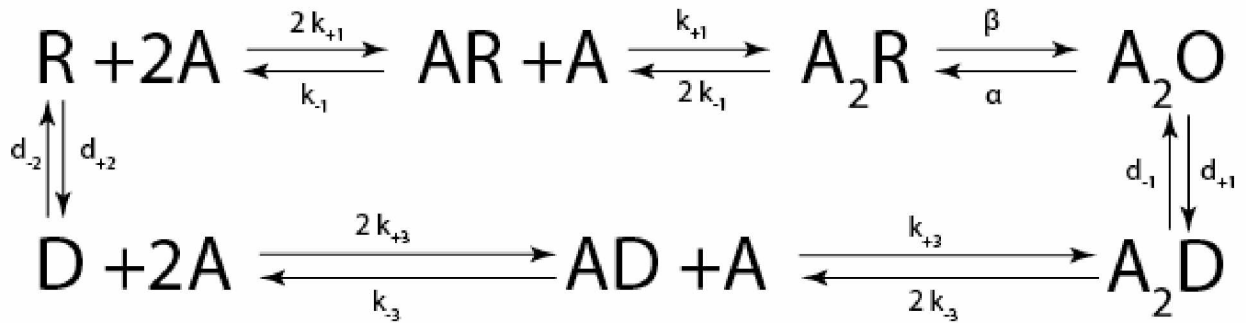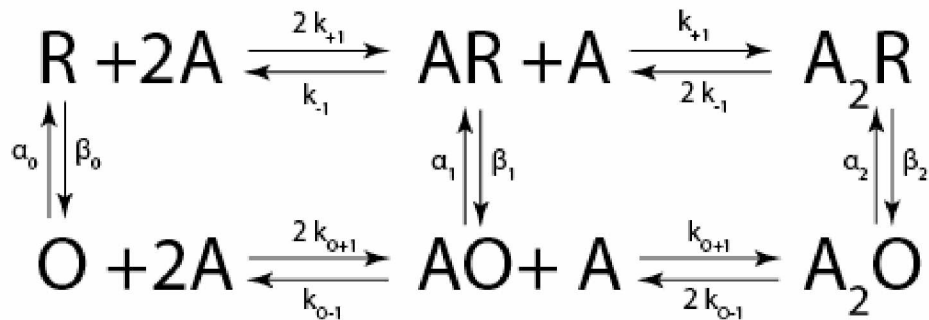
Figure 1.2: Classical Mechanisms. (A) Mechanism proposed by del Castillo and Katz (1957) to describe receptor-ligand interactions. (B) More recent model developed by Katz and Thesleff (1957) and modified to include two ligand binding sites as well as desensitized states. (C) A Monod-Wyman-Changeux (MWC) mechanism. A is agonist, R is receptor in the closed conformation, D is a receptor in the desensitized state, and O is receptor in the open conformation.
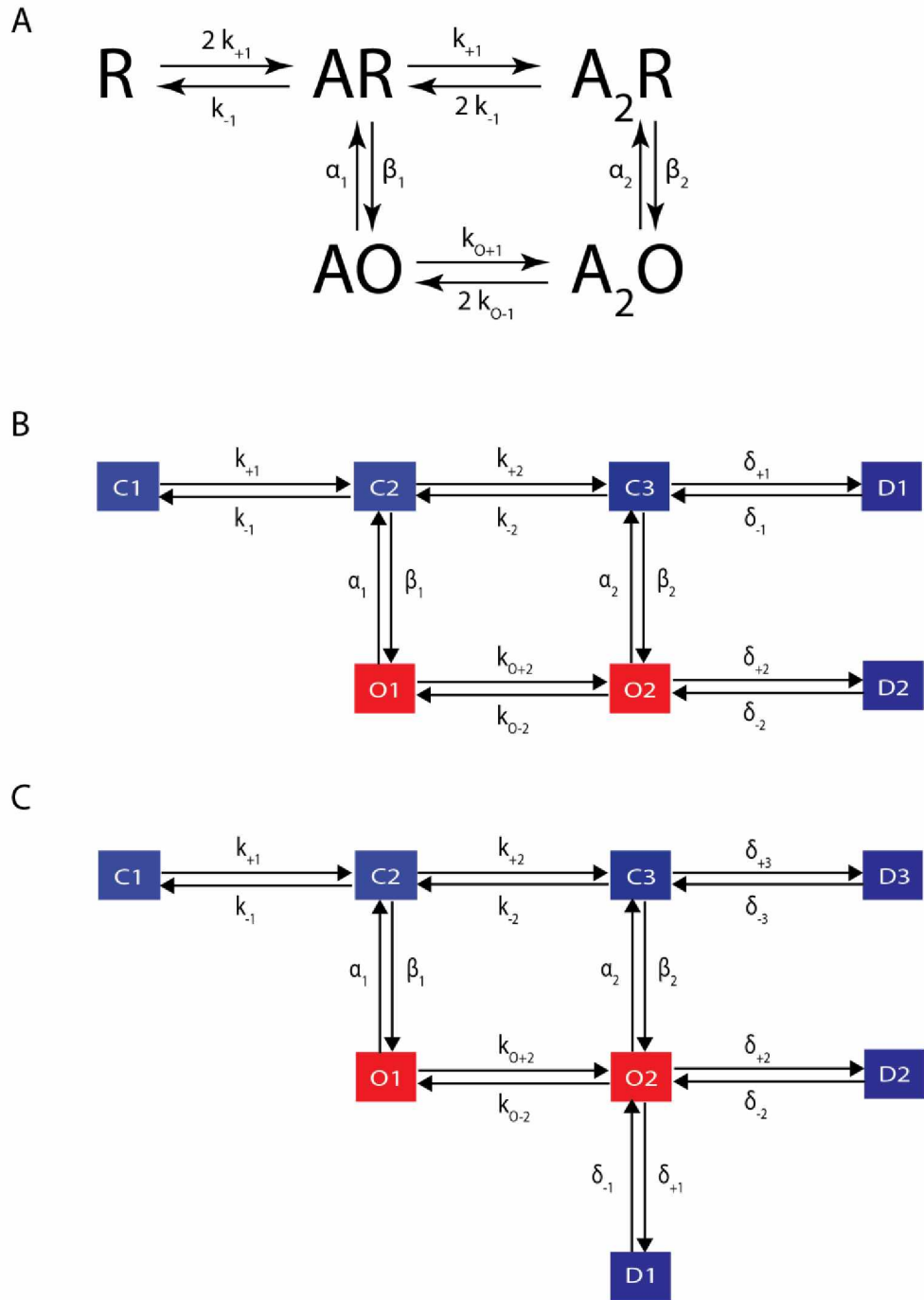
Figure 1.3: Complex Mechanisms. (A) A common example of a mechanism used to describe the nicotinic receptor with two ligand binding steps and mono and di-liganded openings. (B) Mechanism used to fit LS $\alpha 4\beta 2$ nAChR data. (C) Mechanism used to fit the HS $\alpha 4\beta 2$ nAChR data.

1.3 References

Agnati, L.F., M. Zoli, I. Stromberg, and K. Fuxe. 1995. Intercellular communication in the
brain: wiring versus volume transmission. *Neuroscience*. 69:711–726.

Albuquerque, E.X., E.F.R. Pereira, M. Alkondon, and S.W. Rogers. 2009. Mammalian
Nicotinic Acetylcholine Receptors: From Structure to Function. *Physiol. Rev.* 89:73–
120. doi:10.1152/physrev.00015.2008.

Breese, C.R., M.J. Lee, C.E. Adams, B. Sullivan, J. Logel, K.M. Gillen, M.J. Marks, A.C.
Collins, and S. Leonard. 2000. Abnormal regulation of high affinity nicotinic
receptors in subjects with schizophrenia. *Neuropsychopharmacology*. 23:351–364.
doi:10.1016/S0893-133X(00)00121-4.

Buisson, B., and D. Bertrand. 2001. Chronic exposure to nicotine upregulates the
human (alpha)4((beta)2 nicotinic acetylcholine receptor function. *J. Neurosci.*
21:1819–1829. doi:21/6/1819 [pii].

Buisson, B., M. Gopalakrishnan, S.P. Arneric, J.P. Sullivan, and D. Bertrand. 1996.
Human alpha4beta2 neuronal nicotinic acetylcholine receptor in HEK 293 cells: A
patch-clamp study. *J. Neurosci.* 16:7880–7891.

Castillo, J. Del, and B. Katz. 1957. Interaction at End-Plate Receptors between Different
Choline Derivatives. *Proc. R. Soc. London. Ser. B - Biol. Sci.* 146:369 LP-381.

Changeux, J.-P. 2010. Nicotine addiction and nicotinic receptors: lessons from
genetically modified mice. *Nat. Rev. Neurosci.* 11:389–401. doi:10.1038/nrn2849.

Charnet, P., C. Labarca, B.N. Cohen, N. Davidson, H.A. Lester, and G. Pilar. 1992.
Pharmacological and kinetic properties of a4B2 Neuronal Nicotinic Acetylcholine
receptors expressed in Xenopus Oocytes. *J. Physiol.* 450:375–394.

Christner, C., M. Radina, M. Zerlin, C. Ullmer, E.F.R. Pereira, H.L. Ubbert, E.X. Albuquerque, and A. Maelicke. 2003. Galantamine Is an Allosterically Potentiating Ligand of Neuronal Nicotinic but Not of Muscarinic Acetylcholine Receptors. 305:1024–1036. doi:10.1124/jpet.102.045773.trols.

Coe, J.W., P.R. Brooks, M.G. Vetelino, M.C. Wirtz, E.P. Arnold, J. Huang, S.B. Sands, T.I. Davis, L. a Lebel, C.B. Fox, A. Shrikhande, J.H. Heym, E. Schaeffer, H. Rollema, Y. Lu, R.S. Mansbach, L.K. Chambers, C.C. Rovetti, D.W. Schulz, F.D. Tingley 3rd, and B.T. O'Neill. 2005. Varenicline: an α4β2 nicotinic receptor partial agonist for smoking cessation. *J Med Chem*. 48:3474–3477. doi:10.1021/jm050069n.

Dani, J.A., and D. Bertrand. 2007. Nicotinic acetylcholine receptors and nicotinic cholinergic mechanisms of the central nervous system. *Annu Rev Pharmacol Toxicol*. 47:699–729. doi:10.1146/annurev.pharmtox.47.120505.105214.

Dome, P., J. Lazary, M.P. Kalapos, and Z. Rihmer. 2010. Smoking, nicotine and neuropsychiatric disorders. *Neurosci. Biobehav. Rev*. 34:295–342. doi:10.1016/j.neubiorev.2009.07.013.

Edelstein, S.J., O. Schaad, E. Henry, D. Bertrand, and J.P. Changeux. 1996. A kinetic mechanism for nicotinic acetylcholine receptors based on multiple allosteric transitions. *Biol. Cybern*. 75:361–79. doi:10.1007/s004220050302.

Fenster, C.P., T.L. Whitworth, E.B. Sheffield, M.W. Quick, and R.A.J. Lester. 1999. Upregulation of Surface α4β2 Nicotinic Receptors Is Initiated by Receptor Desensitization after Chronic Exposure to Nicotine. *J. Neurosci*. 19:4804–14.

Grupe, M., A.A. Jensen, P.K. Ahring, J.K. Christensen, and M. Grunnet. 2013.

Unravelling the mechanism of action of NS9283, a positive allosteric modulator of

(??4)3(??2)2 nicotinic ACh receptors. *Br. J. Pharmacol.* 168:2000–2010.

doi:10.1111/bph.12095.

Guan, Z.-Z., X. Zhang, R. Ravid, and A. Nordberg. 2000. Decreased Protein Levels of

Nicotinic Receptor Subunits in the Hippocampus and Temporal Cortex of Patients

with Alzheimer's Disease. *J. Neurochem.* 74:237–243. doi:10.1046/j.1471-

4159.2000.0740237.x.

Hajos, M., and B.N. Rogers. 2010. Targeting alpha7 nicotinic acetylcholine receptors in

the treatment of schizophrenia. *Curr Pharm Des.* 16:538–554. doi:CPD-Mihaly

Hajos (Albert Adell) [pii].

Harpsøe, K., P.K. Ahring, J.K. Christensen, M.L. Jensen, D. Peters, and T. Balle. 2011.

Unraveling the high- and low-sensitivity agonist responses of nicotinic acetylcholine

receptors. *J. Neurosci.* 31:10759–66. doi:10.1523/JNEUROSCI.1509-11.2011.

Jones, G.M., B.J. Sahakian, R. Levy, D.M. Warburton, and J.A. Gray. 1992. Effects of

acute subcutaneous nicotine on attention, information processing and short-term

memory in Alzheimer's disease. *Psychopharmacology (Berl).* 108:485–494.

Katz, B., and S. Thesleff. 1957. A study of the desensitization produced by acetylcholine

at the motor end-plate. *J Physiol.* 138:63–80. doi:10.1113/jphysiol.1957.sp005838.

Khiroug, S.S., L. Khiroug, and J.L. Yakel. 2004. Rat nicotinic acetylcholine receptor

alpha2beta2 channels: comparison of functional properties with alpha4beta2

channels in Xenopus oocytes. *Neuroscience.* 124:817–22.

doi:10.1016/j.neuroscience.2004.01.017.

Kim, J.S., A. Padnya, M. Weltzin, B.W. Edmonds, M.K. Schulte, and R.A. Glennon. 2007. Synthesis of desformylflustrabromine and its evaluation as an α4β2 and α7 nACh receptor modulator. *Bioorganic Med. Chem. Lett.* 17:4855–4860. doi:10.1016/j.bmcl.2007.06.047.

Lee, C.H., C. Zhu, J. Malysz, T. Campbell, T. Shaughnessy, P. Honore, J. Polakowski, and M. Gopalakrishnan. 2011. ??4??2 neuronal nicotinic receptor positive allosteric modulation: An approach for improving the therapeutic index of ??4??2 nAChR agonists in pain. *Biochem. Pharmacol.* 82:959–966. doi:10.1016/j.bcp.2011.06.044.

Levin, E.D., and A.H. Rezvani. 2000. Development of nicotinic drug therapy for cognitive disorders. *Eur. J. Pharmacol.* 393:141–146. doi:10.1016/S0014-2999(99)00885-7.

Li, P., and J.H. Steinbach. 2010. The neuronal nicotinic α4β2 receptor has a high maximal probability of being open. *Br. J. Pharmacol.* 160:1906–1915. doi:10.1111/j.1476-5381.2010.00761.x.

Liu, X. 2013. Positive allosteric modulation of ??4??2 nicotinic acetylcholine receptors as a new approach to smoking reduction: Evidence from a rat model of nicotine self-administration. *Psychopharmacology (Berl).* 230:203–213. doi:10.1007/s00213-013-3145-2.

Mansvelder, H.D., Z.M. Fagen, B. Chang, R. Mitchum, and D.S. McGehee. 2007. Bupropion inhibits the cellular effects of nicotine in the ventral tegmental area. *Biochem. Pharmacol.* 74:1283–1291. doi:10.1016/j.bcp.2007.07.034.

Mansvelder, H.D., J.R. Keath, and D.S. McGehee. 2002. Synaptic mechanisms underlie nicotine-induced excitability of brain reward areas. *Neuron.* 33:905–919. doi:10.1016/S0896-6273(02)00625-6.

Mansvelder, H.D., and D.S. McGehee. 2000. Long-term potentiation of excitatory inputs to brain reward areas by nicotine. *Neuron.* 27:349–357. doi:10.1016/S0896-6273(00)00042-8.

Martin-Ruiz, C.M., J.A. Court, E. Molnar, M. Lee, C. Gotti, A. Mamalaki, T. Tsouloufis, S. Tzartos, C. Ballard, R.H. Perry, and E.K. Perry. 1999. α4 but Not α3 and α7 Nicotinic Acetylcholine Receptor Subunits Are Lost from the Temporal Cortex in Alzheimer's Disease. *J. Neurochem.* 73:1635–1640. doi:10.1046/j.1471-4159.1999.0731635.x.

Marutle, A., U. Warpman, N. Bogdanovic, L. Lannfelt, and A. Nordberg. 1999. Neuronal nicotinic receptor deficits in Alzheimer patients with the Swedish amyloid precursor protein 670/671 mutation. *J. Neurochem.* 72:1161–1169. doi:10.1046/j.1471-4159.2000.0721161.x.

Mohamed, T.S., S.S. Jayakar, and A.K. Hamouda. 2015. Orthosteric and Allosteric Ligands of Nicotinic Acetylcholine Receptors for Smoking Cessation. *Front. Mol. Neurosci.* 8:1–9. doi:10.3389/fnmol.2015.00071.

Monod, J., J. Wyman, and J.P. Changeux. 1965. on the Nature of Allosteric Transitions: a Plausible Model. *J. Mol. Biol.* 12:88–118. doi:10.1016/S0022-2836(65)80285-6.

26

Moore, M.A., and M.P. McCarthy. 1995. Snake venom toxins, unlike smaller

   antagonists, appear to stabilize a resting state conformation of the nicotinic

   acetylcholine receptor. *BBA - Biomembr.* 1235:336–342. doi:10.1016/0005-

   2736(95)80022-8.

Nelson, M.E., A. Kuryatov, C.H. Choi, Y. Zhou, and J. Lindstrom. 2003. Alternate

   Stoichiometries of alpha 4beta 2 Nicotinic Acetylcholine Receptors. *Mol Pharmacol.*

   63:332–341. doi:10.1124/mol.63.2.332.

Ni, R., A. Marutle, and A. Nordberg. 2013. Modulation of ??7 nicotinic acetylcholine

   receptor and fibrillar amyloid-?? interactions in Alzheimer's disease brain. *J.*

   Alzheimer's Dis. 33:841–851. doi:10.3233/JAD-2012-121447.

Nordberg, A., and B. Winblad. 1986. Reduced number of [3H]nicotine and

   [3H]acetylcholine binding sites in the frontal cortex of Alzheimer brains. *Neurosci.*

   Lett. 72:115–120. doi:10.1016/0304-3940(86)90629-4.

Olsen, J.A., J.S. Kastrup, D. Peters, M. Gajhede, T. Balle, and P.K. Ahring. 2013. Two

   distinct allosteric binding sites at ??4??2 nicotinic acetylcholine receptors revealed

   by NS206 and NS9283 give unique insights to binding activity-associated linkage at

   cys-loop receptors. *J. Biol. Chem.* 288:35997–36006.

   doi:10.1074/jbc.M113.498618.

Pandya, A., and J.L. Yakel. 2011. Allosteric modulators of the ??4??2 subtype of

   neuronal nicotinic acetylcholine receptors. *Biochem. Pharmacol.* 82:952–958.

   doi:10.1016/j.bcp.2011.04.020.

Paradiso, K.G., and J.H. Steinbach. 2003. Nicotine is highly effective at producing desensitization of rat alpha4beta2 neuronal nicotinic receptors. *J. Physiol.* 553:857–71. doi:10.1113/jphysiol.2003.053447.

Paterson, D., and A. Nordberg. 2000. Neuronal nicotinic receptors in the human brain. *Prog. Neurobiol.* 61:75–111. doi:10.1016/S0301-0082(99)00045-3.

Rusted, J.M., and D.M. Warburton. 1992. Facilitation of memory by post-trial administration of nicotine: evidence for an attentional explanation. *Psychopharmacology (Berl).* 108:452–455. doi:10.1007/BF02247420.

Sala, F., J. Mulet, K.P. Reddy, J.A. Bernal, P. Wikman, L.M. Valor, L. Peters, G.M. König, M. Criado, and S. Sala. 2005. Potentiation of human α4β2 neuronal nicotinic receptors by a Flustra foliacea metabolite. *Neurosci. Lett.* 373:144–149. doi:10.1016/j.neulet.2004.10.002.

Staley, J.K. 2006. Human Tobacco Smokers in Early Abstinence Have Higher Levels of beta2* Nicotinic Acetylcholine Receptors than Nonsmokers. *J. Neurosci.* 26:8707–8714. doi:10.1523/JNEUROSCI.0546-06.2006.

Terry, A. V., P.M. Callahan, and C.M. Hernandez. 2015. Nicotinic ligands as multifunctional agents for the treatment of neuropsychiatric disorders. *Biochem. Pharmacol.* 97:388–398. doi:10.1016/j.bcp.2015.07.027.

Timmermann, D.B., K. Sandager-Nielsen, T. Dyhring, M. Smith, A.M. Jacobsen, E. Nielsen, M. Grunnet, J.K. Christensen, D. Peters, K. Kohlhaas, G.M. Olsen, and P.K. Ahring. 2012. Augmentation of cognitive function by NS9283, a stoichiometry-dependent positive allosteric modulator of ??2- and ??4-containing nicotinic acetylcholine receptors. *Br. J. Pharmacol.* 167:164–182. doi:10.1111/j.1476-5381.2012.01989.x.

Weltzin, M.M., and M.K. Schulte. 2010. Pharmacological Characterization of the Allosteric Modulator Desformylflustrabromine and Its Interaction with a4b2 Neuronal Nicotinic Acetylcholine Receptor Orthosteric Ligands. *Am. Soc. Pharmacol. Exp. Ther.* 334:917–926. doi:10.1124/jpet.110.167684.2006.

Wevers, A., L. Monteggia, S. Nowacki, W. Bloch, U. Schütz, J. Lindstrom, E.F.R. Pereira, H. Eisenberg, E. Giacobini, R.A.I. De Vos, E.N.H.J. Steur, A. Maelicke, E.X. Albuquerque, and H. Schröder. 1999. Expression of nicotinic acetylcholine receptor subunits in the cerebral cortex in Alzheimer's disease: histotopographical correlation with amyloid plaques and hyperphosphorylated-tau protein. *Eur. J. Neurosci.* 11:2551–2565. doi:10.1046/j.1460-9568.1999.00676.x.

Whitehouse, P.J., and K.S. Au. 1986. Cholinergic receptors in aging and Alzheimer's disease. *Prog. Neuropsychopharmacol. Biol. Psychiatry.* 10:665–676.

Williams, D.K., J. Wang, and R.L. Papke. 2011. Positive allosteric modulators as an approach to nicotinic acetylcholine receptor-targeted therapeutics: Advantages and limitations. *Biochem. Pharmacol.* 82:915–930. doi:10.1016/j.bcp.2011.05.001.

World Health Organization. 2015. Who Report on the Global Tobacco Epidemic, 2015. 2–103.

Chapter 2: Destabilization of Desensitized States of Low Sensitivity Nicotinic Acetylcholine Receptors[1]

Abstract

A description of mechanisms that underlie modulation of nAChRs by allosteric ligands is critical for understanding the effects of modulation on cholinergic signaling in the CNS. We used single-channel methods to investigate the mechanism of potentiation of the human low-sensitivity, $\alpha 4_3 \beta 2_2$ nicotinic acetylcholine receptor by the allosteric ligand desformylflustrabromine (dFBr). Markov model analysis of steady-state, low concentration data from receptors expressed in HEK293 cells yielded a 7 state model with unique rate constants for naive and modulated receptors. The model consisted of two sequential binding reactions, mono- and diliganded open states, and two desensitized states, D1 and D2, accessible from the diliganded closed state and diliganded open state, respectively. We found that dFBr decreased the mean lifetimes of D1 (77 ms to 7.6 ms) and D2 (1.7 s to 490 ms). In simulations of macroscopic responses to concentration jumps, the EC_{50} of naive receptors was 74 μM for peak currents, with a maximal P_{open} of 0.9, and profound desensitization (steady-state $P_{open} <$ 0.05 for all ACh concentrations) that developed rapidly (τ_{fast} = 70 ms) at high ACh concentration. dFBr increased the apparent affinity (EC_{50} = 18 μM) of receptors and potentiated steady-state, desensitized responses (~ 5-fold). To investigate the contribution of destabilization of desensitized states to modulation, we examined state occupancy probabilities for both models when driven by various profiles of ACh

concentration. Potentiation of desensitized responses arose from a lower probability of occupancy of D2, whereas destabilization of D1 slowed the initial, fast rate of macroscopic desensitization. Recovery from desensitization was substantially faster with dFBr and correlated with decreased lifetimes of D1 and D2. Finally, we found that desensitization of LS receptors plays an important role in hastening the time course of deactivation following a brief pulse of agonist concentration[1]

---

[1] Demmerly, A., Edmonds, B.W. 2015. Destabilization of desensitized states underlies modulation of (α4)3(β2)2 receptors by desformylflustrabromine. *J. Gen. Physiol.*

2.1 Introduction

A major class of nicotinic receptors in brain is formed from $\alpha4$ and $\beta2$ subunits that assemble as pentamers with alternate stoichiometries, a high-sensitivity (HS; $\alpha4_2\beta2_3$) receptor with an EC_{50} of ~ 1 μM and a low-sensitivity (LS; $\alpha4_3\beta2_2$) receptor with an EC_{50} of ~ 75 μM (Nelson et al., 2003; Moroni et al., 2006). $\alpha4\beta2$ receptors are targets for compounds that bind allosteric sites and modulate responses to ACh. Compounds that potentiate and show selectivity for $\alpha4\beta2$ receptors may mitigate signaling deficiencies in Alzheimer's disease (Warpman and Nordberg, 1995; Martin-Ruiz et al., 1999) and other cognitive disorders associated with insufficient receptor activation or expression. As an alternative to allosteric ligands, partial agonists (Sullivan et al., 1997; Coe et al., 2005) or inhibitors of acetylcholinesterase (Friedman, 2004) have been used as strategies to activate nAChRs; however, those options offer little opportunity for selectivity (Pandya and Yakel, 2011). Moreover, tonic occupation of orthosteric sites produces desensitization, resulting in a profound reduction in responsiveness to ACh (Paradiso and Steinbach, 2003). If cholinergic inputs are at least partially intact, allosteric ligands may yield better functional outcomes.

Novel, $\alpha4\beta2$-selective allosteric ligands are of particular interest as leads for development of additional compounds with distinct functional properties. NS9283 is an allosteric modulator with selectivity for the LS $\alpha4\beta2$ receptor subtype (Timmerman et al, 2012). In whole-cell recordings, NS9283 produces a marked increase in the potency of ACh with no apparent change in efficacy

(Timmermann et al., 2012; Grupe et al., 2013). In response to brief, 1 ms applications of ACh, NS9283 prolongs the time course of deactivation (τ increased from 18 ms to 65 ms); however, the time course of desensitization is unaffected, and desensitized receptors are not reactivated by application of the modulator (Grupe et al., 2013).

Desformylflustrabromine is a metabolite originally isolated from *Flustra foliacea* that potentiates a mixture (HS and LS) of $\alpha 4\beta 2$ receptors, but not $\alpha 3\beta 4$ or homomeric $\alpha 7$ receptors (Sala et al., 2005). The reported mechanism of potentiation is different from NS9283. dFBr increases the potency and efficacy of ACh (Kim et al., 2007), yielding up to 3-fold potentiation of peak current at high agonist concentration. The observation that dFBr activates desensitized receptors in whole-cell recordings led to the hypothesis that potentiation arises from stabilization of open states relative to desensitized states (Weltzin and Schulte, 2010); however, this would require that for steps into high concentrations of agonist, a significant fraction of the receptors is desensitized at the time of peak current. In a study of nonstationary noise of $\alpha 4\beta 2$ receptors expressed in HEK293 cells, the maximal open probability of LS receptors was reported to be large (> 0.8) (Li and Steinbach, 2010), which is at least inconsistent with marked potentiation of LS receptors for any mechanism other than recruitment of silent receptors (Fenster et al., 1999; Zhang and Steinbach, 2003; Li and Steinbach, 2010).

In this study, we used a single-channel approach to gain a better understanding of LS receptor gating and the mechanism of potentiation by dFBr. Gating models developed from low concentration data exhibited characteristics typical of whole-cell responses previously reported for LS receptors (Nelson et al., 2003; Li and Steinbach, 2010; Grupe et al., 2013). We found evidence for two desensitized states, both of which were destabilized by dFBr. Simulations of macroscopic responses showed that dFBr produced marked potentiation of the steady-state response and accelerated recovery from desensitization. At saturating agonist, the peak open probability of naïve receptors was 0.9, and peak response was not potentiated.

2.2 Materials and Methods

2.2.1 Cell Techniques

HEK293 cells were maintained in Eagle's Minimum Essential Medium (MEM; Sigma Aldrich) supplemented with 1% GlutaMAX (Gibco), 10 % bovine growth serum (Hyclone, Thermo Scientific), penicillin (200 U/mL; Cellgro), and streptomycin (200 µg ml^{-1}; Cellgro), pH adjusted to 7.4. Cells were incubated at 37°C in a humidified atmosphere of 5% CO_2, passaged weekly and plated onto 35mm tissue culture dishes (Becton Dickinson) two days prior to transfection. Human α4 and β2 cDNAs [provided in pcDNA3.1/Hygro vectors (Invitrogen) by Dr. Marvin Schulte, University of the Sciences in Philadelphia] were purified using a Plasmid Midi Kit (Qiagen) and transiently transfected (SuperFect

Transfection Reagent, Qiagen) into HEK293 cells. Recordings were made approximately 2 days following transfection.

2.2.2 Electrophysiology Techniques

Desformylflustrabromine hydrochloride was obtained from Tocris. All other reagents, including acetylcholine chloride, were obtained from Sigma Aldrich. To minimize receptor rundown, patch-clamp recordings were made in the cell-attached configuration (Hamill et al., 1981). The membrane potential was nominally zeroed with a high K^+ extracellular solution containing (in mM): 142 KCl, 5.4 NaCl, 2 $CaCl_2$, 1.7 $MgCl_2$, 5 HEPES, and 10 glucose, pH adjusted to 7.4. Pipette solutions were made by addition of either 1 μM ACh or, alternatively 1 μM ACh and 1 μM dFBr to (in mM) 5.4 KCl, 142 NaCl, 2 $CaCl_2$, 1.7 $MgCl_2$, and 5 HEPES, pH adjusted to 7.4, on the day of the experiment. All recordings were made at room temperature ($\sim$ 22°C).

Recording pipettes (thick-walled borosilicate glass; Warner Instruments) were pulled to a resistance of 10-14 MΩ using a PMP-102 micropipette puller (MicroData Instrument, Inc.). To reduce pipette capacitance, tips were coated with Sylgard (Dow Corning). Prior to recording, the pipettes were front- and then back-filled with the pipette solution containing ACh with or without dFBr. Cells were viewed with a Nikon FN1 Eclipse compound microscope, and patches were made (minimum seal resistance 5 GΩ) and then voltage-clamped at an applied potential +80 mV with a HEKA EPC-10 Double amplifier using PATCHMASTER

36

software. Data were low-pass filtered at 5 kHz (4-pole Bessel, -3dB) and

digitized to the computer at 20 kHz.

Amplitude distributions (Figure 3.1) were fitted with the sum of 2 Gaussian

components. Dose-response data for peak responses in Figure 3.4 were fitted

with the Hill equation:

$$y = y_{max}/[1 + (EC_{50}/A)^n], \qquad (1)$$

where A is agonist concentration, EC_{50} is the concentration of agonist at which y

= $y_{max}/2$, and n is the Hill coefficient. Values for simulated steady-state

responses were obtained at 15 s following a simulated jump into ACh.

2.2.3 Model Fitting

Idealized records for patches that appeared to contain 1 channel were

constructed using the segmental k-means method (Qin, 2004), and fitted rate

constants were obtained for models using a maximum likelihood algorithm (MIL)

in QuB (Qin et al., 1996, 1997). Imposed dead times of 200 µs provided the

most reasonable lifetimes for state C3 as well as the fit of the probability density

function (thick line in distributions). The number of components in closed and

open duration distributions indicated that at least 5 closed states and two open

37

states were needed to fit a full model that included desensitized states, which, prior to fitting, could not be assigned to particular gaps in the data record because of the low agonist concentration. The scheme shown in Model 1 was used to fit rate constants for 0.1 μM, 1 μM ACh and 1 μM ACh + 1 μM dFBr data, where A is the ACh concentration, k_{+1} and k_{+2} are association rate constants for binding of 1st and 2nd ligand, and k_{-1} and k_{-2} are dissociation rate constants. Likewise, k_{O+2} governs the concentration dependent rate between O1 and O2, and k_{O-2} is the dissociation rate constant. β_1 and β_2 are opening rate constants for mono- and diliganded receptors, and α_1 and α_2 are corresponding closing rate constants. Rate constants $\delta_{1+/-}$ and $\delta_{2+/-}$ govern transitions into and out of states D1 and D2, respectively.

2.2.4 Definition of Bursts

Single-channel recordings often contain several channel openings in succession (bursts) followed by long periods of closings that occur spontaneously. Analysis of bursts allows us to obtain information on how burst characteristics can be changed in the presence of a modulator as well as how accurate the model is. We use bursts to determine the accuracy of our model by comparing mean burst open time and mean burst length values obtained from the physical data to those computed by the model. If the values obtained from the model resemble those obtained from our data, then we have more

38

confidence that the model is an accurate representation of the data. To do this

we define bursts in the data with a critical value (t_{crit}) using the equation:

$$Amp_{1}* e^{-Tcrit/Tau1}=Amp_{2}* (1 - e^{-Tcrit/Tau2})$$

T_{crit} is the cutoff duration between exponential components and equalizes

the area under the overlapping tails of the distributions. Where Amp_1 and Amp_2

are the weights of the first and second components respectively for bursts. Tau1

and tau2 are the time constants computed from MIL. Each tau in the distribution

contributes one exponential component to the probability density function (thick

line in distributions). Bursts that held doubles were discarded from the analysis,

and values were compared to burst durations calculated from the model.

2.2.5 Calculation of Burst Parameters

We define bursts as a series of openings that occurs before ligand

unbinds from the receptor. Burst parameters were calculated from transition

probabilities (Colquhoun and Hawkes, 1982). Since ligand remains bound, a

burst was defined as 1 or more openings consisting of transitions between O2

and C3 only. The burst begins with an opening to O2 and ends with a transition

to D2 or, alternatively, to C3 from which the receptor does not reopen (next

transition to D1 or C2). O1 openings were not included due to the low occupancy

39

of O1. To determine the distribution of the number of openings per burst, we calculated the probability that a burst contains 1, 2, 3,..., r openings. For a burst to consist of a single opening, the open channel must make a transition to C3 followed directly by a transition to C2 or D1 (state 7 → state 3 → state 2 or state 7 to state 3 → state 4; see state number assignments, Model 1). Alternatively, the open channel can desensitize to D2 (state 7 → to state 5) without entering C3. The probability that the burst consists of a single opening (P (1)) is therefore given by the sum of the probabilities of these events. P (1) = $\pi_{73} \cdot \pi_{32}$ + $\pi_{73} \cdot \pi_{34}$ + π_{75}, where $\pi_{73} = \alpha_2/(\alpha_2 + \delta_{2+})$, $\pi_{32} = k_{-2}/(k_{-2} + \beta_2 + \delta_{1+})$, $\pi_{34} = \delta_{1+}/(\delta_{1+} + k_{-2} + \beta_2)$, and $\pi_{75} = \delta_{2+}/(\delta_{2+} + \alpha_2)$.

For the probability that the burst consists of two openings, $P(2)$ = $\pi_{73} \cdot \pi_{37} \cdot \pi_{73} \cdot \pi_{32}$ + $\pi_{73} \cdot \pi_{37} \cdot \pi_{73} \cdot \pi_{34}$ + $\pi_{73} \cdot \pi_{37} \cdot \pi_{75}$. The probability of r openings is given by:

$$P(r) = \pi_{73}{}^{r} \cdot \pi_{37}{}^{r-1} \cdot (\pi_{32} + \pi_{34}) + \pi_{73}{}^{r-1} \cdot \pi_{37}{}^{r-1} \cdot \pi_{75} \qquad (6)$$

Using the identities π_{32} + π_{34} = 1 − π_{37} and π_{75} = 1− π_{73}, the expression can be simplified to the form for a geometric distribution:

$$P(r) = (\pi_{73} \cdot \pi_{37})^{r-1} \cdot (1 - \pi_{73} \cdot \pi_{37}) \qquad (7)$$

40

The mean number of openings per burst, $m_r = \sum_{r=1}^{\infty} r \cdot P(r)$, was calculated from the mean of the geometric distribution:

$$m_r = \frac{1}{1 - \pi_{73} \cdot \pi_{37}} \qquad (8)$$

The sum of the mean open time per burst [$m_r \cdot m_{O2}$, where $m_{O2} = 1/(\alpha_2 + \delta_{2+})$] and the mean closed time per burst [$(m_r - 1) \cdot m_{C3}$, where $m_{C3} = 1/(\beta_2 + k_{-2} + \delta_{1+})$], gives the mean burst duration. The probability of being open during the burst was then calculated by dividing the mean open time per burst by the mean burst duration.

Model 1.
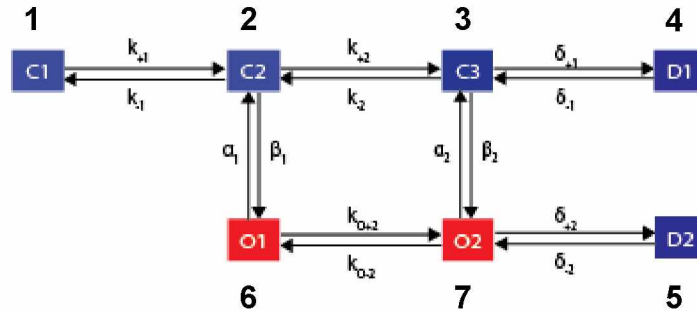
2.2.6 Estimation of Channel Open Probability

Estimates of the probability that each patch contained only a single channel were made using an approximation given by Colquhoun & Hawkes

(Colquhoun and Hawkes, 1990). For **N** independent channels with two states (open and closed), the probability that, if one channel is open, the next transition will be closing of the open channel rather than opening of the second channel is given by:

$$\pi \approx \frac{1 - P_{open}}{1 - P_{open}/N},$$ (2)

where $P_{open} = m_o/(m_o + m_c)$ (m_o and m_c are the mean open time and mean closed time, respectively) is the probability that a channel is open on an observed record of single openings, and **N** is the number of channels in the patch. The probability of observing r consecutive single openings before the first double opening is $P(r) = \pi^{r-1}(1 - \pi)$. The probability of observing at least n_o consecutive single openings is then given by the cumulative form of the geometric distribution.

$$P(r \geq n_o) = \pi^{n_o - 1}.$$ (3)

When channels exhibit long (desensitized) closed periods punctuated by bursts with high P_{open}, a better (more stringent) estimate of the probability of two channels is obtained by treating bursts as single openings (Colquhoun and Hawkes, 1990). We therefore adjusted n_o to reflect the number of bursts (n_o/

m_{r_exp},) by dividing the number of bursts by the openings per burst, where m_{r_exp}

is the experimentally determined number of openings per burst). m_{r_exp} (no

correction for missed events) was obtained in QuB by defining a t_{crit} separating

components 1 and 2, or components 2 and 3 of closed duration distributions for

experiments in ACh and ACh + dFBr, respectively. We defined the t_{crit} for dFBr

as between 2 and 3 due to the components of 1 and 2 being extremely close to

each other. Bursts were defined as runs of openings containing gaps less than

t_{crit}. For the probabilities reported here as P $(r \geq n_0)$, r and n_0 are bursts, not

openings.

2.2.7 Simulations

All simulations shown for control (ACh model) and modulated (dFBr

model) responses were made using rate constants from the best model of the set

as determined by the total number of openings (> 1700, includes openings and

closings) (see Table 1). A set was defined as patches that were obtained with

the same ACh/dFBr concentration profile. Monte Carlo simulations of

macroscopic currents in Figure 2.4A were made in QuB Express for 10,000

channels with a unitary amplitude of 1 pA and standard deviation (SD) of

Gaussian noise of 0.15 pA (Nicolai and Sachs, 2013). Current values were

converted to and displayed as open probabilities (P_{open}) in Igor Pro

(WaveMetrics).

43

For a Markov process, the evolution of state occupancy probabilities is given by:

$$\frac{ds_i}{dt} = \sum_{j=1}^{n} s_j r_{ji} - \sum_{j=1}^{n} s_i r_{ij} \quad , \qquad (4)$$

where s_i is the fraction of channels in state S_i, and r_{ji} and r_{ij} are the rate constants governing transitions into and out of state S_i, respectively (Colquhoun and Hawkes, 1981). Given an initial condition of $P_{C1}=1$ and a concentration profile $c(t)$, which sets the values of concentration dependent rates, $s(t)$ was integrated in xpp (v. 7.0, Bard Ermentrout; www.math.pitt.edu/~bard/xpp/xpp.html) using a Runge-Kutta method and 10 μs time steps.

To examine trajectories of occupancy probabilities, simulations were driven by three different agonist concentration profiles: 1) a jump, 2) a slowly rising exponential function, and 3) a brief pulse of agonist given by an alpha function to mimic transmitter concentration at a fast synapse (τ=500 μs).

$$c(t) = A * (t/\tau) * e^{-(t-\tau)/\tau} \qquad (5)$$

2.3 Results

2.3.1 Conductance of LS Receptors

Channel openings with two distinct amplitudes were observed in cell-attached recordings with a low concentration of ACh (1 μM). Figure 2.1A shows 1 s records and corresponding open-point amplitude histograms for typical low- and high-amplitude channels recorded at -80 mV. Assuming a reversal potential of 0 mV, fitted histograms yielded chord conductance (g) estimates of 19.9 ± 1.4 pS (mean$\pm$SD; n=13 cells) and 28.6 ± 2.5 pS (n=19 cells). Consistent with previous reports of inward rectification of $\alpha 4 \beta 2$ receptors (Buisson et al., 1996; Sabey et al., 1999), we did not observe LS receptor openings at assumed patch membrane potentials above 0 mV; however, I-V data collected between -80 and -20 mV for two patches (one in dFBr; Figure 2.1C, open circles) were well fitted by a linear equation, yielding a slope conductance estimate (30 pS) similar to our estimate of g, and a predicted reversal potential near 0 mV (-2.7 mV). Assuming inward currents rectify for depolarizations above -20 mV, our estimate of g may be somewhat high due to an underestimate of the driving force.

In patches that appeared to contain only one channel conductance, based on the observation of openings to only one level over a minimum recording period of 2.5 min, 71% (15 out of 21 patches) contained LS receptors. Differences in apparent affinity for ACh for the two subtypes of $\alpha 4 \beta 2$ receptors (LS, $\alpha 4_3 \beta 2_2$ $EC_{50} \sim 75$ μM vs HS, $\alpha 4_2 \beta 2_3$ $EC_{50} \sim 1$ μM (Buisson and Bertrand, 2001; Nelson et al., 2003; Moroni et al., 2006)) favors activation of HS receptors;

therefore, our data is consistent with reports that at least 70% of functional $\alpha4\beta2$ receptors expressed in HEK 293 cells are LS receptors (Li and Steinbach, 2010; Grupe et al., 2013). Modulation of LS receptor currents by dFBr could arise from effects on channel gating, unitary conductance, or recruitment of silent receptors (Fenster et al., 1999; Zhang and Steinbach, 2003; Li and Steinbach, 2010) (not investigated here). Fitting of open point amplitude histograms for ACh + dFBr (Figure 2.1B) yielded a mean conductance of 28.4±2.0 pS (mean±SD, n=12 cells), similar to the value for ACh. Accordingly, dFBr does not modulate receptor function by altering single channel conductance. Sublevels were observed in patches with and without dFBr (Figure 2.1B, inset). Sublevels appeared more frequently dFBr; however, because they were brief and, even in dFBr, occurred too infrequently to analyze, they were fitted as full amplitude events.

2.3.2 Gating of LS Receptors in ACh and ACh + dFBr

Recordings in 1 μM ACh or, alternatively, 1 μM ACh + 1 μM dFBr yielded 3 patches for each condition (out of a total of ~ 150 patches containing LS receptors) that contained runs of 30 pS openings of sufficient length (> 250 openings, average of 560) and no evidence of simultaneous openings of two channels. When the probability of a channel being open is low, as it was in our experiments (P_{open} ~ 0.01), more than one channel may be present despite the observation of openings to only one level (Colquhoun and Hawkes, 1990). We

46

estimated the probability of obtaining the observed run of single openings

(corrected for high P_{open} bursts, see Methods) for each patch if, in fact, two

channels were present (see Methods). Values of $P(r \geq n_o)$ were 0.01, 0.23, and

0.53 for ACh, and 0.03, 0.45, and 0.11 for ACh + dFBr. Figure 2.2 shows 50 s

segments from ACh and dFBr patches with the lowest probability of having two

channels.

In single-channel recordings it is often observed that several channel

openings occur in rapid succession, where the individual openings are separated

by brief closings (Colquhoun and Hawkes, 1982). Analyzing bursts allows all the

openings within one burst to be attributed to a single channel, allowing shut

periods within bursts to tell us about characteristics of a channel or the effects a

modulator has on burst structure. Figure 2.3 shows burst length and open

lifetime for 1μM ACh (A) and 1 μM ACh + 1 μM dFBr (B). Two exponentials were

needed to fit the distributions of burst length and open time per burst. Burst

length and open lifetime decrease in the presence of dFBr; the fast (τ_f) and slow

(τ_s) time components decrease for burst length from 2.86 ms to 1.6 ms for τ_f and

42.1 ms to 14.7 ms for τ_s. Burst open lifetime distributions showed a similar

trend, with τ_f being reduced from 3 to 0.75ms and τ_s being reduced from ~16 to

~11 ms. dFBr decreases the mean burst length and burst open lifetime, which is

counter-intuitive to how a potentiator is expected to behave. The decrease in

burst length is due to dFBr effectively reducing the intra-burst duration via

decreasing the mean lifetime of desensitized state D1 (See 2.3.7), allowing

greater simultaneous activation of receptors when exposed to agonist. Burst

parameters for the patches, calculated for zero agonist concentration, were in agreement with the time constants obtained from the fitted burst distributions. The calculated mean burst duration was 51.4 ms (42.1 ms from fits) and 25.7 ms (~15 ms from fits) for ACh and dFBr respectively. The calculated mean open time was also in agreement with values of 12.4 ms (~16 ms for the fits) and 8.1 ms (~11 ms for the fits) in ACh and dFBr respectively. These results give us more confidence that our model is a fairly accurate representation of LS $\alpha 4 \beta 2$ nAChR gating.

The stability of the patches for all concentrations (0.1 and 1 μM) and in the presence of modulator (1 μM ACh + 1 μM dFBr) is shown in Figure 2.4. P_{open} was larger when calculated from the stability plots (0.1 μM ACh: 0.13, 1 μM ACh: 0.16, and + dFBr: 0.14) due to the inclusion of periods of high occupancy.

2.3.3 Fitting Mechanisms to Single Channel Data

We investigated the mechanism of modulation for dFBr on $\alpha 4_3 \beta 2_2$ nACh receptors by fitting a wide range of models directly to the single-channel data. Figure 2.5 shows models tested (left) along with the final model for 1 μM ACh and 1 μM ACh +1 μM dFBr. Rates plus standard deviations (0.1 μM and 1 μM ± dFBr). Models on the left include Katz and Thesleff, Monod Wyman Changeux (MWC), modified MWC models that include desensitization and two models that did not contain activations steps, linear and star. All models were constrained by the requirement of microscopic reversibility for the cycle, while activation rates

were not constrained. Due to the low probability of unliganded openings under our conditions these states were omitted from MWC and similar models.

More classical mechanisms such as the Katz and Thesleff and MWC models were initially utilized in order gain a better understanding of the data. The Katz and Thesleff model fit the closed time distributions well for all concentrations and one open state fit the 1 μM ACh data but not the 0.1 μM data (Figure A.2.1). Activation rates are 10-fold higher for 1 μM data than the 0.1 μM data, whereas the concentration dependent rates of $2k_{+2}$ and k_{+1} are 100 to 1000x larger for the 0.1 μM data than the 1 μM data (Table A.2.1). Lifetime of C3 is also extremely low and well below our dead time, giving less confidence in the rates leaving C3. The basic MWC model had similar problems in regards to the activation rates being 10 to 100 x larger for 0.1 μM vs 1 μM ACh data. Activation rates for the 1 μM data set were low and gave low P_{open} in simulated macroscopic currents (not shown). The MWC model clearly showed that more than 3 closed states are required to fit the closed time distributions for our data. Recent work using concatenated receptors provides evidence that $\alpha 4_3 \beta 2_2$ receptors possess two high affinity binding sites at α-β interfaces in addition to a 3rd, high affinity site at the α-α interface (Harpsoe et al., 2011). Attempts to fit permutations of the MWC mechanism that included an additional agonist binding reaction always produced unreasonably large or small values for at least 1 rate constant. It may be that the additional activation step and subsequent open state have a lifetime very similar to that of either the mono or diliganded activation

steps and open states in our data, thus we are unable to distinguish them from the other states.

2.3.4 Modified MWC Mechanisms

From the classical mechanisms we tested various scenarios of desensitization and its connections to the models. In order to improve fits, we added desensitized states to the MWC mechanism. The MWC modified mechanisms gave the most reliable results for all the cases we tested so we will focus on those mechanisms here. We tested various locations of two or more desensitized states. These included single desensitized states off of either O1, O2, or C3 (not discussed), two desensitized states off of O1/O2, O1/C3, or O2/C3, and a few variations with three desensitized states. Only a few of these variations are discussed in detail here. For these modified models two desensitized states or more gave better results in terms of fits to the closed distributions and reasonable simulated currents. For mechanisms that contained three desensitized states we excluded testing configurations that contained a D state off of O1. This is because any configuration that included a state off of O1 resulted in a difference in the activation rates between concentrations, as well as dFBr not potentiating current when simulations were performed (data not shown), which does not agree with previous findings on dFBr's apparent activity in whole cell experiments (Weltzin and Schulte, 2010). Desensitized states off of O1 and O2 gave decent fits (Figure A.2.3), but still had the issue of activation rates being

10 to 100x higher for the 0.1μM data and the rates between O1 and O2 are high (Table A.2.3). It was found that a desensitized state was required off of state O2 and off of C3 in order for the activation rates to agree with each other.

We further tested the existence of an additional desensitized state off of O2, leading to two desensitized states off of O2 and one off of C3. The fits to closed and open time distributions improved marginally with this addition and it was difficult to determine if an additional desensitized state was required from the fit alone (Figure A.2.4). With this configuration we saw a large discrepancy between the activation rates and rates entering O1 when comparing multiple concentrations of ligand (Table A.2.4). Simulated macroscopic currents also showed an increase in desensitization compared to the two desensitized state models.

The mechanism that gave us consistent activation rates as well as reasonable simulations for EC_{50} was a two desensitization state configuration with states off of O2 and C3. Consistent with reports in which 2 desensitized states were identified for LS $\alpha4\beta2$ receptors (Sabey et al., 1999; Nelson et al., 2003; Paradiso and Steinbach, 2003; Grupe et al., 2013). Rate constants from our two best patches (shown in Figure 2.2) that contained the largest number of events (ACh: 1754; ACh + dFBr: 1785), are shown in Table 2.1 were used for simulations. The average data from analysis of all 3 data sets in each condition are shown in Table 2.2.

For the maximum likelihood fitting algorithm, model rate constants are adjusted to maximize the likelihood of the data (sequence and durations of openings and closings) with correction for missed events (Qin et al., 1996). Estimated rate constants for our model (Figure 2.5) yielded distributions of open and closed durations that agree with the observed data (Figure 2.6). A comparison of the data sets collected under each parameter (ACh and ACh + dFBr) indicated that rate constants for transitions to O1 (β1), from O1 to O2 (k_{+2}) and transitions out of D1 and D2 (δ_{1-} and δ_{2-}) were significantly larger in dFBr (P values: 0.061, 0.008, 0.001 and 0.047 for two-tailed t-test, respectively; Table 2.2). For the fitted rate constants in Figure 2.5, the increase in δ_{1-} corresponds to a decrease in the mean lifetime of D1 ($1/\delta_{1-}$) from 77 ms to 7.6 ms, and the increase in δ_{2-} yields a reduction in the mean lifetime of D2 from 1.7 s to 493 ms.

2.3.5 Desensitization Based Mechanisms

At high concentrations of ACh almost all current can be attributed to the activity of diliganded AChRs (Elenes and Auerbach, 2002). The lifetimes of diliganded closed mouse AChRs (~10 μs) are too brief to be detected (Maconochie and Steinbach, 1998). If concentrations are high enough, then the lifetimes of diliganded closed states are too brief to be detected. To account for this possibility are we fitted models that contained a doubly liganded open state and only desensitization like states for closed states. We made two desensitization based models, linear and star. For the linear and the star models the fits are relatively good for closed time distributions, but open time

52

distributions for 0.1 μM and 1 μM ACh +1 μM dFBr requires more than one open

state (Figure A.2.5 and A.2.6). Majority of rates agreed in the models between

concentrations. The exceptions were for linear k_{23} and k_{21}, and for star k_{O4}, k_{30},

and k_{1O} (Table A.2.5 and A.2.6). Simulations testing the decay time course for

these models (starting in state O) revealed dFBr increased the decay time

course, which does not coincide with previous reports on the effects of dFBr (Kim

et al., 2007; Weltzin and Schulte, 2015). It is not surprising that these schemes

failed to describe open-time distributions that clearly contain more than one open

component. Also, if our data did not contain any information on activation, then

we would see a strong case for dFBr as a potentiator that destabilizes

desensitized states in models that lack activation rates. We are confident that

the concentrations utilized in the low-sensitivity experiments are low enough to

allow the observation of activation kinetics for the $\alpha 4\beta 2$ LS subtype.

2.3.6 Simulations of Macroscopic Currents

To determine if our estimated kinetic parameters supported potentiation

over a range of ACh concentrations, we simulated macroscopic responses to

concentration jumps (Figure 2.7A). Potentiation of the peak response by dFBr

was apparent at 10 μM ACh, less at 100 μM, and negligible at 1 mM ACh where

the peak open probability for ACh alone was ~ 0.8. At concentrations of ACh

above 1 mM, peak responses were inhibited in dFBr (Figure 2.7B). dFBr yielded

3-3.5-fold potentiation of desensitized (near steady-state) responses, as

53

expected for shorter lifetimes of desensitized states. Fitted Hill equations to peak

responses yielded (mean±SD) EC_{50} values and Hill slopes of 58±4 μM and

0.76±0.04 for ACh, and 17±1 μM and 0.98±0.05 for dFBr. The concentration

dependence of dFBr-induced differences (increases) in responses are shown for

ACh concentrations up to 1 mM in Figure 2.7C. Our model yielded a maximal

P_{open} of ~ 0.9, consistent with an estimate from noise analysis for LS receptors of

> 0.8 (Li and Steinbach, 2010).

When driven with a jump into 1 mM ACh, desensitization exhibited a

biphasic, exponential decay with a time constant of 55 ms for the fast, major

amplitude component (relative amplitude 0.33) and 220 ms for the slow

component (Figure 2.7A). The fitted, steady-state value was 0.07, with steady-

state values of P_{open} for all concentrations (assessed from mean response

amplitudes near the end of a 15 s jump) are shown in Figure 2.7B (open

squares).

2.3.7 Occupancy Probabilities and Desensitization

An advantage of single-channel methods for studies of mechanism is that

once the rate constants for the model are determined, the time-dependent

probability of occupancy of each state can be determined for any concentration

profile. One aim of examining occupancy probabilities was to determine how

changes in occupancy of D1 and D2 contribute to potentiation. Figure 2.8 shows

occupancy probabilities for concentration jumps into 10 μM, 100 μM, and 1 mM

54

ACh. The open probability was approximated by P_{O2} (P_{O1} is less than 0.005 for all simulations). For jumps into a low concentration of ACh (10 μM), dFBr increased the peak response by a factor of 2 (P_{O2_ACh} = 0.13, P_{O2_dFBr} = 0.26).

During the early phase of macroscopic desensitization (right panels Figure 2.8), the reduction in P_{D1} by dFBr was the significant contributor to potentiation. Even though entry into D1 occurs earlier, P_{D1_dFBr} is lower and drops faster compare to that of P_{D1_ACh}. Potentiation is almost entirely due to destabilization of D1. This is most notable at larger concentrations and appears to be negligible at concentrations of ~1 μM. As P_{O2} approaches steady-state (best seen for 1 mM simulation, lower panels), the difference between P_{D1_ACh} and P_{D1_dFBr} declines due to the relatively slow relaxation of ACh model receptors from D1 into D2. Steady-state differences in P_{O2} arise almost entirely from destabilization of D2. The early versus late contribution of destabilization of D1 and D2 are also seen for higher concentration simulations, where the fraction of bound receptors are close to 1 shortly after P_{O2} reaches the peak.

2.3.8 Slow Solution Exchange and Potentiation

In a recent study in which $\alpha 4_3 \beta 2_2$ receptors were in excess, 3-fold potentiation was observed for 1 μM dFBr with 100 μM ACh (EC_{75} for that preparation) (Weltzin and Schulte, 2015). Our models yielded a prediction of less than 1.1-fold potentiation at EC_{75} (~ 300 μM) because of the high P_{open} (~ 0.68) at the peak response to ACh alone. Differences between oocyte results

and model predictions could arise from different gating properties of LS receptors in HEK cells, recruitment of receptors from a large population of nonfunctional, silent receptors (Fenster et al., 1999; Zhang and Steinbach, 2003; Li and Steinbach, 2010), or from a relatively slow activation profile in oocytes due to slow solution exchange (Joshi et al., 2004). To determine if slow solution exchange predicted larger potentiation, we calculated occupancy probabilities using an exponential function for the concentration profile $c(t) = cmax * (1 - \exp(-t/\tau_c))$ (Figure 2.9). A time constant (τ_c) of 4 s yielded a time to peak of ~ 400 ms (ACh model) for 300 μM ACh, similar to published results for $\alpha4\beta2$ responses in oocytes (Kim et al., 2007; Weltzin and Schulte, 2010). A 400 ms rise time is also expected for the vertical flow exchange apparatus used in those experiments (Joshi et al., 2004). Figure 2.9A shows that a slow rise in ACh concentration yielded a lower peak P_{open} for the naive receptor and a large increase in response (1.64-fold) compared to jumps (lower panel).

2.3.9 Deactivation Following a Pulse of High Agonist Concentration

To examine macroscopic responses to an agonist concentration profile typical of fast synapses (Clements et al., 1992; Silver et al., 1996; Beato, 2008), we drove models with an alpha function with peak concentration of 1 mM and half maximum width of 1.2 ms (Figure 2.10). The peak open probability for the ACh model ($P_{O2\_ACh} = 0.28$) was low in comparison to that found for sustained jumps into the same concentration of ACh. dFBr yielded a 1.6-fold increase in

response amplitude (P_{O2_dFBr} = 0.45) due to an increase in the fraction of bound receptors. For the ACh model, the decay of P_{O2} (deactivation) exhibited a fast, major amplitude (0.72) phase with a time constant of 44 ms, in addition to two smaller, slow components with time constants of 133 ms and 5.4 s. The slow time constants matched time constants describing relaxation of P_{D1} and P_{D2}, consistent with the view that the time course of LS receptor deactivation reflects a fast phase of channel closing followed by delayed openings arising from receptors leaving D1 and D2.

In single channel recordings of $\alpha7$ nAChRs, individual openings were found to terminate not by channel closing, but by entry into desensitized states (daCosta et al., 2011) (see also, (Marabelli et al., 2015)). For the LS receptor, relaxation of receptors into D1 and D2 exhibited a time course similar to the fast decay of P_{O2} (Figure 2.10A) indicating that bursts of openings may terminate in D1 or D2. To test the hypothesis that the initial phase of deactivation is accelerated by entry into desensitized states, responses were simulated with δ_{1+} and δ_{2+} set to zero. The inset shows that the mean decay time of P_{O2} was prolonged ~ 3-fold (τ=157 ms). The deactivation time course of LS receptors was therefore not a simple reflection of channel closing.

For the dFBr model, the decay of P_{O2} was fitted with the sum of two exponential components. The time constant of the major amplitude (A_1=0.97), fast phase (45 ms) was slightly faster than the value found for naïve receptors, and the time course of the slow phase (τ_2=649 ms) was similar to the time course

of decay of P_{D2} (τ=653 ms). A decay component for P_{O2} reflecting recovery of

receptors from D1 was not observed because the fast time constant for

relaxation of P_{D1} (τ_1 = 76 ms; A_1 = 0.97) was the same as the fast time constant

for P_{O2}. P_{D1} is scaled in Figure 2.11B to show this relationship. Despite the fact

that deactivation was faster in dFBr, charge transfer at 100 ms was still 1.4-fold

larger. In contrast to naïve receptors, removal of desensitization for the dFBr

model only produced a small increase in the time constant (τ=50 ms) of a single

exponential fit to the decay of P_{O2} (inset). With only δ1+ set to zero (trace not

shown), the time constant was slightly shorter (τ=39 ms); therefore, elimination of

D1 offsets the effect of removing D2. The calculated mean burst duration in dFBr

was 26 ms (P_{open}=0.98, m_r=3.1) with desensitization, so a functional burst in dFBr

includes, on average, ~1 sojourn in D1. When burst P_{open} is high, the mean burst

duration is a good approximation of the time constant fitted to the decay of

aligned bursts (no latency to first opening). Removal of desensitization increased

the mean burst duration from 51 ms (P_{open}=0.98, m_r=4.1) to 154 ms (P_{open}=0.98,

m_r=8.5).

The development of and recovery from desensitization following a pulse of

agonist concentration was faster in dFBr (Figure 2.11). dFBr decreased the time

to peak of P_{D1} + P_{D2} from 187 ms to 69 ms. Recovery from desensitization

reflected recovery of both P_{D1} and P_{D2} for ACh and P_{D2} only for dFBr. Despite

the fact that receptors were only exposed to saturating agonist for ~1 ms, 54% of

naïve receptors bound by agonist were desensitized. In dFBr, only 18% were

desensitized.

2.4 Discussion

Studies of $\alpha4\beta2$ receptors in whole cells are complicated by expression of two subtypes of receptors (Nelson et al., 2003; Moroni et al., 2006). With oocytes, the ratio of injected RNAs can be altered to favor one subtype (Nelson et al., 2003; Moroni et al., 2006; Weltzin and Schulte, 2015); however, for studies of fast receptors, cell lines are often preferable because solution exchange times are shorter for small cells. When $\alpha4\beta2$ receptors are expressed in HEK293 cells, most of the functional surface receptors are the low-sensitivity ($\alpha_{4}3\beta_{2}2$) subtype (Nelson et al., 2003; Li and Steinbach, 2010), and this preparation has been used successfully to characterize macroscopic properties of LS receptors and, recently, to investigate mechanism for the LS-selective modulator NS9283 (Grupe et al., 2013). Unfortunately, dFBr potentiates both subtypes (Weltzin and Schulte, 2015) so, for us, a single-channel approach provided the most straightforward option for circumventing problems with heterogeneity, with the added benefit of gaining greater insight into mechanism. If full gating models can be obtained (or at least ones that give a fairly complete representation of function), as we did here for naïve and modulated receptors, simulations of macroscopic responses can be made for any profile of agonist concentration. This could prove useful for predicting the consequences of dFBr modulation for signaling at LS receptors because receptors may experience quite different profiles in ACh concentration due to different spatial relationships between receptors and release sites (Descarries et al., 1997; Ren et al., 2011) and, as we

59

suggest here, the change in the postsynaptic signal may depend on the concentration profile, with larger effects for profiles that favor desensitization.

The model for the naive receptor presented in this study generated predictions for macroscopic behavior that agree with results for human LS receptors from other studies. Our finding of two desensitized states with short and long lifetimes is supported by observations of two phases of current decay in concentration jump experiments (Nelson et al., 2003; Paradiso and Steinbach, 2003; Grupe et al., 2013), and also by experiments documenting corresponding fast and slow phases for recovery of receptors from desensitization (Paradiso and Steinbach, 2003; Grupe et al., 2013). Except perhaps for the slow the time course of desensitization recovery (discussed below), the values of time constants (of fitted exponentials) reported by other groups agree with our values (Nelson et al., 2003; Grupe et al., 2013). The fitted rate constants for our model also yielded expected values for potency and Hill coefficients (Nelson et al., 2003; Moroni et al., 2006; Grupe et al., 2013). Ideally, we would like to perform additional experiments with a range of ACh + dFBr concentrations to verify if the potentiation exhibited by dFBr on a single-channel level depends on agonist concentration. Overall, the model does a remarkably good job of replicating high concentration results.

The primary finding of this study was that dFBr decreased the mean lifetimes of two desensitized states. Our conclusions, and the validity of our models, depend on obtaining correct estimates for the lifetimes of C1, D1, and D2, the longest closed durations in our single-channel records and, therefore, the

60

most susceptible to underestimation due to the possibility that patches contained

multiple channels. For the patches used to fit rate constants for simulations, we

found low values (<0.05) for the estimates of the probability that a second

channel is present [P (r ≥ n_0)]; however, the estimates for P(2) channels were

larger for other patches. Moreover, if a second channel were active for only part

of the record, P (r ≥ n_0) is less reliable. D2 is isolated from other closed states

and has a long mean lifetime (1.7 s); therefore, if undetected channels were

present, the value of δ_{2-} should be correlated with P (r ≥ n_0). Regression analysis

showed that P (r ≥ n_0) and (normalized) δ_{2-} were not correlated (Pearson r = -

0.29, $P(r)$ = 0.57). The finding of shorter lifetimes of D1 and D2 in dFBr appears

to be well supported; however, we are less certain about the precise values of δ_{2-}

and k_{+1}. For rat $\alpha4\beta2$ receptors activated by ACh, the reported slow time

constant for recovery from desensitization was 17 s (Paradiso and Steinbach,

2003). In a recent study of human, mostly LS receptors expressed in HEK 293

cells, the slow phase of recovery was 12.8 s (Grupe et al., 2013). In simulations

(not shown), decreasing the value of δ_{2-} from 0.6 s^{-1} to 0.2 s^{-1} (a value well within

the error reported for group data) prolonged the slow recovery time constant from

5 s to 10 s, and decreased the steady-state P_{open} from 0.05 to 0.025. Effects on

other macroscopic parameters were negligible. Additional studies are needed to

obtain better estimates of δ_{2-} and k_{+1}.

Our findings have potential implications for signaling. First, in cases

where receptors are subject to a prolonged elevation in transmitter concentration

(Descarries et al., 1997; Zoli, 1999; Ren et al., 2011), destabilization of

61

desensitized states would result in a substantial increase in charge transfer. Interestingly, dFBr had no effect on response amplitude for agonist concentrations below 1μM, so the possibility exists for functional selectivity based on a threshold of agonist concentration.

At fast synapses, for which low-sensitivity receptors are better suited (Nelson et al., 2003), receptors are exposed to a brief concentration and are far from steady state. Our results predict a steep dependence of receptor occupancy on transmitter concentration. For glutamatergic synapses, estimates of the time constants for the decay of transmitter range from 1.2 to 4 ms (Clements et al., 1992; Diamond and Jahr, 1995). For our model, increasing the duration of the pulse of 1 mM ACh from 1 ms to 4 ms increased the estimated P_{open} from 0.25 to 0.68. From the perspective of development of positive allosteric ligands, if receptors are saturated at fast cholinergic synapses, dFBr and other compounds that exhibit potentiation by scaling the current, will be relatively ineffective at boosting postsynaptic signals that arise from low frequency inputs. Compounds that enhance charge transfer by prolonging deactivation may be more effective, e.g. NS9283 (Grupe et al., 2013). For high frequency stimuli, compounds that accelerate recovery from desensitization may be preferable.

Paradiso and Steinbach showed that prolonged application of ACh promotes entry into a desensitized state that recovers slowly; the relative amplitude of the slowly recovering component of desensitization increased with longer jumps into agonist (Paradiso and Steinbach, 2003). Our results do not

62

fully account for their observations, which suggest the existence of a third desensitized state; however, we do observe a redistribution of receptors from D1 to D2 at longer times ($\tau \sim 1$ s). For experiments in which desensitized receptors were found to be reactivated by dFBr (Weltzin and Schulte, 2010), the only mechanism that, for our model, can account for their observed rapid increase in the fraction of open receptors is via an increase in the rate out of D2. Our results do not support the large increases in peak current with high agonist concentrations found in oocyte experiments (Kim et al., 2007; Weltzin and Schulte, 2015); however, at least part of the discrepancy is likely due to slow solution exchange, which allows time for desensitization to develop.

In conclusion, we provide the first model for gating of human $\alpha 4_3 \beta 2_2$ receptors from single channel data. We provide evidence favoring the view that the allosteric modulator dFBr improves LS receptor responsiveness by destabilization of desensitized states. The consequences of modulation for signaling will likely depend on the frequency and profile of agonist concentration at the receptors.

2.5 Acknowledgments
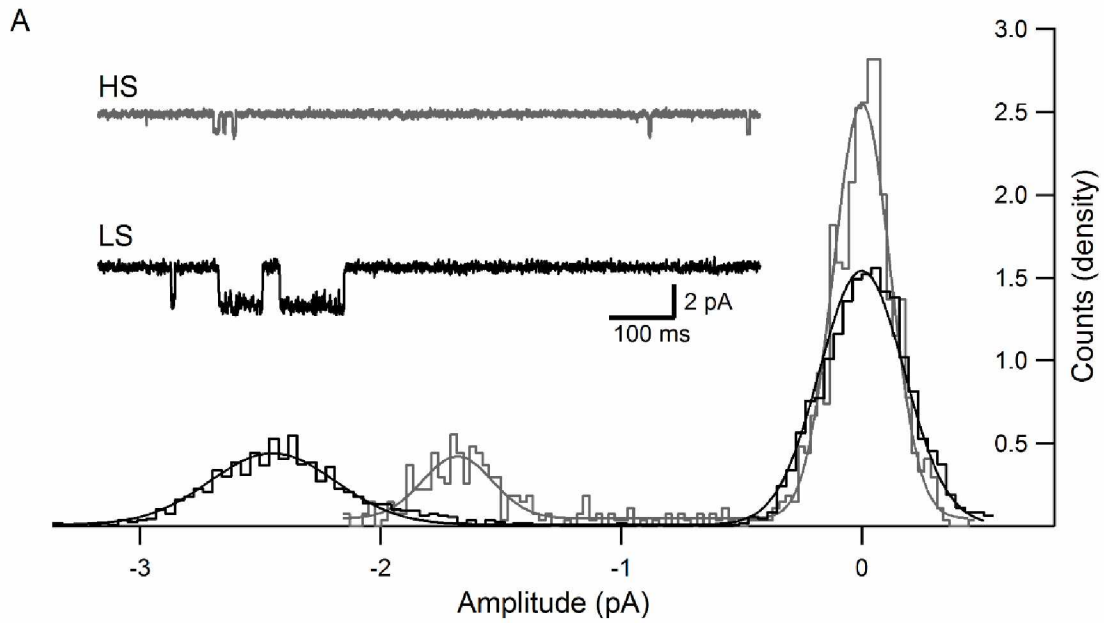
Figure 2.1A: Unitary conductance's of α4β2 receptors. (A) Sample traces and open point amplitude histograms are shown for low [21.0±1.9 pS (mean±SD); HS receptor; gray traces] and high [30.6±3.3 pS (mean±SD); LS receptor; black traces] conductance channels recorded in 1 μM ACh.
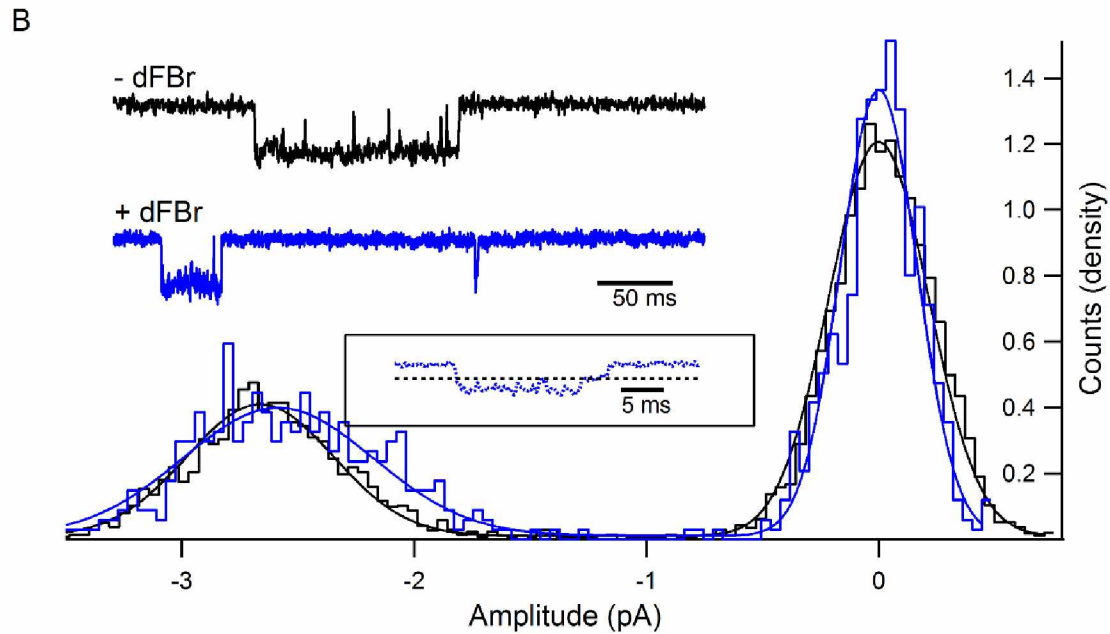
Figure 2.1B: Unitary conductance's of $\alpha4\beta2$ receptors. (B) Fitted amplitude histograms and traces are shown for an LS receptor in 1 μM ACh [33.5±3.9 pS (mean±SD)] and a receptor in 1 μM ACh and 1 μM dFBr [32.3±5.1 pS (mean±SD)]. Inset shows example of occasional sublevel [dotted line at 1.38 pA (17.3 pS)] primarily seen in dFBr.

C
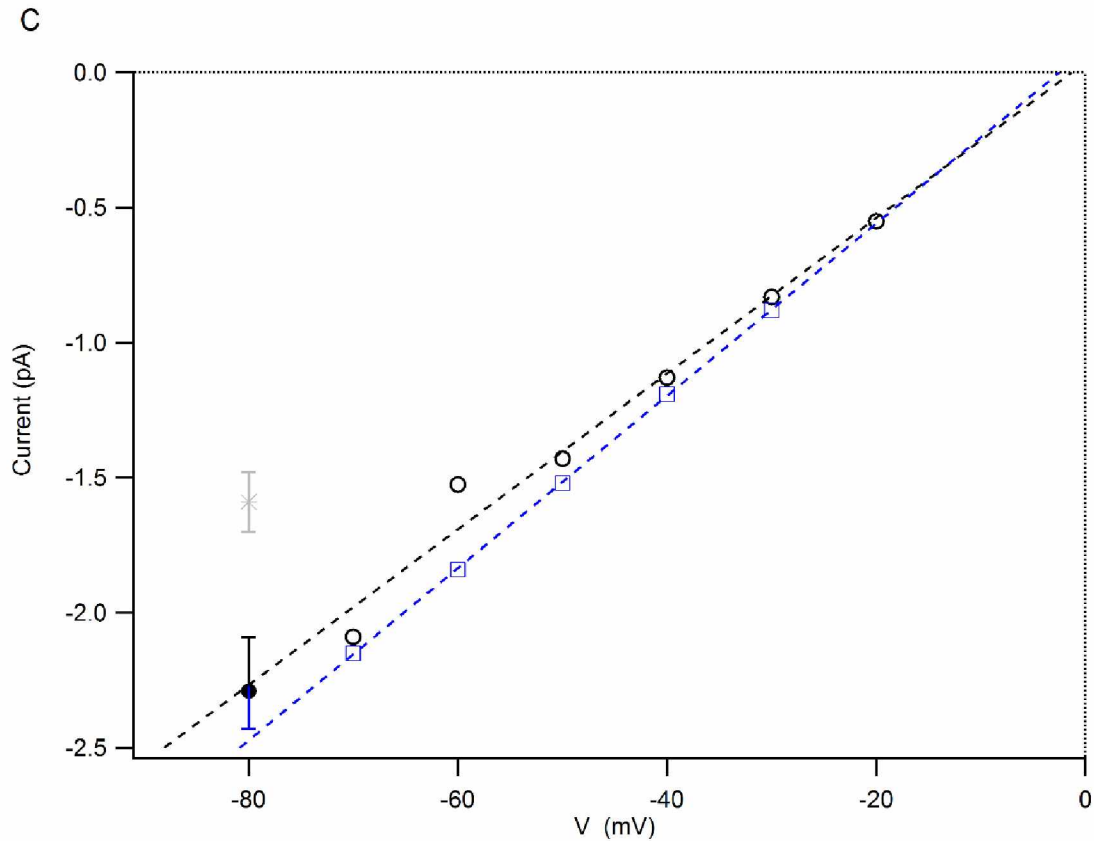
Figure 2.1C: Unitary conductance's of $\alpha4\beta2$ receptors. (C) I-V plot shows mean

values ($\pm$ SD) of HS (19.9$\pm$1.4 pS; n=13 cells; gray star) and LS (28.6$\pm$2.5 pS;

n=19 cells; black circle, obscured) receptors recorded in 1 μM ACh and LS

receptors in 1 μM ACh + 1 μM dFBr (28.4$\pm$2.0 pS; n=12 cells; blue square).

Additional I-V data fitted with linear equations yielded slopes of ~30 pS and

extrapolated reversal potentials near -3 mV
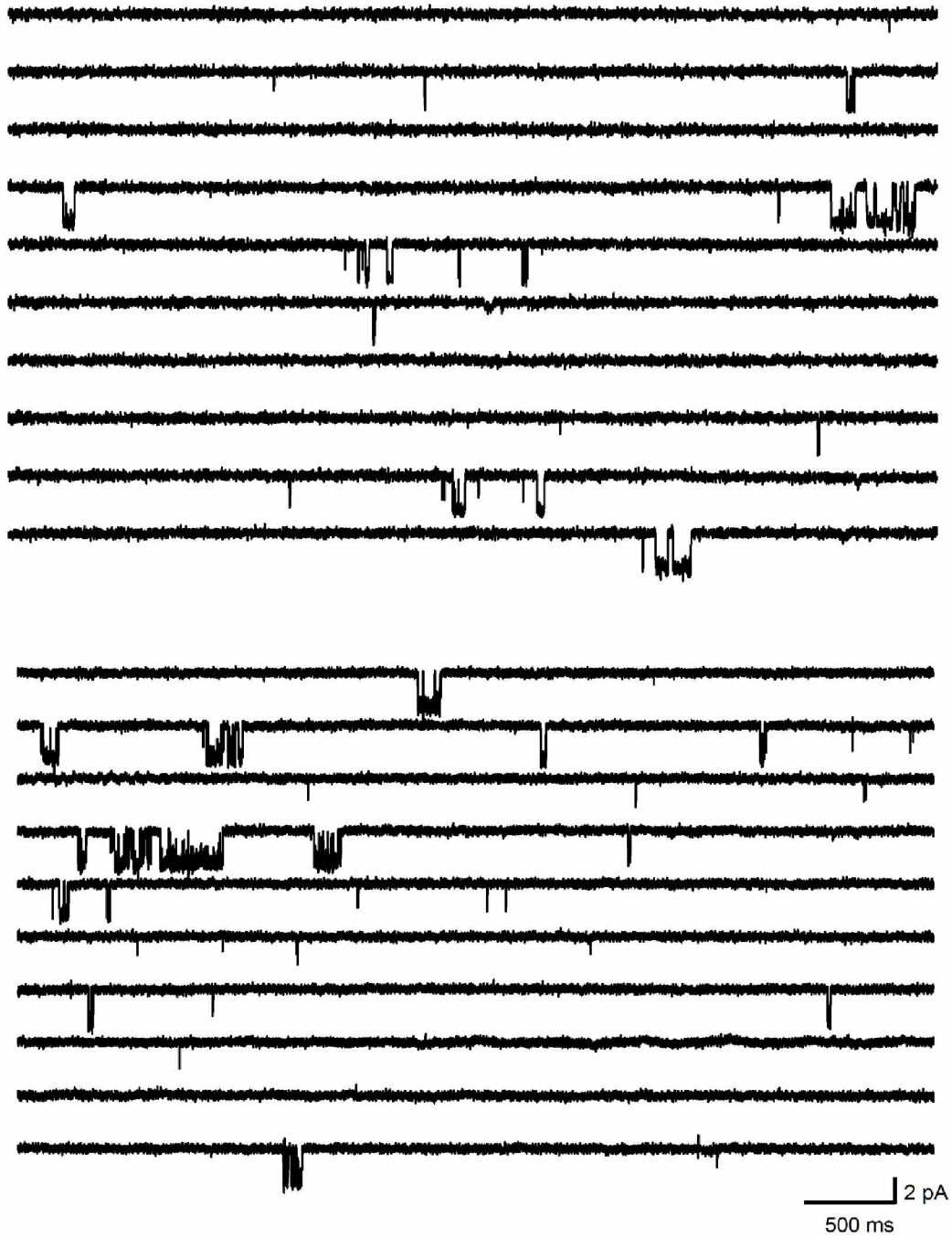
Figure 2.2: Steady-state recordings of $\alpha 4_3\beta 2_2$ receptors. Recordings shown are

for 1 μM ACh (top) or 1 μM ACh + 1 μM dFBr (bottom). Contiguous traces

represent 50 s of data filtered at 1 kHz (-3 dB, 4-pole Bessel).

68
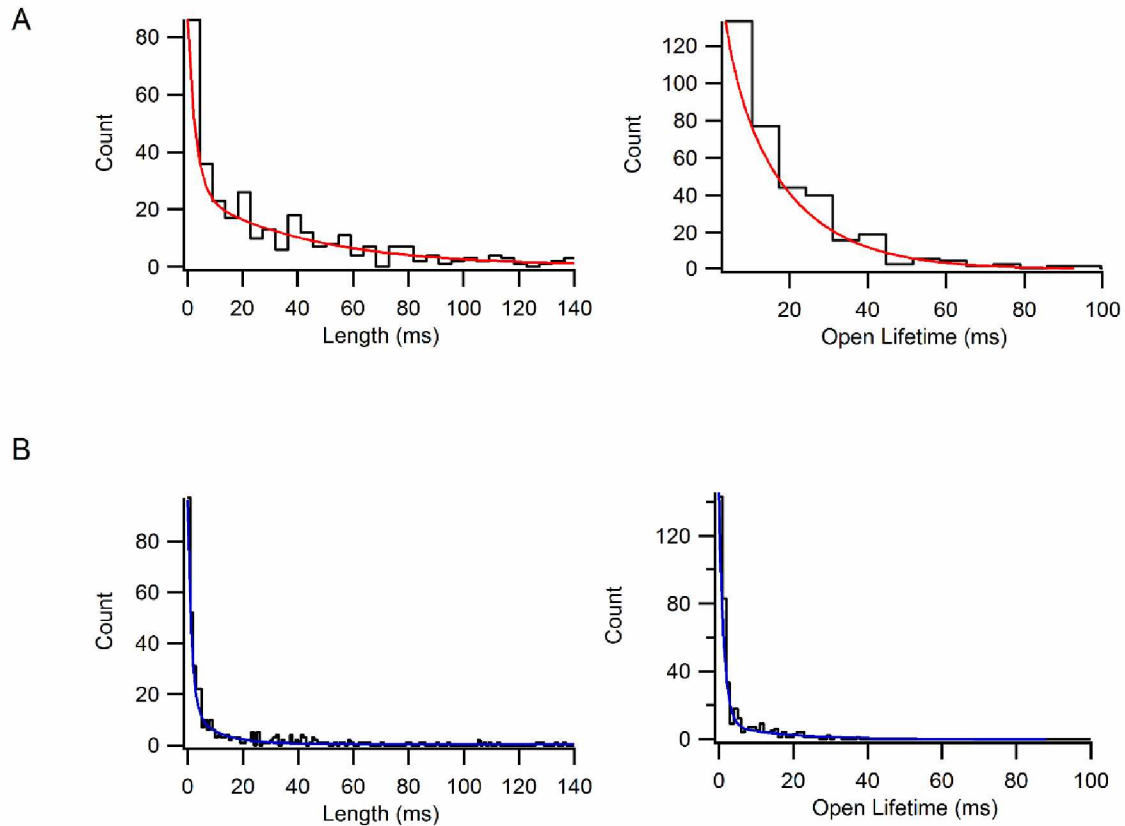
Figure 2.3: Burst characteristics for $\alpha 4_3 \beta 2_2$ receptors. Distributions are fitted

with two exponentials for 1 μM ACh (red; tcrit: 1.22 ms) and 1 μM ACh + 1 μM

dFBr (blue; tcrit: 1.99 ms). Determination of critical time is described in methods.

Distributions are plotted up to 140 ms for burst Length and 100 ms for burst open

lifetime for comparison between control and dFBr. (A) Distributions for 1 μM

ACh burst length (left; τ_1: 2.86ms, τ_2: 42.1 ms) and burst open lifetime (right; τ_1:

3.0 ms, τ_2: 15.9 ms). (B) Distribution for 1 μM ACh + 1 μM dFBr burst length

(left; τ_1: 1.6 ms, τ_2: 14.7 ms) and burst open lifetime (right; τ_1: 0.75 ms, τ_2: 10.9

ms). The presence of dFBr decreases burst length and open lifetime fast and

slow time components.
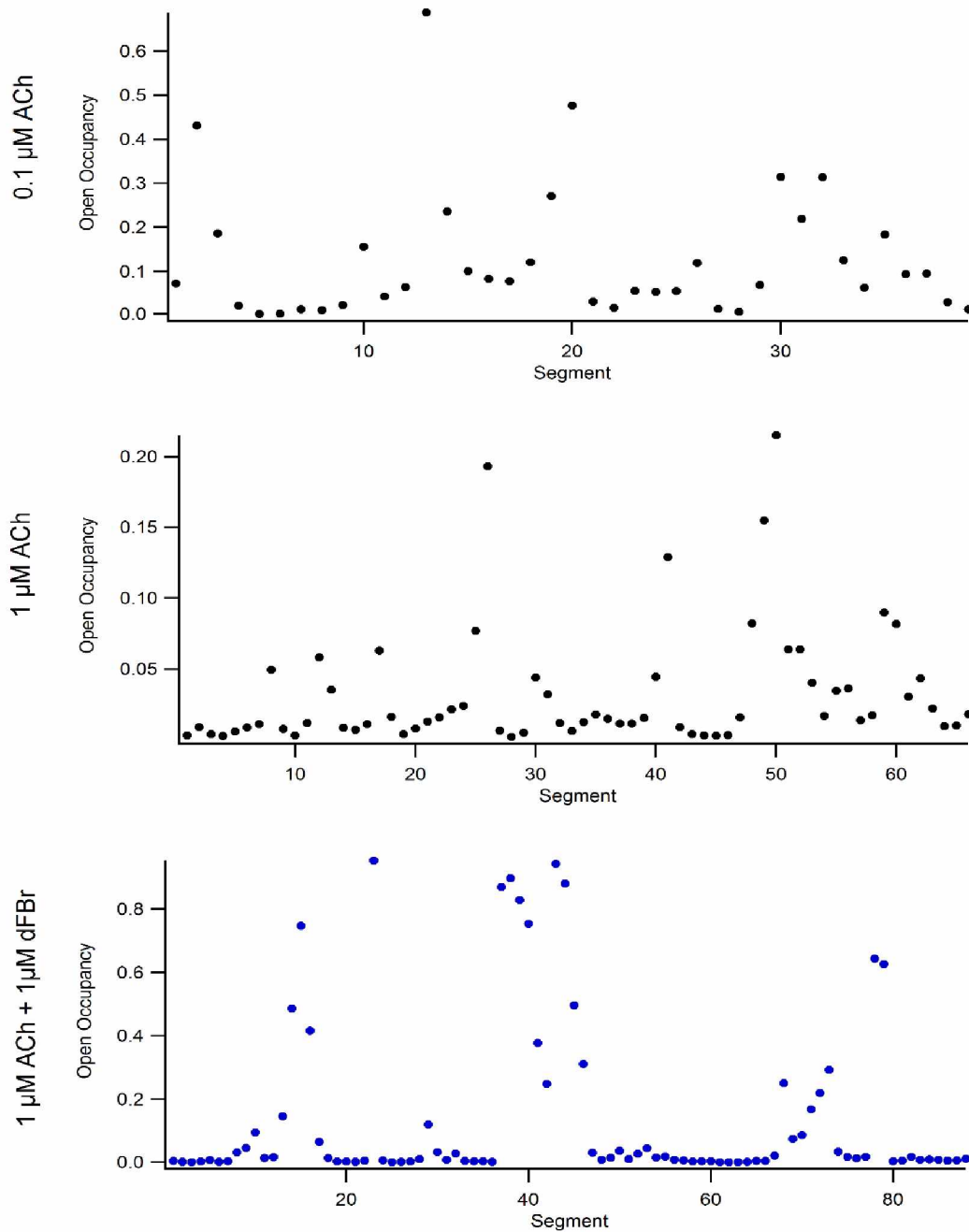
Figure 2.4: Stability plots for $\alpha 4_3 \beta 2_2$ receptors. Stability plots obtained from QuB

(50 events per segment, overlap of 25 events) for 0.1 (top) and 1 μM ACh

(middle) and 1 μM ACh 1 μM dFBr are displayed as segment vs occupancy of

opening. An event is composed of either an opening or a closing. All patches

are relatively stable with intermittent spikes in occupancy.
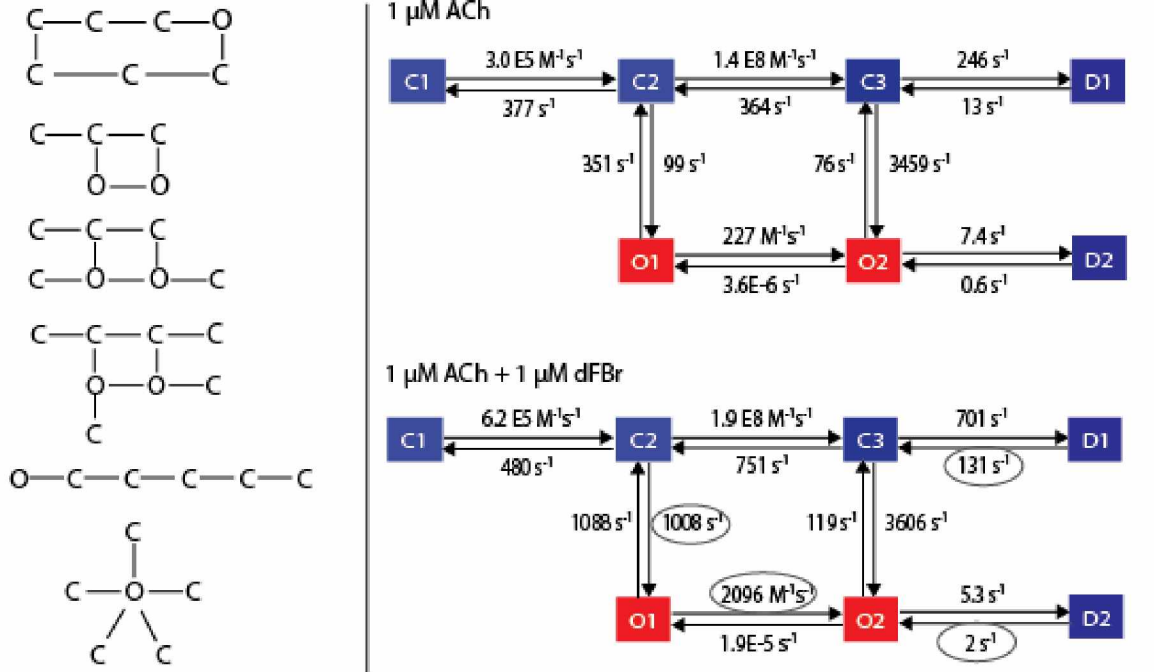
Figure 2.5: Models tested on $\alpha 4_3\beta 2_2$ receptors. Left: Examples of models tested, included are activation based mechanisms (from top) Katz and Thesleff, MWC, MWC with 2 desensitized, MWC with 3 desensitized and the desensitization models linear, and star. Right: Final model utilized with rate constants. Rate constants governing transitions C2→O1, O1→O2 and out of desensitized states D1 and D2 (circled) were significantly larger (P < 0.05) in dFBr.
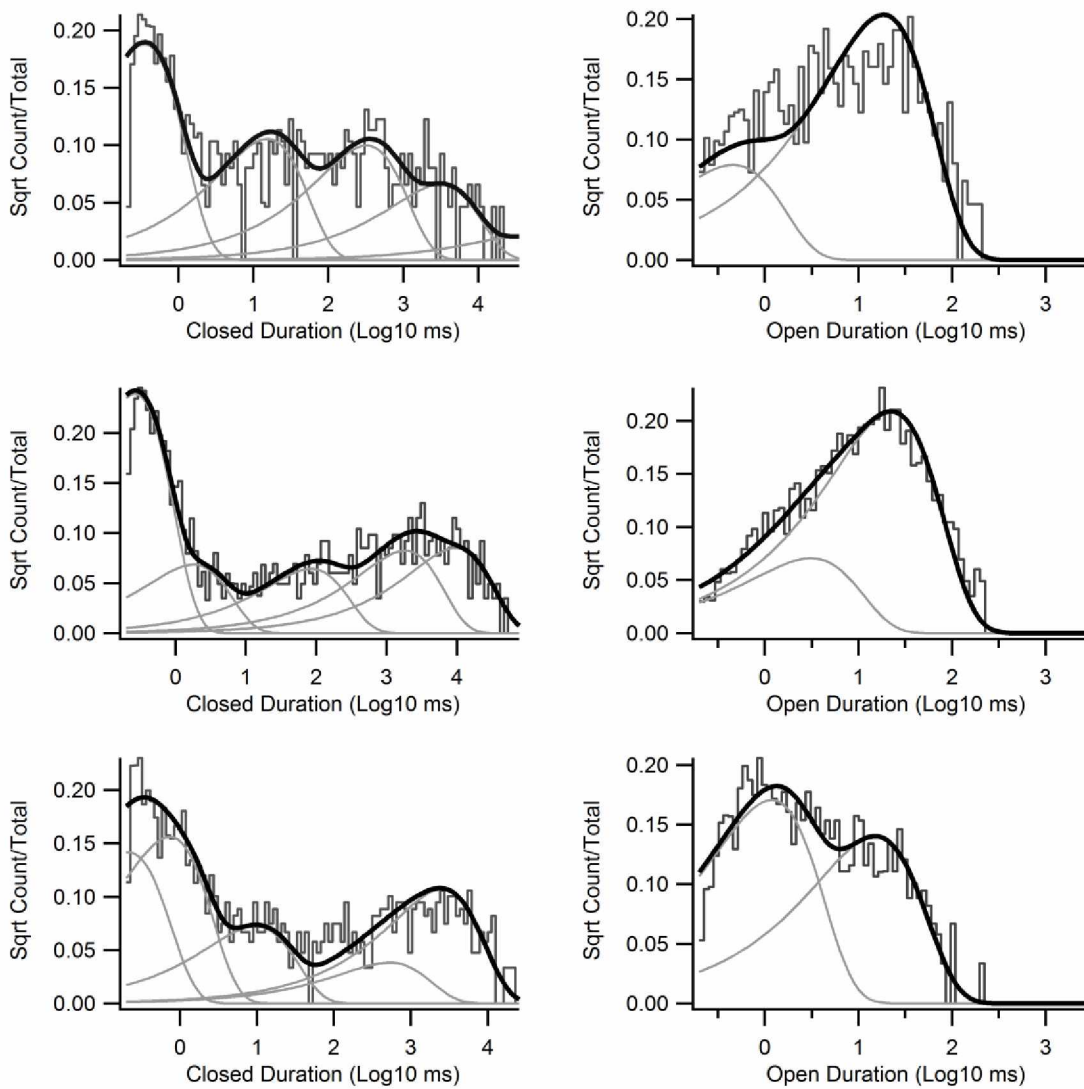
Figure 2.6: Gating models for naive and modulated LS $\alpha4\beta2$ receptors. Open and closed duration distributions from patches shown in Figure 2.2 for 0.1 μM ACh (top), 1 μM ACh (middle) and 1 μM ACh + 1 μM dFBr fitted with the gating model shown in Figure 2.5.

A
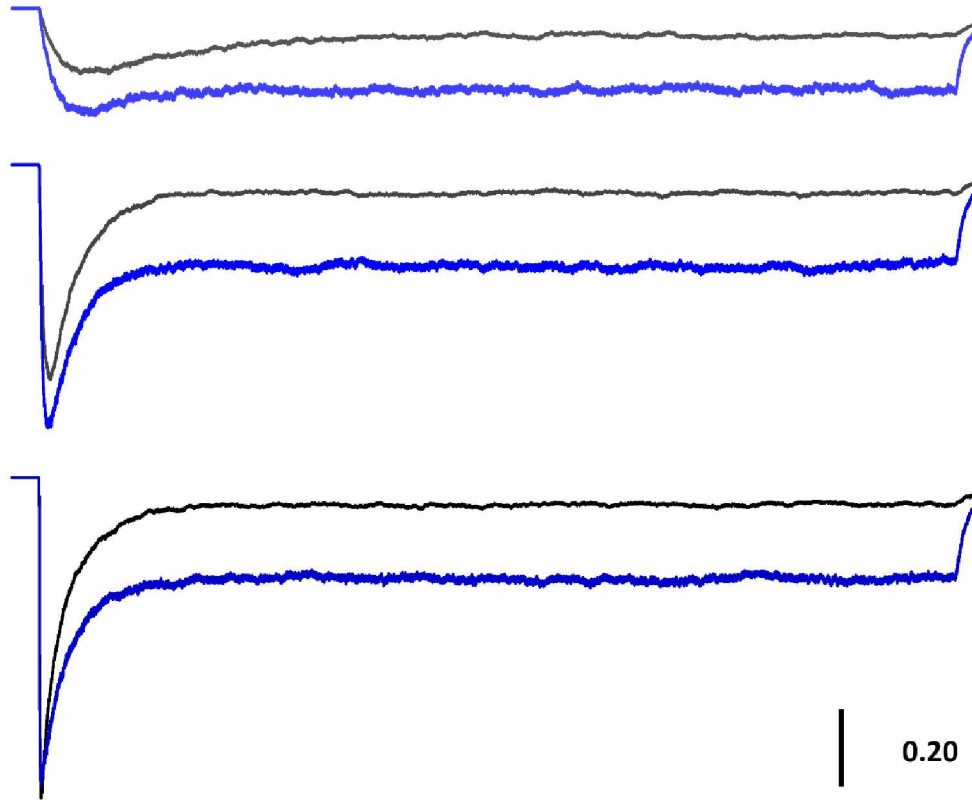
Figure 2.7A: Concentration dependence of potentiation of peak and steady-state currents. (A) Simulated currents are shown for the ACh (black traces) and dFBr (blue traces) models driven by 5 s jumps into 10 μM (top), 100 μM (middle), and 1 mM (bottom) ACh. Exponential functions fitted to the decay phase of currents for 1 mM ACh traces are superimposed (black traces). ACh model: A_1= 0.33, τ_1= 55 ms, A_2=0.45, τ_2=220 ms, y_0= 0.07. dFBr model: τ=157 ms, y_0=0.26. Rise times (10 – 90%) for ACh and dFBr models with 1 mM ACh were 9.2 ms and 7.5 ms, respectively. Calibration bar: units of open probability (P_{open}).

73

B
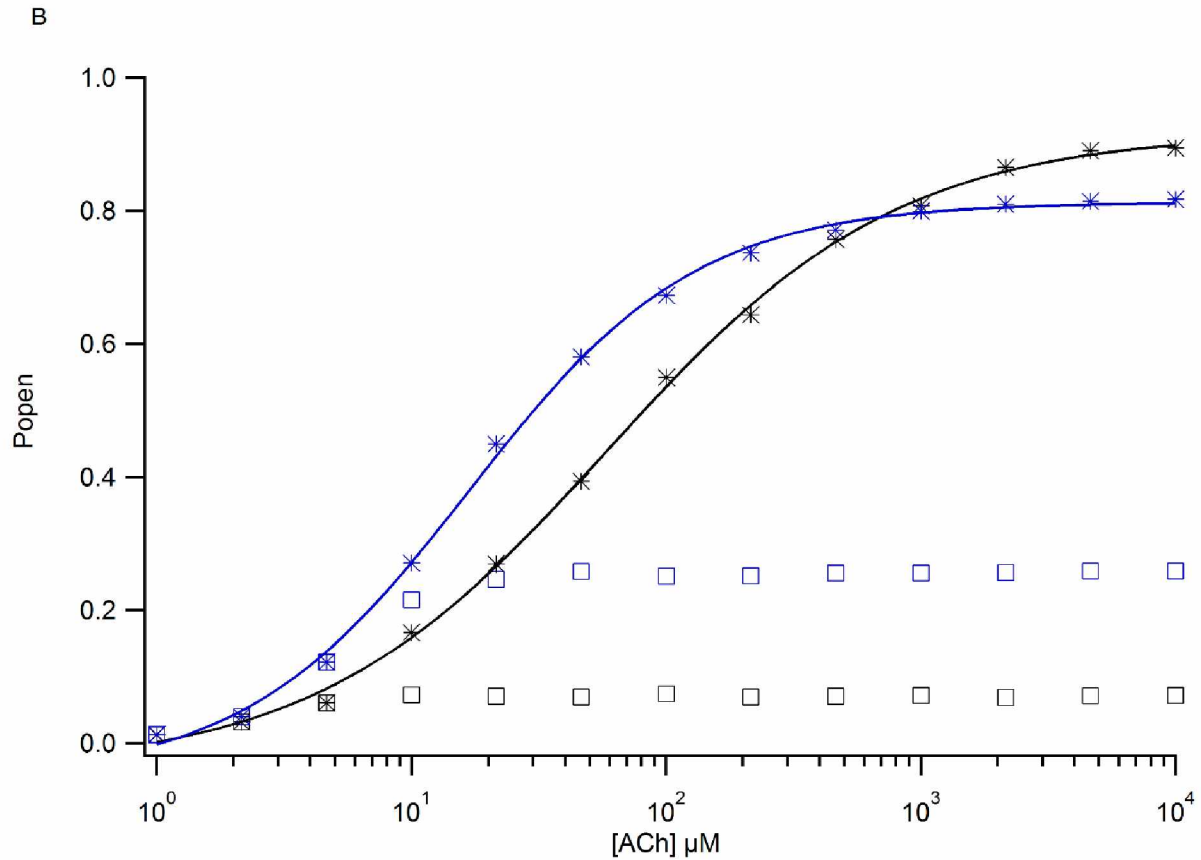
Figure 2.7B: Concentration dependence of potentiation of peak and steady-state currents. (B) The channel open probability (P_{open}) of peak (stars) and steady-state (squares) responses are plotted for ACh (black) and dFBr (blue) models as a function of ACh concentration (1, 2.15, 4.64, 10, 21.5, 46.4, 100, 215, 464, 1000, 2150, 4640, and 10000 μM). The maximal (peak) P_{open} for saturating ACh concentration was ~ 0.92 for ACh and 0.81 for dFBr. Slope and EC_{50} values from fitted Hill equations were 0.76$\pm$0.04 and 58$\pm$3.6 μM for ACh, and 0.98$\pm$0.05 and 17$\pm$1.1 μM for dFBr.

C
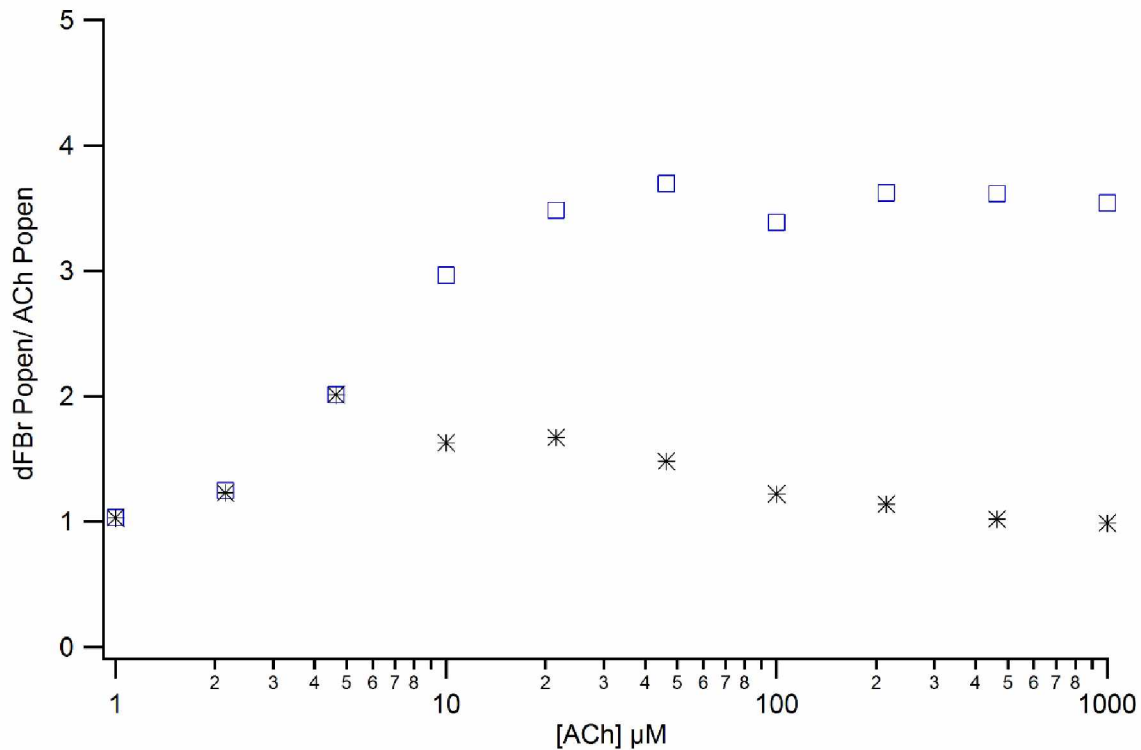
Figure 2.7C: Concentration dependence of potentiation of peak and steady-state currents. (C) The ratio of dFBr model to ACh model P_{open} is shown as a function of ACh concentration. Potentiation of peak response (stars) was largest at low ACh (101% increase for 4.64 μM ACh) and declined to zero at 1 mM ACh. At concentrations higher than 1mM, dFBr responses were smaller (shown in B). Steady-state, desensitized responses (blue squares) were potentiated 3-3.5-fold above 10 μM ACh.
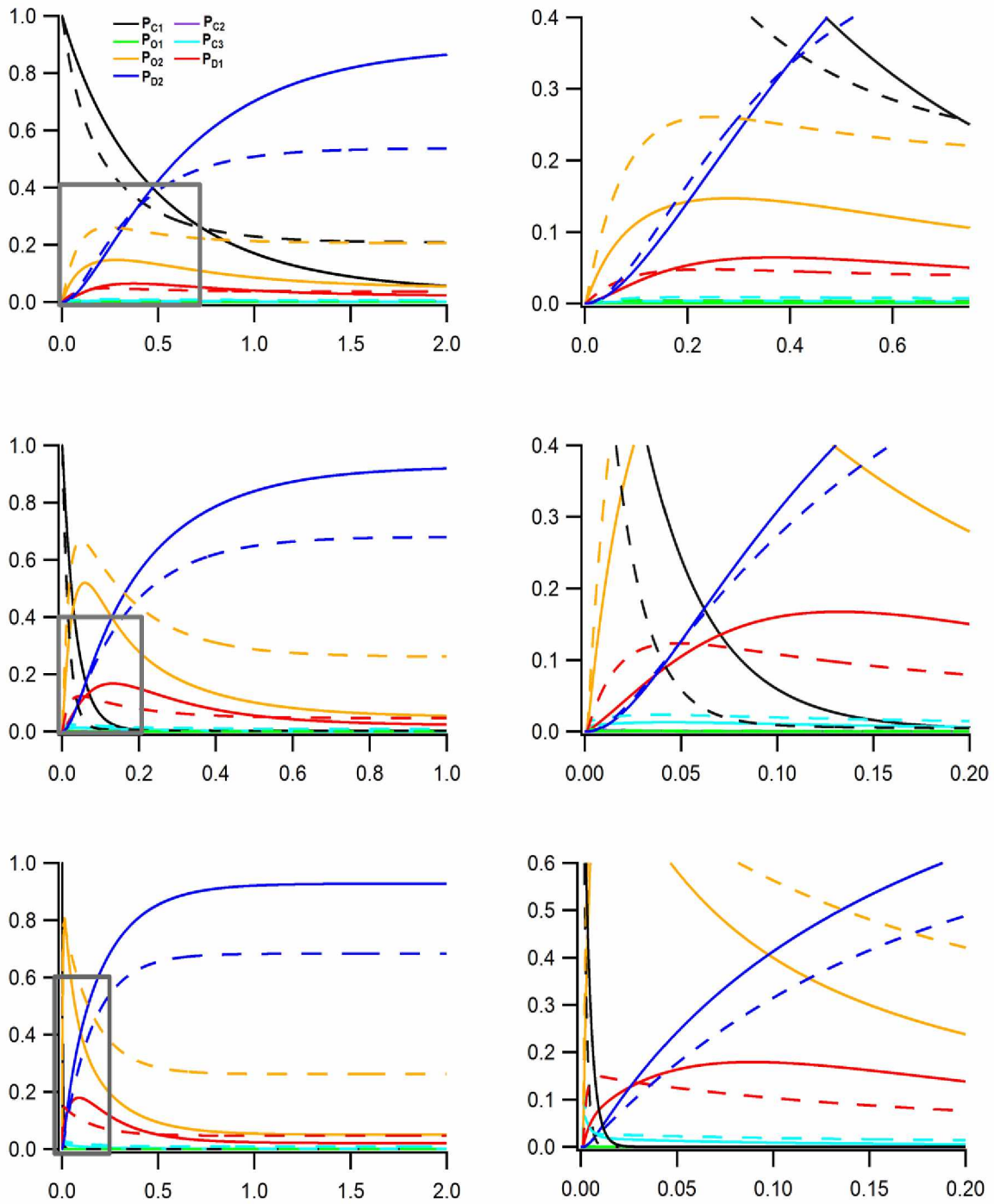
Figure 2.8: Occupancy probabilities using a concentration jump profile for $\alpha 4_3 \beta 2_2$

receptors. See caption on next page.

Figure 2.8: Occupancy probabilities using a concentration jump profile for $\alpha 4_3 \beta 2_2$ receptors. Occupancy probabilities (y-axis) of channel states following a concentration jump are shown for 10 (top), 100 (middle), and 1000 (bottom) μM ACh for ACh (solid lines) and dFBr models (dashed lines). The maximum probability of occupancy of O1 was low (< 0.005) and changes in P_{O1} with dFBr were negligible; therefore, P_{O2} was used as an estimate of open probability. Occupancy probabilities of states C2 and C3 were also low, except for the first few milliseconds of the high concentration simulation where P_{C3} reached ~ 0.1 in dFBr.
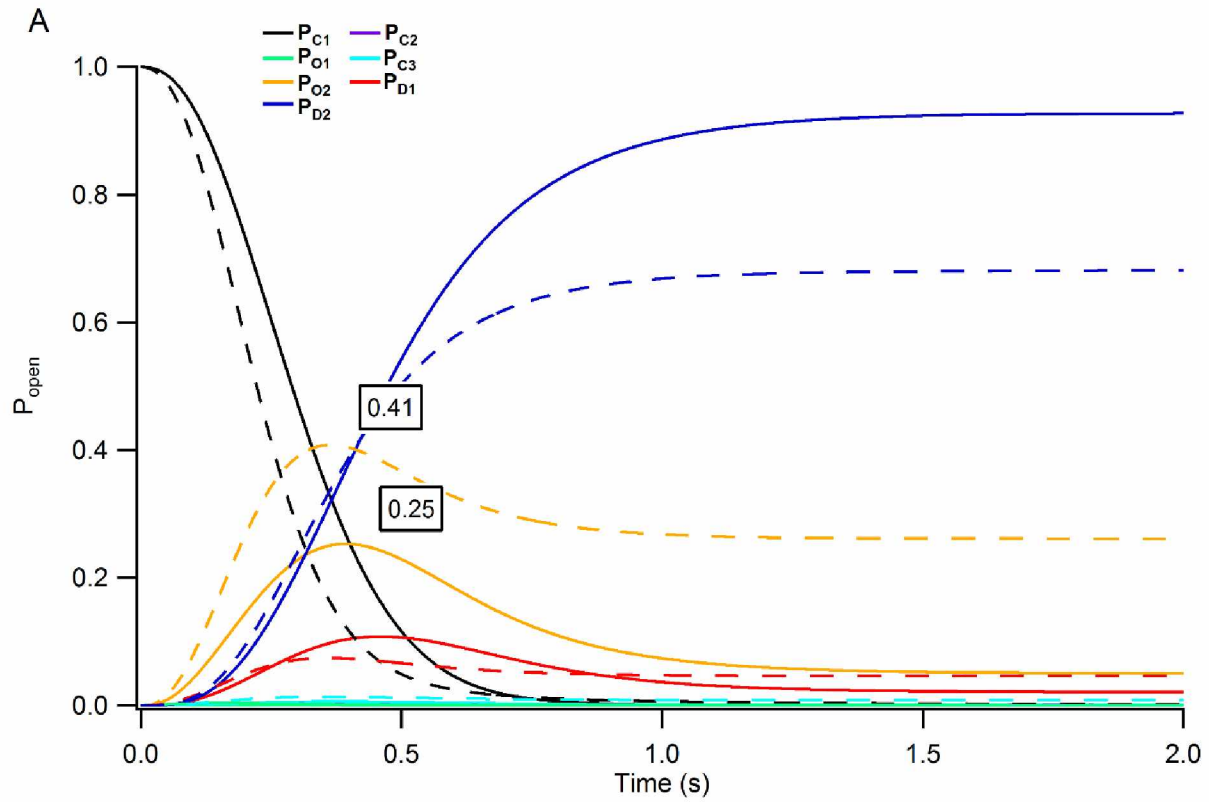
Figure 2.9A: Slowly rising concentration profile decreases peak P_{open} and increases potentiation with dFBr. (A) Occupancy probabilities are shown for a slow, exponential rise in ACh concentration according to: $c(t) = A * (1 - \exp(-t/\tau))$ where A = 300 μM (EC$_{75}$) and τ = 4 s.

B
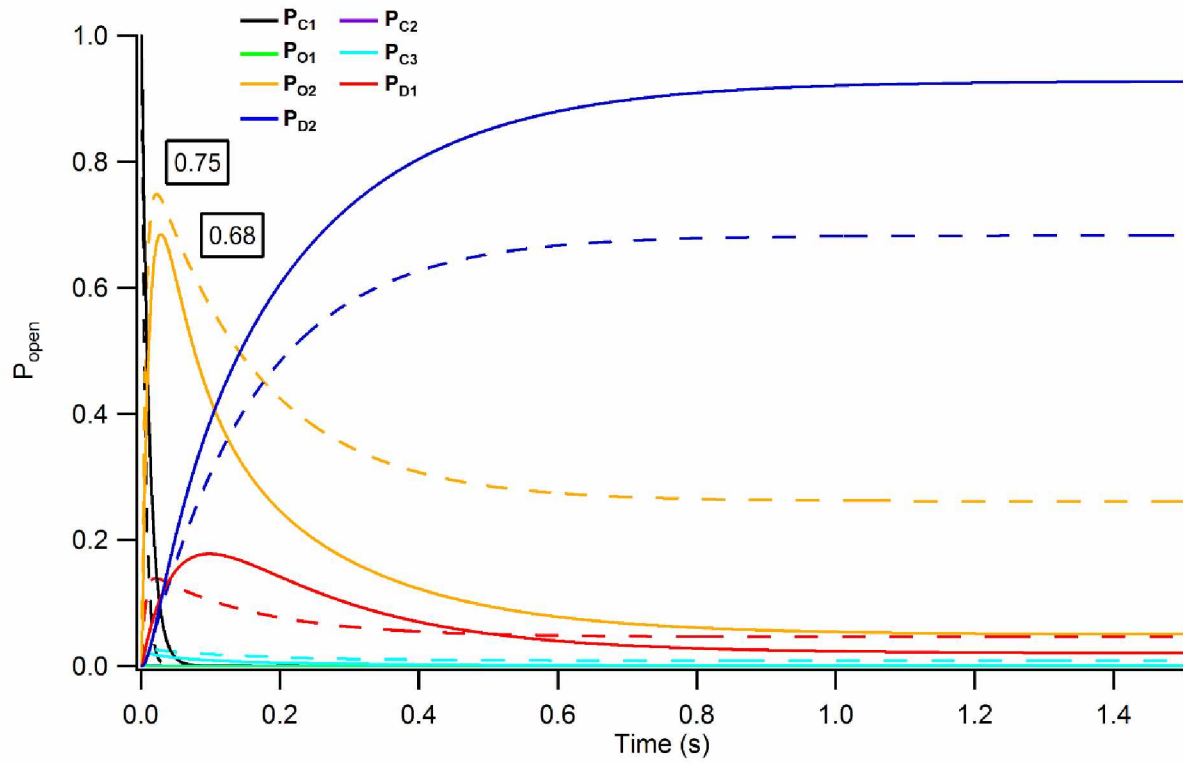
Figure 2.9B: Slowly rising concentration profile decreases peak P_{open} and increases

potentiation with dFBr. (B) Response to step increase in ACh concentration to 300 μM.

A
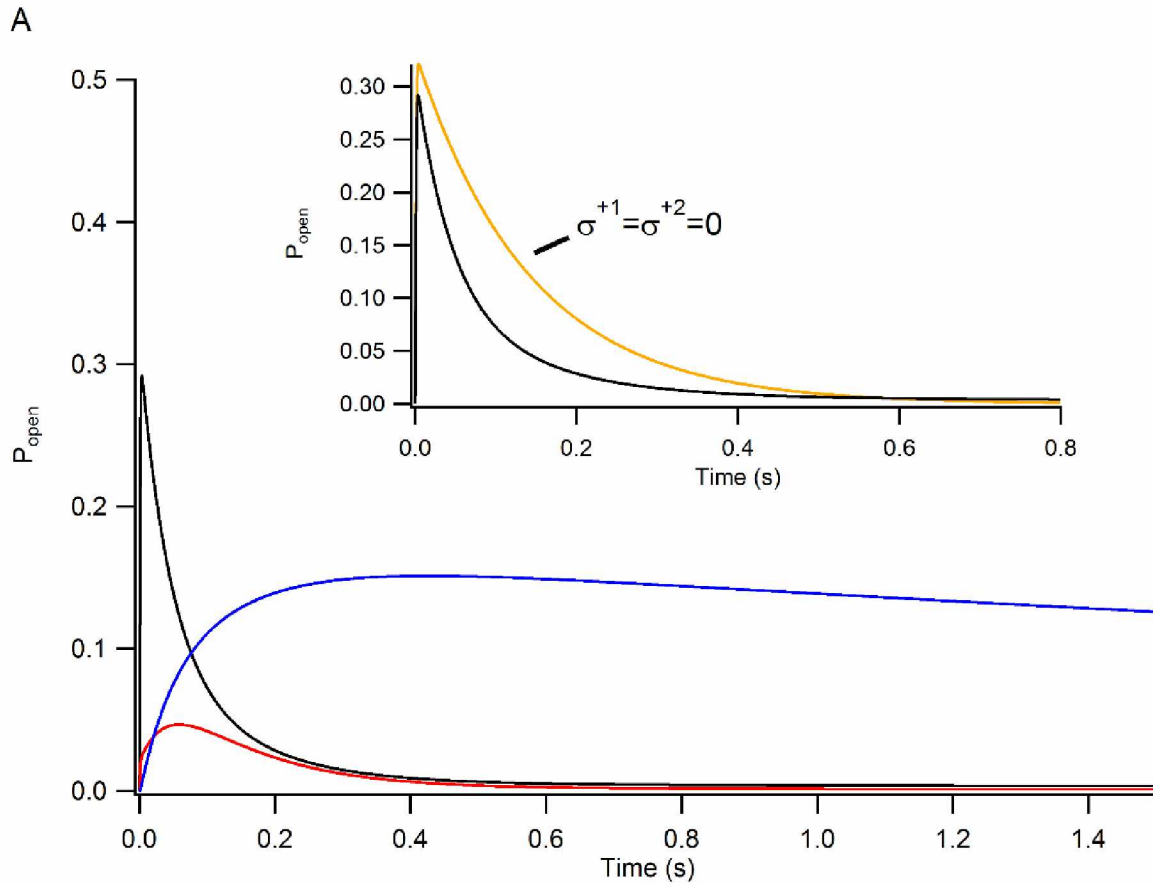
Figure 2.10A: Response to a pulse of a high concentration of agonist. Occupancy probabilities are shown for models driven by an alpha function to mimic a synaptic agonist concentration profile. (A) Responses are shown for the ACh model. Peak open probability (P_{O2}) was 0.28 at 3.7 ms compared with 0.45 at 3.6 ms for dFBr (shown in B; 1.61-fold potentiation). The decay of P_{O2} was fitted with the sum of 3 exponentials (A_1=0.72, τ_1=44 ms, A_2=0.27, τ_2=133 ms, A_3= 0.012, τ_3=5.4 s, y_0= 0). The decay of P_{D1} was fitted with two exponential components (A_1=0.98, τ_1=147 ms, A_2=0.02, τ_2=5.0 s, y_0=0), and P_{D2} was fitted with one component (τ=5.2 s, y_0=0). Main inset shows P_{O2} for the ACh model (black trace) with P_{O2} for a modified model (blue trace) in which rates into desensitized states D1 and D2 were set to zero (δ_{1+} = δ_{2+} = 0). The decay time constant for the fitted exponential was 157 ms (y_0=0).

80

B
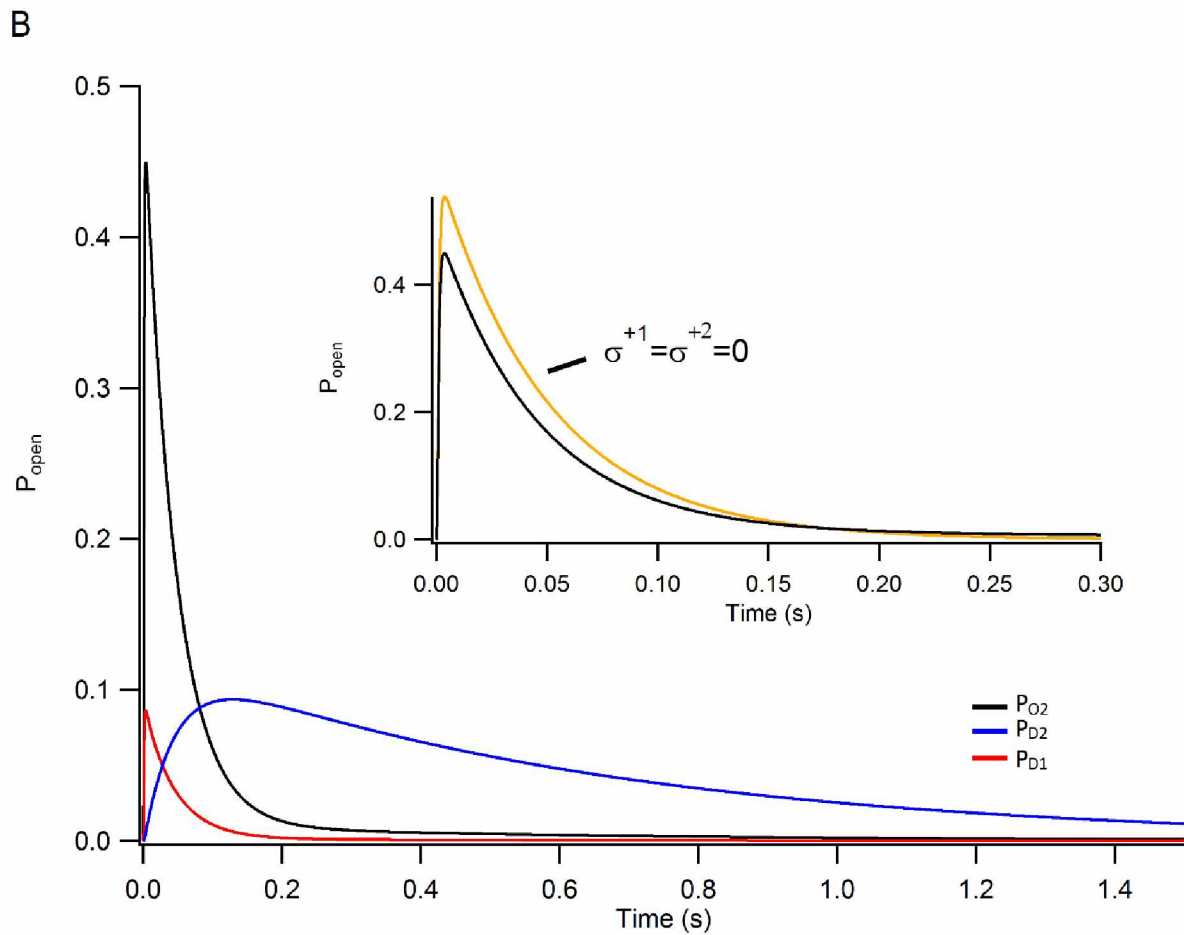
Figure 2.10B: Response to a pulse of a high concentration of agonist. (B) For the dFBr model the decay of P_{O2} was fitted with two exponential components (A_1=0.97 τ_1=45 ms, A_2=0.02, τ_2=649 ms, y_0=0). P_{D1} was fitted with two components (A_1=0.97, τ_1=76 ms, A_2=0.03, τ_2=556 ms, y_0=0), and P_{D2} was fitted with a single exponential (τ=653 ms, y_0=0). For dFBr, the inset shows that removal of desensitization had a negligible effect on the decay time course. The time constant (τ=50 ms; y_0=0) was similar to the time constant for the fast, major component of decay of P_{O2} with desensitization intact (τ=46 ms).

81

A
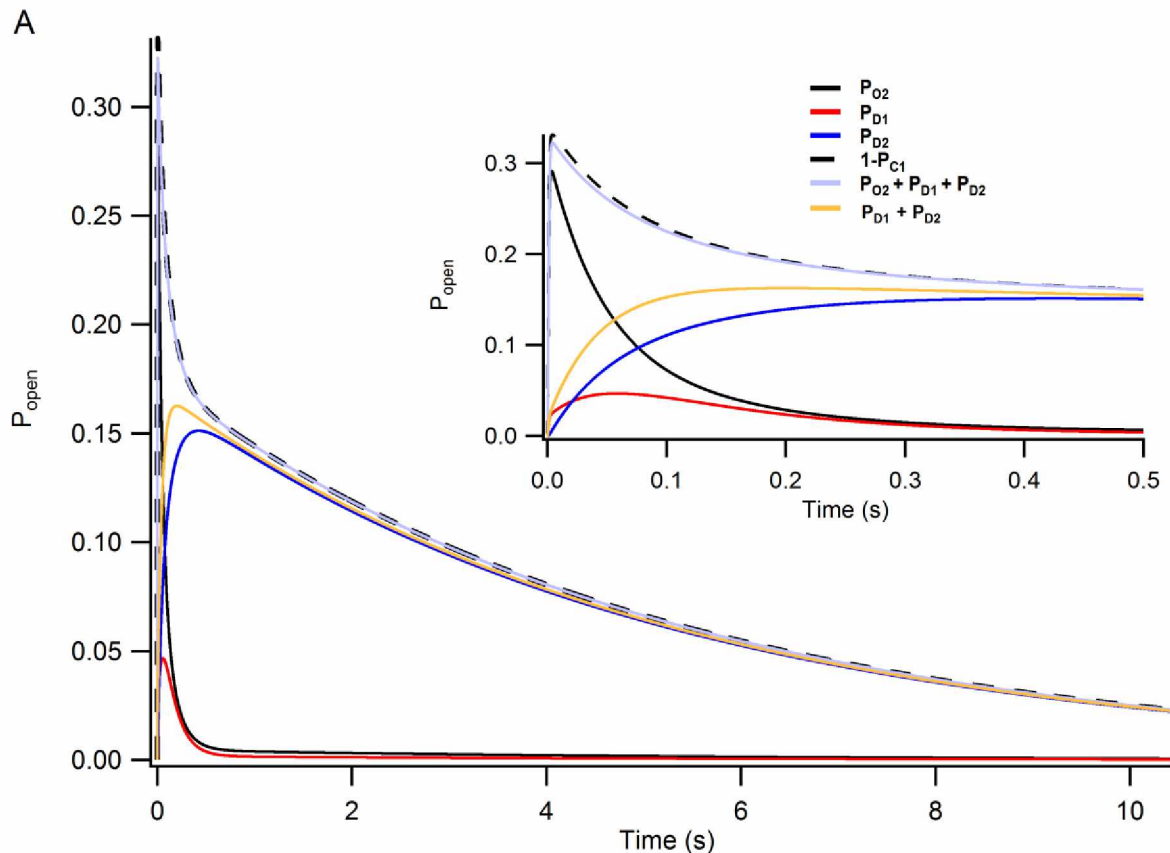
Figure 2.11A: Development and recovery from desensitized states following a brief pulse of agonist concentration. Responses are shown for the same alpha function pulse in Figure 2.10. The fraction of occupied receptors ($1-P_{C1}$) is nominally the same as the sum of receptors in O2, D1, and D2 ($P_{O2+D1+D2}$) for both models. Insets show responses on expanded time scales. (A) For the ACh model, desensitization ($P_{D1 + D2}$) peaked at 197 ms. Relaxation of $P_{D1 + D2}$ was fitted with the sum of two exponentials with time constants ($A_1=0.07$, $\tau_1=200$ ms, $A_2=0.93$, $\tau_2=5.2$ s, $y_0=0$) similar to relaxation time constants for the components P_{D1} and P_{D2} fitted individually.
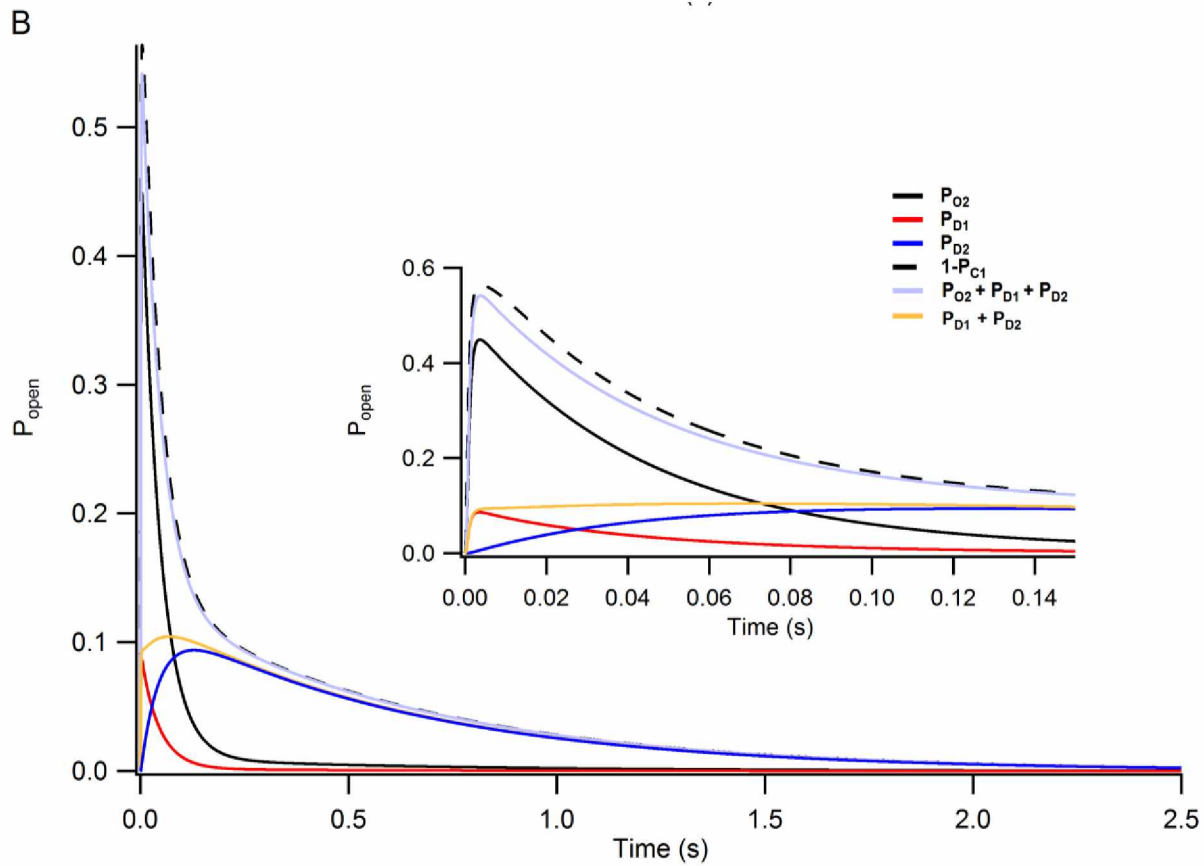
Figure 2.11B: Development and recovery from desensitized states following a brief pulse of agonist concentration. (B) For dFBr, $P_{D1 + D2}$ peaked at 69 ms, and relaxation of $P_{D1 + D2}$ was well fitted with a single exponential with a time constant (τ=654 ms) identical to that for that for P_{D1} alone (Figure 2.10).

Table 2.1. Rate constants used in simulations for $\alpha 4_3\beta 2_2$ receptors. Errors are the relative estimated error in the fits.

Rate Constant	Units	1 μM ACh	(+) dFBr
k_{+1}	$M^{-1}s^{-1}$	3E5 ±23%	6.2E5 ±7.8%
k_{-1}	s^{-1}	377 ±32%	480 ±8.9%
k_{+2}	$M^{-1}s^{-1}$	1.4E8 ±31%	1.9E8 ±18%
k_{-2}	s^{-1}	464 ±19%	751 ±1.7%
β_1	s^{-1}	99 ±38%	1009 ±9.5%
α_1	s^{-1}	351 ±22%	1088 ±6.6%
δ_{1+}	s^{-1}	246 ±18%	703 ±15%
δ_{1-}	s^{-1}	13 ±30%	131 ±15%
β_2	s^{-1}	3456 ±6%	3606 ±15%
α_2	s^{-1}	76 ±5%	119 ±10%
δ_{2+}	s^{-1}	7.4 ±21%	5.3 ±27%
δ_{2-}	s^{-1}	0.6 ±24%	2.0 ±31%
k_{O+2}	$M^{-1}s^{-1}$	227	2096
k_{O-2}	s^{-1}	3.6E-6	1.9E5

Table 2.2. Mean values for $\alpha 4_3\beta 2_2$ receptor rate constants. Errors are the standard deviations between the three patches.

Rate Constant	Rate	0.1 μM ACh		1 μM ACh		1 μM ACh + 1 μM dFBr		
		mean (n=2)	SD	mean (n=3)	SD	mean (n=3)	SD	P
k_{+1}	$M^{-1}s^{-1}$	3.1E5	3.1E3	3E5	5.8E3	3.3E5	2.5E5	0.85
k_{-1}	s^{-1}	20	16	206	176	378	193	0.32
k_{+2}	$M^{-1}s^{-1}$	6E8	3E8	1E8	4.5E7	2.8E8	2.4E8	0.28
k_{-2}	s^{-1}	521	256	557	323	794	287	0.39
β_1	s^{-1}	28	5.3	46	48	679	421	0.06
α_1	s^{-1}	2316	49	536	293	884	333	0.25
δ_{1+}	s^{-1}	464	71	171	68	967	642	0.10
δ_{1-}	s^{-1}	3.9	1.1	9.5	5.3	149	29	0.001
β_2	s^{-1}	2081	1028	3872	984	2867	640	0.21
α_2	s^{-1}	75	7	110	82	131	43	0.72
δ_{2+}	s^{-1}	6	1.4	7	0.3	8.7	4.4	0.36
δ_{2-}	s^{-1}	0.34	0.07	0.31	0.26	1.4	0.6	0.046
k_{O+2}	$M^{-1}s^{-1}$	593	521	579	350	2075	385	0.01
k_{O-2}	s^{-1}	2.2E-6	7E-7	9.5E-5	1.5E-4	1E-4	0.9E-4	0.93

2.6 References

Beato, M. 2008. The time course of transmitter at glycinergic synapses onto

motoneurons. *J Neurosci.* 28:7412-7425.

Buisson, B., and D. Bertrand. 2001. Chronic exposure to nicotine upregulates the

human (alpha)4(beta)2 nicotinic acetylcholine receptor function. *J Neurosci.*

21:1819-1829.

Buisson, B., M. Gopalakrishnan, S.P. Arneric, J.P. Sullivan, and D. Bertrand. 1996.

Human alpha4beta2 neuronal nicotinic acetylcholine receptor in HEK 293 cells: A

patch-clamp study. *J Neurosci.* 16: 7880-7891

Clements, J.D., R.A. Lester, G. Tong, C.E. Jahr, and G.L. Westbrook. 1992. The time

course of glutamate in the synaptic cleft. *Science.* 258:1498-1501.

Coe, J.W., Brooks, P.R., Vetelino, M.G., Wirtz, M.C., Arnold, E.P., Huang, J.,, S.B.

Sands, Davis, T.I., Lebel, L.A., Fox, C.B., Shrikhande, A., Heym, J.H.,, E.

Schaeffer, Rollema, H., Lu, Y., Mansbach, R.S., Chambers, L.K.,, and C.C.

Rovetti, Schulz, D.W., Tingley 3rd, F.D., O'Neill, B.T. 2005. Varenicline: an

alpha4beta2 nicotinic receptor partial agonist for smoking cessation. *J. Med.*

Chem. 48:3474-3477.

Colquhoun, D., and A.G. Hawkes. 1981. On the stochastic properties of single ion

channels. *Proc R Soc Lond B Biol Sci.* 211:205-235.

Colquhoun, D., and A.G. Hawkes. 1982. On the stochastic properties of bursts of single

ion channel openings and of clusters of bursts. *Philos Trans R Soc Lond B Biol*

Sci. 300:1-59.

Colquhoun, D., and A.G. Hawkes. 1990. Stochastic properties of ion channel openings

and bursts in a membrane patch that contains two channels: evidence

concerning the number of channels present when a record containing only single

openings is observed. *Proc R Soc Lond B Biol Sci*. 240:453-477.

daCosta, C.J.B., C.R. Free, J. Corradi, C. Bouzat, and S.M. Sine. 2011. Single-channel

and structural foundations of neuronal alpha7 acetylcholine receptor potentiation.

J Neurosci. 31:13870 - 13879.

Descarries, L., V. Gisiger, and M. Steriade. 1997. Diffuse transmission by acetylcholine

in the CNS. *Prog Neurobiol*. 53:603-625.

Diamond, J.S., and C.E. Jahr. 1995. Asynchronous release of synaptic vesicles

determines the time course of the AMPA receptor-mediated EPSC. *Neuron*.

15:1097-1107.

Elenes, S., and A. Auerbach. 2002. Desensitization of diliganded mouse muscle

nicotinic acetylcholine receptor channels. *J. Physiol.* 541:367–383.

doi:10.1113/jphysiol.2001.016022.

Fenster, C.P., T.L. Whitworth, E.B. Sheffield, M.W. Quick, and R.A. Lester. 1999.

Upregulation of surface alpha4beta2 nicotinic receptors is initiated by receptor

desensitization after chronic exposure to nicotine. *J Neurosci*. 19:4804-4814.

Friedman, J.I. 2004. Cholinergic targets for cognitive enhancement in schizophrenia:

focus on cholinesterase inhibitors and muscarinic agonists. *Psychopharmacology*

(Berl). 174:45-53.

Grupe, M., A.A. Jensen, P.K. Ahring, J.K. Christensen, and M. Grunnet. 2013.
Unravelling the mechanism of action of NS9283, a positive allosteric modulator of
(alpha4)3(beta2)2 nicotinic ACh receptors. *Br J Pharmacol*. 168:2000-2010.

Hamill, O.P., A. Marty, E. Neher, B. Sakmann, and F.J. Sigworth. 1981. Improved
patch-clamp techniques for high-resolution current recording from cells and cell-
free membrane patches. *Pflugers Arch*. 391:85-100.

Harpsoe, K., P.K. Ahring, J.K. Christensen, M.L. Jensen, D. Peters, and T. Balle. 2011.
Unraveling the high- and low-sensitivity agonist responses of nicotinic
acetylcholine receptors. *J. Neurosci*. 31:10759 - 10766.

Joshi, P.R., A. Suryanarayanan, and M.K. Schulte. 2004. A vertical flow chamber for
Xenopus oocyte electrophysiology and automated drug screening. *J Neurosci
Methods*. 132:69-79.

Kim, J.S., A. Padnya, M. Weltzin, B.W. Edmonds, M.K. Schulte, and R.A. Glennon.
2007. Synthesis of desformylflustrabromine and its evaluation as an alpha4beta2
and alpha7 nACh receptor modulator. *Bioorg Med Chem Lett*. 17:4855-4860.

Li, P., and J.H. Steinbach. 2010. The neuronal nicotinic alpha4beta2 receptor has a
high maximal probability of being open. *Br J Pharmacol*. 160:1906-1915.

Maconochie, D.J., and J.H. Steinbach. 1998. The channel opening rate of adult- and
fetal-type mouse muscle nicotinic receptors activated by acetylcholine. *J.
Physiol*. 506:53–72. doi:10.1111/j.1469-7793.1998.053bx.x.

Marabelli, A., R. Lape, and L. Sivilotti. 2015. Mechanism of activation of the prokaryotic
channel ELIC by propylamine: a single-channel study. *J Gen Physiol*. 145:23-45.

Martin-Ruiz, C.M., J.A. Court, E. Molnar, M. Lee, C. Gotti, A. Mamalaki, T. Tsouloufis, S. Tzartos, C. Ballard, R.H. Perry, and E.K. Perry. 1999. Alpha4 but not alpha3 and alpha7 nicotinic acetylcholine receptor subunits are lost from the temporal cortex in Alzheimer's disease. *J Neurochem.* 73:1635-1640.

Moroni, M., R. Zwart, E. Sher, B.K. Cassels, and I. Bermudez. 2006. alpha4beta2 nicotinic receptors with high and low acetylcholine sensitivity: pharmacology, stoichiometry, and sensitivity to long-term exposure to nicotine. *Mol Pharmacol.* 70:755-768.

Nelson, M.E., A. Kuryatov, C.H. Choi, Y. Zhou, and J. Lindstrom. 2003. Alternate stoichiometries of alpha4beta2 nicotinic acetylcholine receptors. *Mol Pharmacol.* 63:332-341.

Nicolai, C., and F. Sachs. 2013. Solving ion channel kinetics with the QuB software. *Biophysical Reviews and Letters.* 08:191-211.

Pandya, A., and J.L. Yakel. 2011. Allosteric modulators of the alpha4beta2 subtype of neuronal nicotinic acetylcholine receptors. *Biochem Pharmacol.* 82:952-958.

Paradiso, K.G., and J.H. Steinbach. 2003. Nicotine is highly effective at producing desensitization of rat alpha4beta2 neuronal nicotinic receptors. *J Physiol.* 553:857-871.

Qin, F. 2004. Restoration of single-channel currents using the segmental k-means method based on hidden Markov modeling. *Biophys J.* 86:1488-1501.

Qin, F., A. Auerbach, and F. Sachs. 1996. Estimating single-channel kinetic parameters from idealized patch-clamp data containing missed events. *Biophys J.* 70:264-280.

Qin, F., A. Auerbach, and F. Sachs. 1997. Maximum likelihood estimation of aggregated Markov processes. *Proc Biol Sci*. 264:375-383.

Ren, J., C. Qin, F. Hu, J. Tan, L. Qiu, S. Zhao, G. Feng, and M. Luo. 2011. Habenula "cholinergic" neurons co-release glutamate and acetylcholine and activate postsynaptic neurons via distinct transmission modes. *Neuron*. 69:445-452.

Sabey, K., K. Paradiso, J. Zhang, and J.H. Steinbach. 1999. Ligand binding and activation of rat nicotinic alpha4beta2 receptors stably expressed in HEK293 cells. *Mol Pharmacol*. 55:58-66.

Sala, F., J. Mulet, K.P. Reddy, J.A. Bernal, P. Wikman, L.M. Valor, L. Peters, G.M. Konig, M. Criado, and S. Sala. 2005. Potentiation of human alpha4beta2 neuronal nicotinic receptors by a Flustra foliacea metabolite. *Neurosci Lett*. 373:144-149.

Silver, R.A., D. Colquhoun, S.G. Cull-Candy, and B. Edmonds. 1996. Deactivation and desensitization of non-NMDA receptors in patches and the time course of EPSCs in rat cerebellar granule cells. *J Physiol*. 493 (Pt 1):167-173.

Sullivan, J.P., D. Donnelly-Roberts, C.A. Briggs, D.J. Anderson, M. Gopalakrishnan, I.C. Xue, M. Piattoni-Kaplan, E. Molinari, J.E. Campbell, D.G. McKenna, D.E. Gunn, N.H. Lin, K.B. Ryther, Y. He, M.W. Holladay, S. Wonnacott, M. Williams, and S.P. Arneric. 1997. ABT-089 [2-methyl-3-(2-(S)-pyrrolidinylmethoxy)pyridine]: I. A potent and selective cholinergic channel modulator with neuroprotective properties. *J Pharmacol Exp Ther*. 283:235-246.

Timmermann, D.B., K. Sandager-Nielsen, T. Dyhring, M. Smith, A.M. Jacobsen, E.O.

Nielsen, M. Grunnet, J.K. Christensen, D. Peters, K. Kohlhaas, G.M. Olsen, and

P.K. Ahring. 2012. Augmentation of cognitive function by NS9283, a

stoichiometry-dependent positive allosteric modulator of alpha2- and alpha4-

containing nicotinic acetylcholine receptors. *Br J Pharmacol*. 167:164-182.

Warpman, U., and A. Nordberg. 1995. Epibatidine and ABT 418 reveal selective losses

of alpha 4 beta 2 nicotinic receptors in Alzheimer brains. *Neuroreport*. 6:2419-

2423.

Weltzin, M.M., and M.K. Schulte. 2010. Pharmacological characterization of the

allosteric modulator desformylflustrabromine and its interaction with alpha4beta2

neuronal nicotinic acetylcholine receptor orthosteric ligands. *J Pharmacol Exp

Ther*. 334:917-926.

Weltzin, M.M., and M.K. Schulte. 2015. Desformylflustrabromine Modulates

alpha4beta2 Neuronal Nicotinic Acetylcholine Receptor High- and Low-Sensitivity

Isoforms at Allosteric Clefts Containing the beta2 Subunit. *J Pharmacol Exp

Ther*. 354:184-194.

Zhang, J., and J.H. Steinbach. 2003. Cytisine binds with similar affinity to nicotinic

alpha4beta2 receptors on the cell surface and in homogenates. *Brain Res*.

959:98-102.

Zoli, M., Picciotto, MR, Ferrari, R, Cocchi, D, Changeux JP. 1999. Increased

neurodegeneration during ageing in mice lacking high-affinity nicotine receptors.

EMBO Journal. 18:1235-1244.
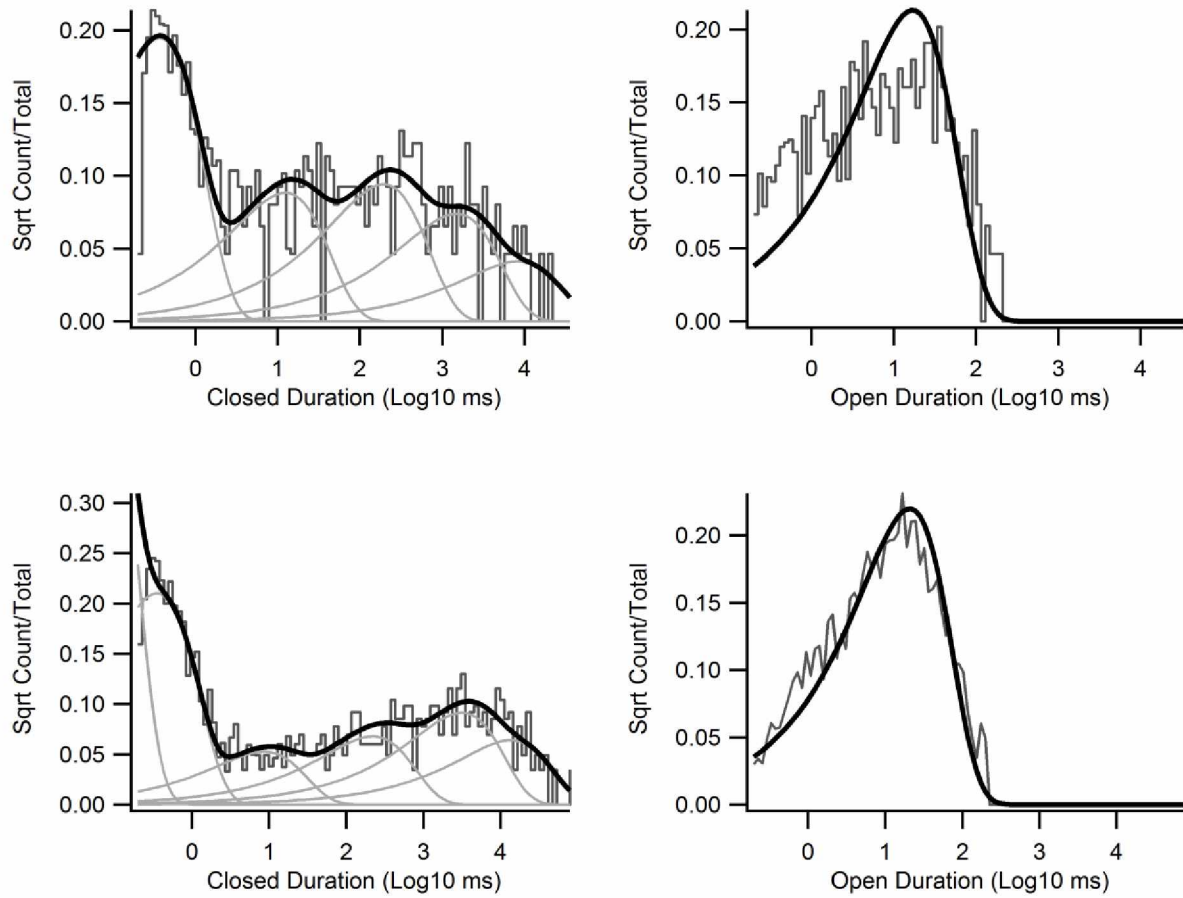
Figure A.2.1: LS Katz and Thesleff model fits. Open and closed duration distributions from patches for 0.1 μM (top) and 1 μM ACh (bottom) group fitted with gating model Katz and Thesleff shown in Figure 2.5.
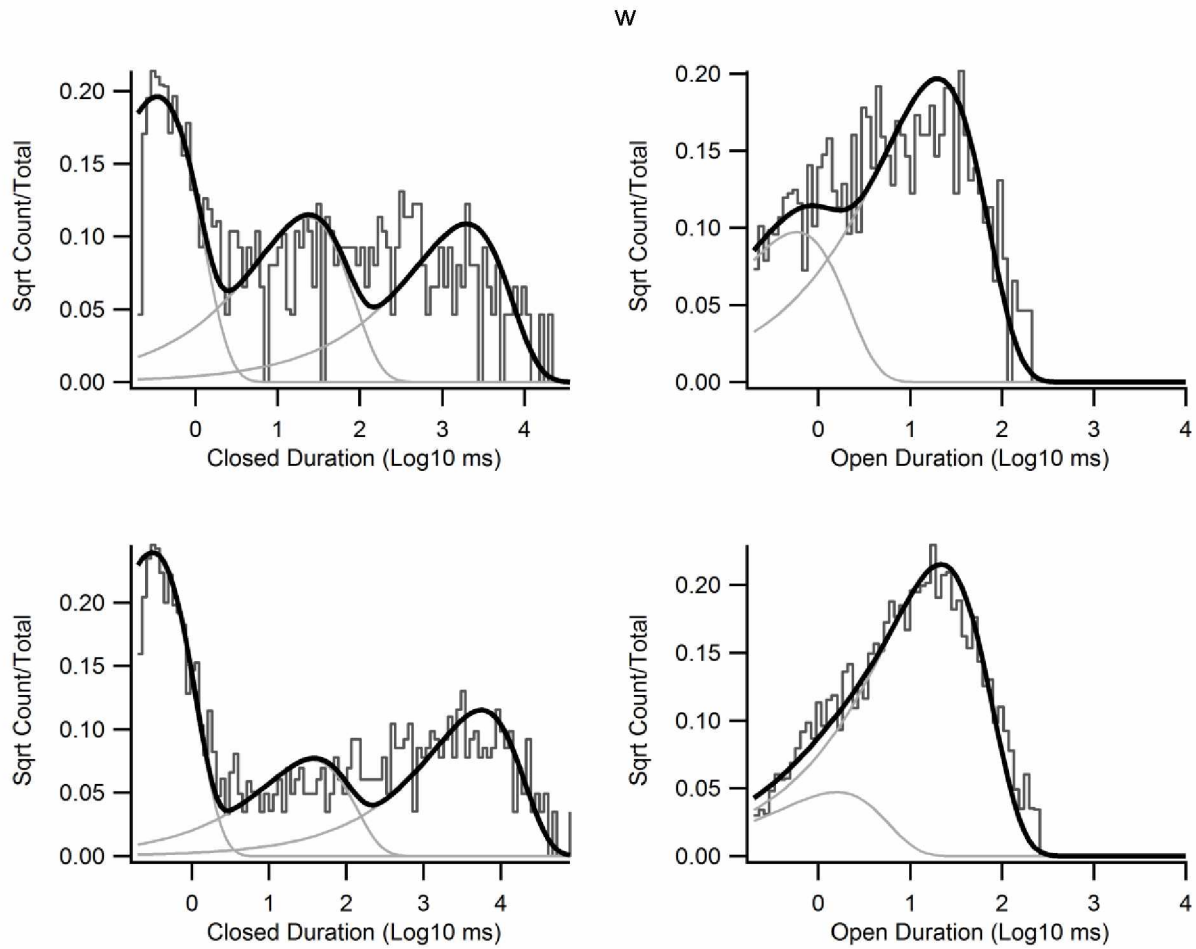
Figure A.2.2: LS MWC model fits. Open and closed duration distributions from patches for 0.1 μM (top) and 1 μM ACh (bottom) group fitted with gating model MWC shown in Figure 2.5.
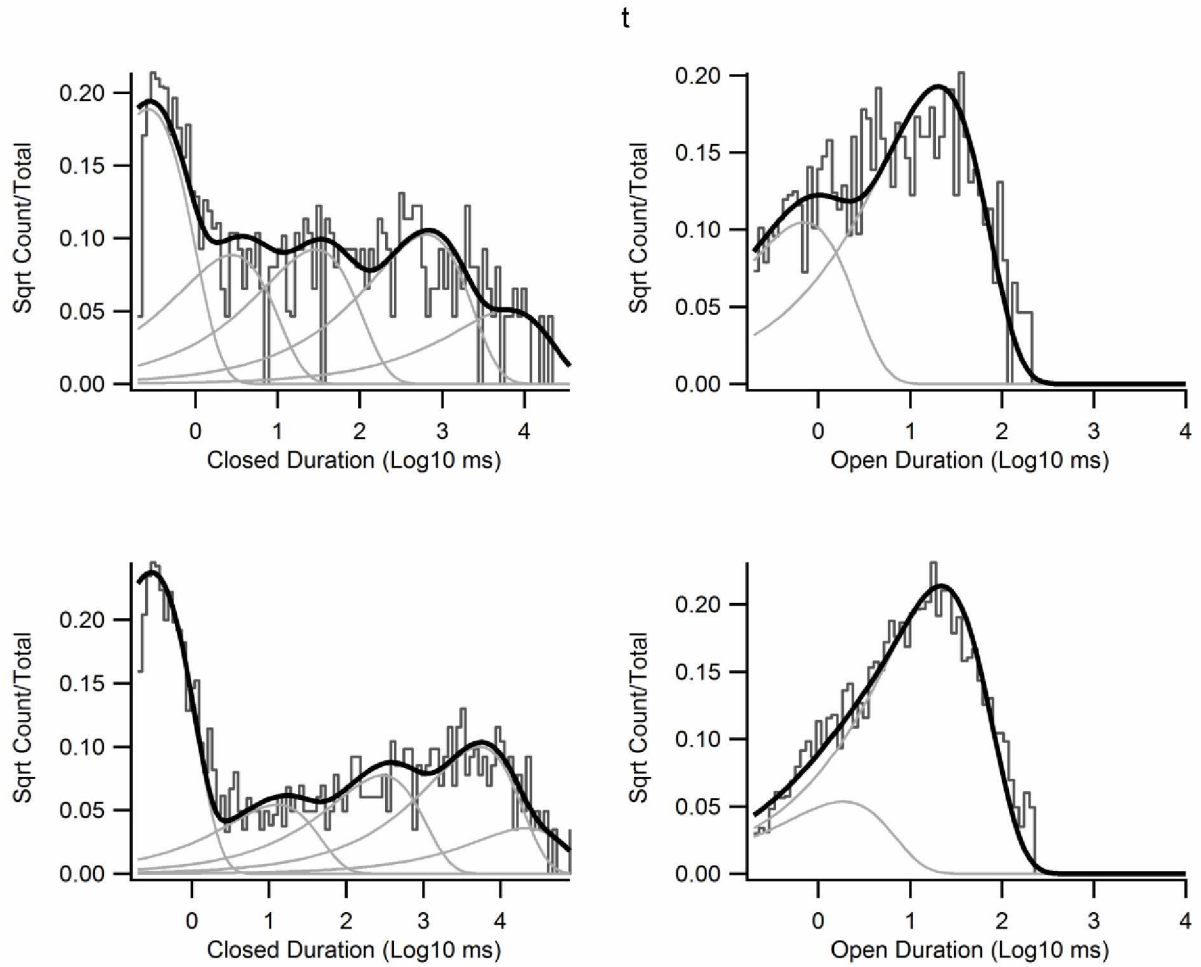
Figure A.2.3: LS modified MWC model fits. Open and closed duration distributions
from patches for 0.1 μM (top) and 1 μM ACh (bottom) group fitted with gating model
modified from classical MWC mechanism shown in Figure 2.5 (third from the top).
Model is modified to contain two desensitized states off of the mono and di-liganded
open states.
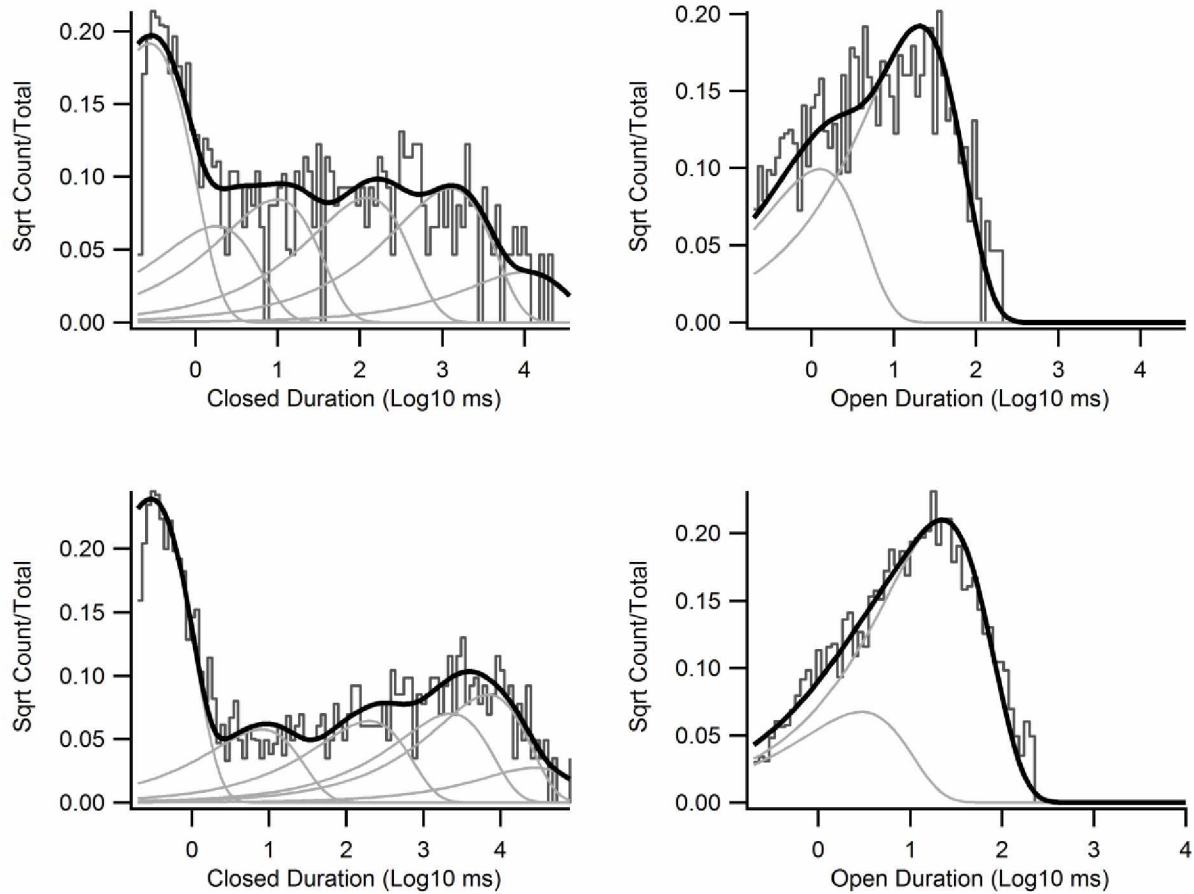
Figure A.2.4: LS modified MWC model fits with three desensitized states. Open and closed duration distributions from patches for 0.1 μM (top) and 1 μM ACh (bottom) group fitted with gating model modified from classical MWC mechanism shown in Figure 2.5 (fourth from the top). Model is modified to contain three desensitized states. One off of the doubly liganded closed state and an additional two off of the di-liganded open states.
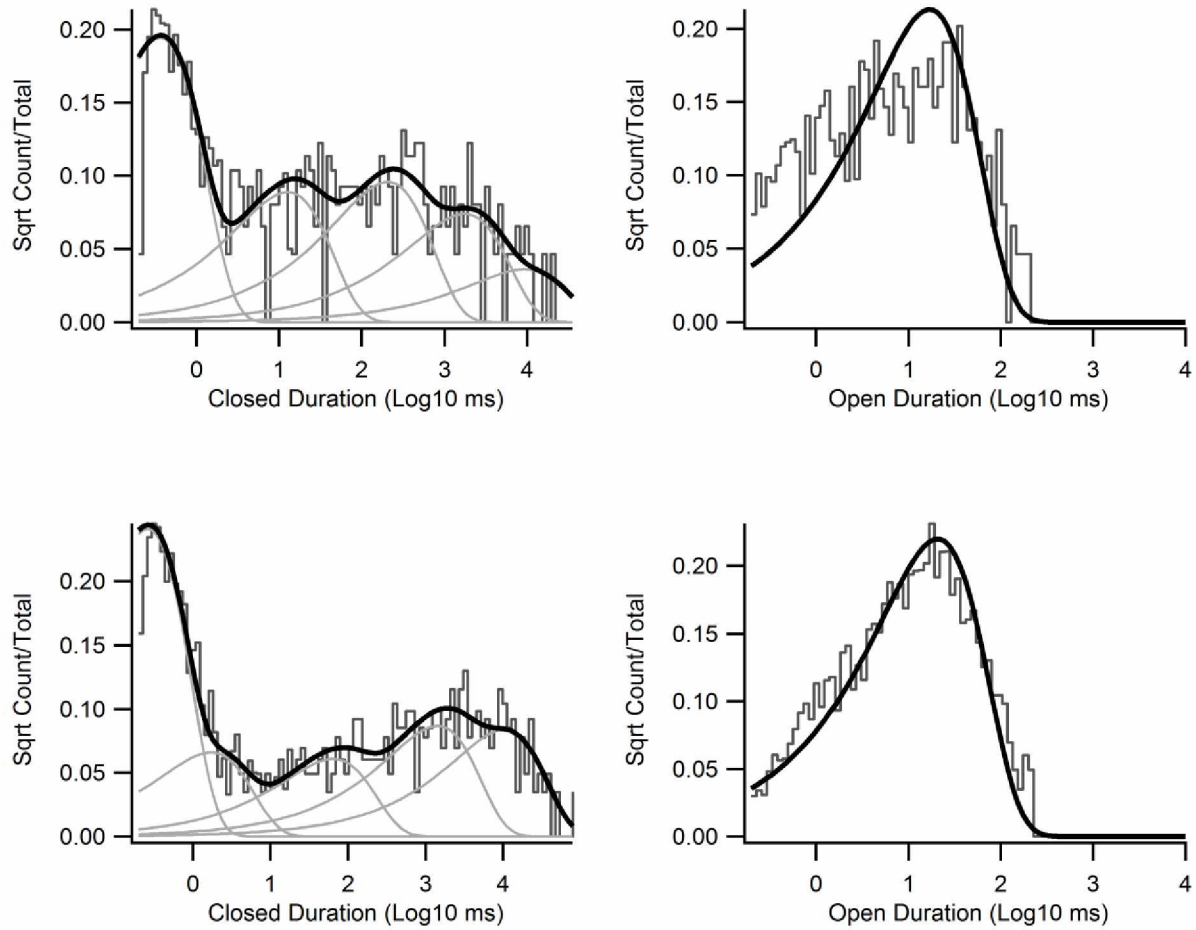
Figure A.2.5: LS linear model fits. Open and closed duration distributions from patches for 0.1 μM (top) and 1 μM ACh (bottom) group fitted with gating model lacking activation and containing 5 desensitized states shown in Figure 2.5 (fifth from the top). Model lacks activation and effectively begins in the doubly liganded open state. This model assumes that we are not seeing any activation rates in our data.
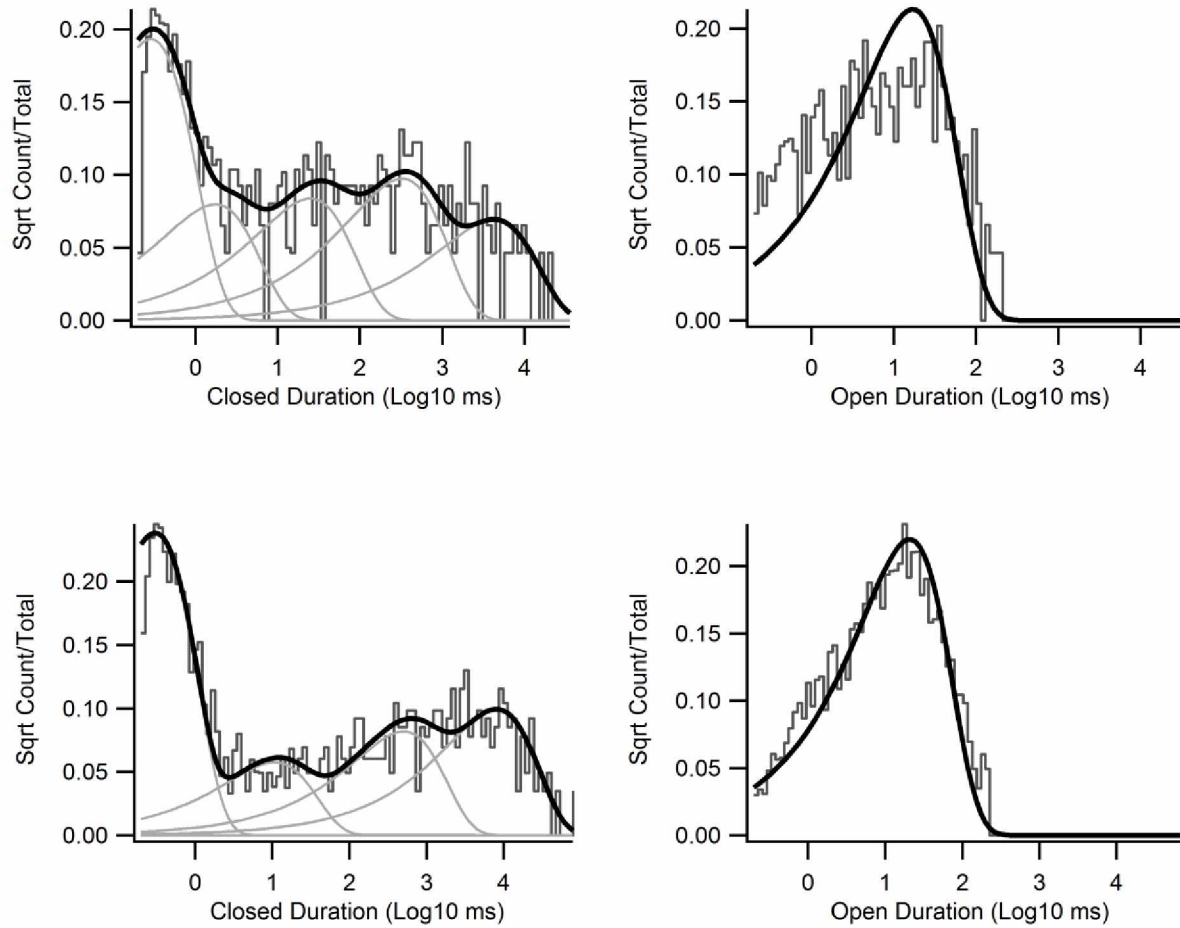
Figure A.2.6: LS star model fits. Open and closed duration distributions from patches for 0.1 μM (top) and 1 μM ACh (bottom) group fitted with gating model lacking activation and containing 5 desensitized states in a star shape shown in Figure 2.5 (bottom). Model lacks activation and effectively begins in the doubly liganded open state.

Table A.2.1: Rate constants for Katz and Thesleff mechanism.

$$\text{C} \underset{k_{-1}}{\overset{2k_{+1}}{\rightleftharpoons}} \text{C} \underset{2k_{-1}}{\overset{k_{+1}}{\rightleftharpoons}} \text{C} \underset{\alpha 2}{\overset{\beta 2}{\rightleftharpoons}} \text{O}$$

$$d_{-2} \updownarrow d_{+2} \qquad\qquad\qquad d_{-1} \updownarrow d_{+1}$$

$$\text{C} \underset{k_{-2}}{\overset{2k_{+2}}{\rightleftharpoons}} \text{C} \underset{2k_{-2}}{\overset{k_{+2}}{\rightleftharpoons}} \text{C}$$

Table A.2.1			
Rate Constant	Unit	0.1 μM	1 μM
$2k_{+1}$	$M^{-1}s^{-1}$	1.6E6 ± 44%	1E9 ± 37%
k_{+1}	$M^{-1}s^{-1}$	8.7E8 ± 38%	2.2E9 ± 61%
$2k_{-1}$	s^{-1}	547 ± 29%	1485 ± 89%
k_{-1}	s^{-1}	16 ± 100%	947 ± 99%
β_1	s^{-1}	2360 ± 29%	2420 ± 63%
α_1	s^{-1}	67 ± 27%	919 ± 99%
$2k_{+2}$	$M^{-1}s^{-1}$	1.2E9 ± 98%	2.3E6 ± 75%
k_{+2}	$M^{-1}s^{-1}$	1.1E7 ± 41%	0.14 ± 100%
$2k_{-2}$	s^{-1}	1.5 ± 41%	5E-8 ± 100%
k_{-2}	s^{-1}	0.83 ± 46%	0.88 ± 77%
d_{+1}	s^{-1}	20 ± 29%	4.4 ± 93%
d_{-1}	s^{-1}	3.7 ± 29%	0.08 ± 70%
d_{+2}	s^{-1}	9E-4 ± 65%	94 ± 70%
d_{-2}	s^{-1}	0.3 ± 99%	10.5 ± 71%

Table A.2.2: Rate constants for MWC mechanism.
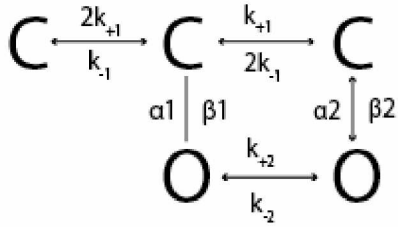
Table A.2.2			
Rate Constant	Unit	0.1 μM	1 μM
$2k_{+1}$	$M^{-1}s^{-1}$	9.5E6 ± 15%	4E5 ± 19%
k_{+1}	$M^{-1}s^{-1}$	1.8E8 ± 99%	3.2E6 ± 97%
$2k_{-1}$	s^{-1}	896 ± 55%	707 ± 95%
k_{-1}	s^{-1}	5 ± 99%	5 ± 98%
β_1	s^{-1}	66 ± 55%	74 ± 93%
α_1	s^{-1}	1106 ± 50%	349 ± 97%
β_2	s^{-1}	2060 ± 55%	2640 ± 94%
α_2	s^{-1}	77 ± 45%	78 ± 92%
k_{+2}	$M^{-1}s^{-1}$	6.9E2 ± 99%	138 ± 44%
k_{-2}	s^{-1}	7.9e-6 ± 56%	1.9E-6 ± 53%

Table A.2.3: Rate constants for a MWC modified mechanism

$$\begin{array}{ccccc}
C & \underset{k_{-1}}{\overset{2k_{+1}}{\rightleftharpoons}} & C & \underset{2k_{-1}}{\overset{k_{+1}}{\rightleftharpoons}} & C \\
& & \alpha_1 \updownarrow \beta_1 & & \alpha_2 \updownarrow \beta_2 \\
C & \underset{d_{+1}}{\overset{d_{-1}}{\rightleftharpoons}} & O & \underset{k_{-2}}{\overset{k_{+2}}{\rightleftharpoons}} & O & \underset{d_{-2}}{\overset{d_{+2}}{\rightleftharpoons}} & C
\end{array}$$

Table A.2.3

Rate Constant	Unit	0.1 μM	1 μM
$2k_{+1}$	M^{-1}s^{-1}	4.6E8 ± 24%	1.1E7 ± 24%
k_{+1}	M^{-1}s^{-1}	4E9 ± 39%	2.1E7 ± 99%
$2k_{-1}$	s^{-1}	1208 ± 34%	43 ± 98%
k_{-1}	s^{-1}	603 ± 30%	404 ± 19%
β_1	s^{-1}	681 ± 30%	560 ± 90%
α_1	s^{-1}	272 ± 18%	86 ± 69%
β_2	s^{-1}	4360 ± 18%	4640 ±68%
α_2	s^{-1}	61 ± 18%	76 ± 68%
k_{+2}	M^{-1}s^{-1}	2E9 ± 29%	2.4E8 ± 73%
k_{-2}	s^{-1}	21 ± 32%	53 ± 71%
$d+1$	s^{-1}	151 ± 21%	68 ± 26%
$d-1$	s^{-1}	1 ± 21%	0.2 ± 9.5%
$d+2$	s^{-1}	2 ± 50%	1 ± 69%
$d-2$	s^{-1}	0.12 ± 33%	0.04 ± 42%

Table A.2.4: Rate constants for a three desensitized state MWC mechanism.

Table A.2.4			
Rate Constant	Unit	0.1 μM	1 μM
$2k_{+1}$	$M^{-1}s^{-1}$	1.05E9 ± 36%	3.1E7 ± 32%
k_{+1}	$M^{-1}s^{-1}$	3.7E9 ± 85%	3.8E8 ± 33%
$2k_{-1}$	s^{-1}	758 ± 85%	419 ± 50%
k_{-1}	s^{-1}	296 ± 22%	350 ± 99%
β_1	s^{-1}	0.001 ± 99%	74 ± 73%
α_1	s^{-1}	9.8e-5 ± 99%	855 ± 55%
β_2	s^{-1}	2710 ± 81%	3570 ± 43%
α_2	s^{-1}	315 ± 82%	79 ± 44%
k_{+2}	$M^{-1}s^{-1}$	1E9 ± 81%	2E4 ± 99%
k_{-2}	s^{-1}	279 ± 83%	4E-5 ± 99%
d_{+1}	s^{-1}	44 ± 23%	82 ± 18%
d_{-1}	s^{-1}	4.5 ± 25%	0.14 ± 19%
d_{+2}	s^{-1}	6.8 ± 91%	0.59 ± 99%
d_{-2}	s^{-1}	0.11 ± 54%	0.003 ± 66%
d_{+3}	s^{-1}	262 ± 25%	332 ± 20.5%
d_{-3}	s^{-1}	0.69 ± 43%	96 ± 1%

Table A.2.5: Rate constants for a linear mechanism.

$$O \underset{k_{1O}}{\overset{k_{O1}}{\rightleftarrows}} C \underset{k_{21}}{\overset{k_{12}}{\rightleftarrows}} C \underset{k_{32}}{\overset{k_{23}}{\rightleftarrows}} C \underset{k_{43}}{\overset{k_{34}}{\rightleftarrows}} C \underset{k_{54}}{\overset{k_{45}}{\rightleftarrows}} C$$
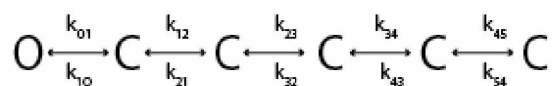
Table A.2.5		
Rate Constant	0.1 μM	1 μM
k1O	1817 ± 10%	3017 ± 9.6%
kO1	87 ± 5.4%	188 ± 5.6%
k12	1086 ± 10%	1062 ± 11%
k21	47 ± 24%	129 ± 65%
k23	49 ± 36%	514 ± 43%
k32	8.8 ± 32%	23 ± 35%
k34	2 ± 36%	12 ± 38%
k43	0.84 ± 43%	1.9 ± 32%
k45	0.1 ± 99%	0.27 ± 46%
k54	0.14 ± 67%	0.185 ± 25%

Table A.2.6: Rate constants for a star mechanism.

Table A.2.6		
Rate Constant	0.1 μM	1 μM
k1O	612 ± 41%	99 ± 42%
kO1	8.9 ± 37%	3.6 ± 18%
k2O	3.3 ± 24%	0.13 ± 11%
kO2	13 ± 14%	11 ± 14%
k3O	43 ± 29%	2.11 ± 44%
kO3	9.8 ± 17%	7.2 ± 16%
k4O	0.25 ± 18%	0.97 ± 99%
kO4	6.7 ± 20%	1e-4 ± 99%
k5O	3696 ± 14%	3553 ± 5.6%
kO5	53 ± 9.6%	62 ± 5.8%

CHAPTER 3: Synchronization of High-Sensitivity $\alpha 4\beta 2$ Nicotinic Acetylcholine Receptors[2]

Abstract

Understanding the mechanism of modulation of nAChRs by potential compounds such as desformylflustrabromine (dFBr) allows for greater insight into the potential uses and drawbacks of the drug on a synaptic level. We tested a variety of classical mechanisms to determine the best kinetic representation of our single-channel data. Our data for the human high sensitivity, ($\alpha 4_2\beta 2_3$), nicotinic receptors was best explained using an 8-state MWC based gating model. It was found that dFBr increased the open probability via an increase in the opening frequency of the diliganded open state in dFBr (by increasing the opening rate of the diliganded receptor). Also, dFBr increased the mean open time of the mono-liganded open state. In order to determine the consequences of the effects of dFBr on signaling at cholinergic synapses, we simulated macroscopic responses to concentration jumps. At high simulated concentrations of ACh, potentiation was primarily exhibited through the increase in open frequency into the diliganded open state, while at low concentrations of ACh, potentiation primarily occurred through the increase in mean open time for the mono liganded open state. For 1 mM ACh simulated macroscopic responses, we found an increase in peak P_{open} in the presence of dFBr, increasing P_{open} from 0.4 to 0.6. The increase in peak P_{open} in the presence of dFBr is due to the synchronization of openings, however, dFBr reduces overall charge transfer at simulated concentrations above 1 μM ACh. The simulated responses demonstrated that the decrease in charge transfer is primarily due to an increase in probability of being in the desensitized state D2. The negative effect dFBr is having on

105

the high sensitivity receptor could be due to the presence of the Good's buffer HEPES

in the recording solution. Future studies will need to consider the buffer's potential

effects when analyzing results.[2]

[2] Demmerly, A., Edmonds, B.W. 2016. Synchronization of high-sensitivity α4β2 nicotinic

acetylcholine receptors. *J. Gen. Physiol.*

3.1 Introduction

The current knowledge on the physiological role and activation of $\alpha4\beta2$ nicotinic acetylcholine receptors (nAChRs) in the central nervous system (CNS) is limited. The heteromeric $\alpha4\beta2$ AChRs are widely distributed throughout the brain and may be involved in nicotine addiction as well as a variety of neurological disorders, including Alzheimer's disease and autism. The high-sensitivity (HS) $\alpha4\beta2$ nAChR is the least studied of the two stoichiometric forms and very little is known about their synthesis and regulation (Changeux, 2010). Due to its potential role in several psychiatric and neurological disorders, HS $\alpha4\beta2$ nAChRs are an important therapeutic target. (Nelson et al., 2003; Khiroug et al., 2004).

A novel strategy in treating a variety of cognitive diseases is to utilize compounds that enhance responses of nAChRs and potentially increase transmission at synapses where nAChRs are deficient, thus restoring functional properties. Allosteric modulators are a class of compounds that bind at a site distinct from the endogenous ligand acetylcholine, and therefore do not compete with the agonist, preserving the natural cholinergic signal. Desformylflustrabromine (dFBr) has been previously identified as a novel positive allosteric modulator (PAM) of $\alpha4\beta2$ nAChRs with no apparent potentiation of other subtypes (Sala et al., 2005). Previous studies have suggested that the potentiation exhibited by dFBr is due to an alteration in channel gating kinetics, but the mechanism by which dFBr modulates the HS $\alpha4\beta2$ receptor is currently unknown (Weltzin and Schulte, 2010; Sala et al., 2005; Kim et al., 2007).

In this study we are taking a first step in determining how dFBr modulates by providing a comprehensive gating model for the high sensitivity receptors. Once it is known how these receptors are activated in the CNS, then our model will provide a framework for how dFBr will potentiate on a synaptic level. Obtaining a mechanism that can describe the effects of the positive allosteric modulator, dFBr, will allow greater insights into its uses and potential shortcomings in future studies.

3.2 Materials and Methods

3.2.1 Cell Techniques

HEK-293 cells were maintained in minimum essential Eagle medium (MEME) supplemented with 1% Glutamax (Gibco), 10 % bovine growth serum, antibiotic penicillin streptomycin (200 µg ml^{-1}), 100 µg/mL G418 (Thermo-Fisher) and pH adjusted to 7.4. Cells were incubated at 37°C in a humidified atmosphere of 5% CO_2, passaged weekly and plated onto 35mm tissue culture dishes (Becton Dickinson) one day prior to experiments. Human α4 and β2 neuronal nicotinic receptor subunits were stably transfected into HEK-293 cells and passaged weekly one day prior to experiments. The cells were provided to us by Dr. Henry Steinbach at Washington University, St. Louis, MO.

3.2.2 Electrophysiology Techniques

All salts were obtained from Sigma Aldrich. To avoid receptor rundown all patch-clamp recordings were made in the cell-attached configuration at room temperature. Membrane potential was zeroed with a K+-based extracellular solution containing (in mM): 142 KCl, 5.4 NaCl, 2 $CaCl_2$, 1.7 $MgCl_2$, 5 HEPES, 10 glucose and pH adjusted to 7.4. Pipette solution contained (in mM): 5.4 KCl, 142 NaCl, 2 $CaCl_2$, 1.7 $MgCl_2$, and 5 HEPES pH adjusted to 7.4. Agonist and PAM solutions were made on the day of the experiment.

Experiments were performed using a Nikon Eclipse FN1 microscope. Pipettes were pulled to a resistance of 10-14 $M\Omega$ using a PMP-102 Micropipette puller (Microdata Instrument Inc.) and thick-walled borosilicate capillary glass tubing with flame polished ends (Warner Instruments). In order to enhance signal to noise ratio pipette tips were coated with Sylgard (Dow Corning 184). Prior to recording the pipettes were front and back filled with the pipette solution containing the appropriate concentration of ACh (0.1 -10 µM) with or without dFBr (1 µM). Patches were voltage-clamped at -80 mV with a HEKA EPC-10 Elektronik amplifier using PATCHMASTER software. Data were low-pass filtered (4-pole Bessel, -3dB) at 10 kHz and digitized to the computer at 100 kHz.*3.2.3*

3.2.3 Definition of Bursts and Clusters

Bursts were defined as in section 2.2.4 and by a critical value (t_{crit}) using the equation:

$$Amp_{1}* \, e^{-Tcrit/Tau1} = Amp_{2}* \, (1 - e^{-Tcrit/Tau2})$$

T_{crit} is the cutoff duration between exponential components and equalizes the area under the overlapping tails of the distributions. Where Amp_1 and Amp_2 are the weights of the first and second components respectively for bursts or second and third components for clusters. Tau1 and tau2 are the time constants computed from MIL. Each tau in the distribution contributes one exponential component to the probability density function (thick line in distributions). Bursts and clusters that held doubles were discarded from the analysis.

3.2.4 Model Fitting and Simulations

Idealized records of single-channel events were constructed and dwell time distributions fitted with models in QuB as previously described. Rate constants were obtained using an algorithm (MIL described) (Qin, 2004; Qin et al., 1997, 1996). All simulations performed utilized scheme 2 for control (1 µM ACh) and modulated (1 µM ACh + 1 µM dFBr). Responses were made using rate constants from a group fit that contained greater than n=3 for all conditions, except 10 µM data. The open and closed distribution used in figures was based on patches that contained the most events

(openings + closings). In order to distinguish between models, we relied on various factors including, the fit of the probability density function to the data, the degree of agreement in activation steps between 0.1 and 1.0 μM ACh, as well as simulated peak P_{open} and EC_{50} values. Log likelihood was not used as a best fit parameter due to its inability to distinguish between models containing a similar number of states (Elenes and Auerbach, 2002). Monte Carlo simulations of macroscopic currents in Figure 3.4A were made in QuB Express for 10,000 channels with a unitary amplitude of 1 pA and standard deviation (SD) of Gaussian noise of 0.15 pA (Nicolai and Sachs, 2013). Current values were converted to and displayed as open probabilities (P_{open}) in Igor Pro (WaveMetrics). Stability plots were generated using QuB's stability function with a window size (events) of 15 and an overlap (events) of 2.

3.3 Results

3.3.1 Conductance of HS Receptors in the Presence of dFBr

Allosteric modulators can exhibit potentiation a variety of ways, including increasing an ion channels conductance. To determine whether dFBr increases chord conductance as a means of potentiating the receptor channel openings with one primary amplitude were analyzed from cell-attached recordings obtained using low concentrations of ACh (0.1 and 1.0 μM ACh). Similar to previous reports we found that $\alpha 4\beta 2$ receptors demonstrated a high sensitivity component to ACh, having a conductance of ~20 pS (Buisson and Bertrand, 2001). Figure 3.1 shows open point amplitude histograms for HS receptors in 1 μM ACh and 1 μM ACh + 1 μM dFBr. Fitted open point amplitude histograms yielded a chord conductance of 19.5±1.8 pS (mean±SD; n=5) and 19.9±0.34 pS (n=4) in the absence and presence of dFBr respectively. The presence of dFBr had no significant effect on the HS conductance levels. Traces (1 s) reveal that dFBr does not significantly alter the mean open time (the mean duration of a single opening). This suggests that when dFBr is applied the average open state lifetime of the receptor is not affected by the drug. Inward rectification of $\alpha 4\beta 2$ has been observed in previous reports (Buisson et al., 1996) and our recordings did not exhibit HS openings above 0 mV. I/V data was collected for 1 μM ACh (n=3) and 1 μM ACh + 1 μM dFBr (n=4) between -80 mV and -30 mV and was fitted with a linear equation. The fit yielded slope conductances of 19.9 for ACh and 19.8 for ACh + dFBr. The I/V relationships demonstrate that dFBr does not increase the chord conductance as a means of potentiation. The control values are very close to the

112

previously reported conductance values of ~20 pS (Buisson et al., 1996). Long

contiguous sweeps (50 s) do not show the obvious effect of dFBr on HS receptor gating.

3.3.2 Gating of HS Receptors in ACh and ACh + dFBr

Recordings of HS $\alpha4\beta2$ in 0.1 (n=4), 1 (n=4), 10 (n=2) μM ACh or 1 μM ACh + 1

μM dFBr (n=3) yielded multiple patches for all conditions that contained enough

openings for analysis. The average number of openings for all ACh patches were

917±395, with a range from 295 to 1250 openings. The average number of openings

for 1 μM ACh + 1 μM dFBr were 1698 openings. Incidents of double openings were

observed in 1 out of 3 of the 0.1 or 1 μM ACh patches, but all other conditions showed

evidence for more than one channel. The probability of a channel being open for the

HS subtype is very low (~ 0.001 to 0.005). These values are taken from the most stable

0.1 and 1.0 μM ACh patches, which contained two observable channels. Figure 3.2

shows 50s segments for 1 μM ACh and 1 μM ACh + 1 μM dFBr. These two data sets

show HS receptor gating for ACh with and without dFBr. Visually an effect is not

immediately apparent.

Single-channel recordings often contain several channel openings in succession

followed by long periods of closings. Our HS data contained none of these classical

bursts, and most 'bursts' in our data contained only one opening. Figure 3.3 shows the

burst length and apparent open lifetime of the bursts for 0.1-10 μM ACh and 1 μM ACh

+ 1 μM dFBr. Two exponentials were needed to fit the distribution of the burst length

and also to fit the total open time per burst. Both of these were very similar since the

majority of bursts consisted of one apparent opening. As the concentration increased, the slower component (time constant τ_s) becomes shorter. The presence of dFBr increased the apparent open lifetime, increasing time constants τ_f from 2.9 to 4.5 ms and τ_s from 3.7 and 10.7 ms. There is a similar effect seen on the burst length increasing constants τ_f from 3.12 to 4.5 ms and τ_s from 3.4 and 5.04 ms. Our calculated burst parameters were in agreement for dFBr (estimated burst open lifetime 4.7 ms) with the time constants obtained from the fits, whereas our ACh calculated burst parameters were larger than our fitted time constants (estimated burst open lifetime 12.9 ms). A possible explanation for this discrepancy is an underestimation in one of the desensitized states by the model. Clusters were defined by a t_{crit} in between 2nd and 3rd components (see methods). Cluster length (Figure 3.4 A) and apparent open lifetime (Figure 3.4 B) required two exponentials to fit. For burst length τ_f showed no significant difference between 0.1 to 10 μM ACh, whereas τ_s decreased from 4.01 ms to 1.83 ms for 0.1 to 10 μM ACh. The slow and fast time constants for the cluster open lifetimes decreased as concentration increased from 0.78 to 0.33 ms for τ_f and 2.1 to 1.6 ms for τ_s for 0.1 to 10 μM ACh. Clusters were dominated primarily by single openings and lower concentrations having more openings (3.4 C).

It is a common problem in the single-channel analysis of low P_{open} receptors to have a level of uncertainty in the number of channels within the data. Therefore, it is beneficial to determine if instability exists in the data and how that will affect kinetic analysis. Stability plots for ACh concentrations of 0.1 μM to 10 μM ACh and 1 μM ACh + 1 μM dFBr were generated using QuB's stability function and segments contained 15

114

events (Figure 3.5, see methods). These plots originated from the same patches used in model analysis, as well as burst and cluster distributions. Both 0.1 and 1 μM ACh data sets contained more than one observable channel and were stable with a P_{open} of 0.0067 and 0.016 respectively. The 0.1 and 1 μM ACh patches were the only completely stable patches despite showing more than one observable channel. Other 0.1 and 1 μM ACh patches had similar low occupancy (<0.01), and contained only one observable channel, but had decreased activity after ~800 segments. The 10 μM ACh patches activity decreased after ~500 segments. The 1 μM ACh + 1 μM dFBr patches were not stable near the end of the recordings and activity decreased after ~1000-1200 segments. The observed occupancy for the 10 μM ACh (0.0011) data was lower when compared to the 0.1 and 1 μM patches, even though more than one channel was observed in the 10 μM data. All 1 μM ACh + 1 μM dFBr patches showed some amount of instability (P_{open}= 0.05, Figure 3.5). This instability is likely caused by channels dropping out as the patch progresses or receptors entering an extremely long lived desensitized state that is concealed by more than one channel being present in the patch. Instability due to channels dropping is the most likely culprit with all of the dFBr data, but this is less likely for the 10 μM data, which begins with very low occupancy and contain more than one observable channel.

3.3.3 Fitting Mechanisms to Single-Channel Data

The mechanism of modulation exhibited by dFBr was investigated by fitting a variety of mechanisms to single-channel data. Mechanisms that contained activation steps were fitted independently to each single-channel concentration group which included 0.1, 1.0 and 10 μM ACh and 1 μM ACh + 1 μM dFBr. A concentration group was defined as all patches of the same concentration, (e.g. all 1 μM), fitted simultaneously as a group. The records were kept intact and were not divided up due to bursts and clusters primarily consisting of single openings (see methods). We tested 4 different types of activation mechanisms, Katz and Thesleff based model, Monod-Wyman-Changeux (MWC) based model, and MWC mechanisms that contained two or three desensitized states. In our MWC models we omitted the unliganded open state due to the low probability of these openings occurring in naïve HS nAChRs. All models utilized activation rate constant constraints of $2k_{+1}$ and k_{+1} for the binding rates, and $2k_{-1}$ and k_{-1} for the unbinding rates, which assumes that both sites on the receptor are available for agonist binding. Mechanisms were also constrained with the requirements of microscopic reversibility.

Classical mechanisms such as the Katz and Thesleff and the MWC have been previously utilized to describe the gating kinetics of ACh receptors. We first tested the Katz and Thesleff based mechanism (See Figure 3.6) and found that 10 μM errors were extremely high (>100%) and most of the rates were vastly different from the other patches (See Table 1). Activation rates between 0.1 and 1 μM ACh changed 5-fold, while the activation rates for the 10μM data were 1000x smaller than for the other two

116

concentrations. The overall fits of the probability density function to the data was

decent, with 10 μM ACh data fitting the worst (Figure 3.7). Deactivation rates in the

Katz and Thesleff model for the dFBr data are much lower when compared to controls,

while $\beta 2$ is 10x lower than control. When simulated, the Katz and Thesleff configuration

gave extremely high P_{open} (~0.85) values and the presence of dFBr displayed inhibition.

The MWC mechanism has been widely used to describe many ion channels.

This mechanism postulates that there are two conformational states a channel can take

on, open and closed, each with different affinities for ligand. For the MWC we imposed

constraints so that the activation rate constants are equivalent for each ligand bound.

For this model type we have two molecules of agonist binding, with one cycle, and 6

free parameters. Of the two classical mechanisms the MWC model gave consistent

activation rates between the 0.1 and 1 μM ACh data. Examples of open and shut time

distributions are shown in Figure 3.8. Since the MWC scheme lacks desensitized states

the fits were poor and thus we decided to use the MWC as a base model. One to three

desensitized states were added to the basic model and their positions tested. Positions

included a D state distal to an O state or to the diliganded closed state.

3.3.4 Modified MWC Schemes

It was difficult to find a desensitization configuration that would result in a slow desensitization time course as observed in previous reports (Weltzin et al., 2014). We first tested multiple two-desensitized state configurations, and scheme 1 is an example of one such configuration (Figure 3.6). This particular configuration gave the lowest errors, unlike configurations that had desensitized states distal to O1 and O2 or C3 and O2. With only two desensitized states, placing one distal to O1 and O2 resulted in no observable desensitization in simulated macroscopic responses. While having the desensitized states distal to C3 and O2 resulted in large error values and the lifetime of C3 being much lower than our imposed dead time (Figure A.3.1 and Table A.3.1). Closed and open time distributions are shown for scheme 1 in Figure 3.9 and rate constants in Table 3.3. Multiple configurations that contained three desensitized states were also tested. Schemes included all three desensitized states off O2 as well as a desensitized state off of O1 and two off of O2. Both configurations resulted in large errors for all conditions and poor fits to the closed time distributions. All three desensitized states being adjacent to O1, O2 and C3 was also tested, but the errors and fits gave us less confidence in the mechanism compared to scheme 2 (Figure 3.10 and Table 3.4).

All of the MWC based models that were tested gave a consistent high P_{open} (>0.6) for 0.1 µM ACh data. The current cause for this is most likely due to larger rate constants between O1 and O2, as lowering those rates in simulations to values seen in the 1 µM ACh model resulted in a lower simulated P_{open} values, which were comparable to the 1 µM data (~0.3- 0.4).

118

3.3.5 Desensitization Based Mechanisms

We also investigated the possibility that our data lacks activation information due to the closed time distributions only displaying closings affiliated with entry into long lived closed states. When agonist concentrations are high, then almost all current can be attributed to the activation of diliganded AChRs (Elenes and Auerbach, 2002). High ACh concentrations can therefore lead to diliganded closed states being too brief to be detected. Mechanisms that only contained desensitized states as closed states were investigated and group fitted to data at different ACh (0.1, 1 and 10 μM ACh) and ACh + dFBr concentrations (1 μM ACh + 1 μM dFBr). Mechanisms are based off of QuB's model search function and were the most common outcomes.

All desensitization models contain only one open state, which results in the probability density function not fitting the open duration distributions. Most group fits of the desensitization based models do not fit 10 μM data as well as the 0.1 or 1 μM ACh data. Scheme 5 (star) (Figure A.3.4) had the best overall visual fits compared to the other desensitization schemes. Whereas, scheme 6 (linear, Figure A.3.5) and scheme 7 (Figure A.3.6) had the worst fits. The 10 μM data fits were poor for all desensitization schemes. In some of the schemes the lifetimes of all of the desensitized states increased with dFBr, including scheme 4 and scheme 7, with scheme 7 fits being equivalent to scheme 6. For all of the schemes it was noted that dFBr reduced the likelihood of entry into the majority (4/5 or 3/4) of the desensitized states within the models. Also, there were cases in all of the desensitized models where dFBr increased the lifetime of some of the desensitized states. Of all of the desensitization schemes

119

the most probable would be Scheme 5 (star) due to the probability density function

fitting the best out of all three and lowest overall errors modulated and unmodulated.

3.3.6 Simulation of Macroscopic Currents

Conducting simulations of macroscopic responses with fitted models is a

powerful tool in determining if the estimated kinetic parameters support potentiation.

Scheme 2 was utilized to investigate dFBr's potentiation over a range of ACh

concentrations by simulating macroscopic responses to concentration jumps (Figure

3.11A). Potentiation of peak currents occurred at all concentrations with the largest

percentile increase occurring at low concentrations (≤ 5 μM), and an increase in peak

current maintained at larger concentrations (≥ 50 μM) (Figure 3.11 B). Fitted Hill

equations to peak responses yielded (mean $\pm$SD) EC_{50} values and Hill slopes of

23.5 ± 1.3 μM and 1.1 ± 0.05 for ACh, and 18.1 ± 0.68 μM and 0.91 ± 0.03 for dFBr. Peak

open probability for 1 mM concentration jumps of ACh was ~0.42, dFBr increased peak

open probability to ~0.63. The concentration dependence of changes induced by dFBr

for macroscopic responses is shown for 1 μM-1 mM ACh (Figure 3.11 C). The decay of

responses at all concentrations were best fit with two exponentials. At concentrations of

1 mM, ACh gave a fast time component of ~17 ms (τ_f) and a slow time component (τ_s)

of ~790 ms. The presence of dFBr significantly reduces these time components,

bringing τ_f down to 5 ms and τ_s down to 6 ms.

We simulated low concentrations of ACh using scheme 2 for ACh and ACh + dFBr in order to determine if dFBr affected low concentrations of agonist the same as high concentrations. Figure 3.12 A shows the effect of dFBr at low concentrations of ACh (1, 3 and 5 μM). At concentrations greater than 3 μM, dFBr gives increased desensitization, whereas at concentrations lower than 1 μM, dFBr increased potentiation without increasing desensitization. We were interested to determine if charge transfer changed significantly in the presence of dFBr, and if that change is correlated to agonist concentration. At ACh concentrations of 1 mM dFBr decreases charge transfer 5.2-fold down to 1.8-fold at 5 μM. Charge transfer did not increase in the presence of dFBr until concentrations were $\leq$1 μM. We were interested to find out if dFBr has a greater impact on the fast (τ_f) or slow (τ_s) time component. While dFBr does decrease τ_f for the HS receptors, it was found that τ_s was more affected by dFBr. For the ACh model, τ_f maintains a steady level at ~100 μM reaching ~17 ms, while in dFBr this occurs at lower concentrations (<10 μM) (Figure 3.12 B). dFBr sees a significant reduction in the slow time course of decay, reducing τ_s to one tenth its ACh value at concentrations greater than 50 μM (Figure 3.12 C).

When individual rate constants were changed during macroscopic simulations it was found that potentiation was different based upon the concentration of ACh used for stimulus. At high (1mM) simulated ACh concentrations the primary mode of potentiation exhibited by dFBr is an increased rate of entry into the diliganded open state O2. This potentiation is offset by an increase into the desensitized state D2, accounting for the observed increase in desensitization as the simulated concentration of ACh increases

121

(Figure 3.11A). At low concentrations (<10 μM) potentiation primarily occurs by an increase in the mean open lifetime of O1. dFBr increases the open probability, synchronizing openings in simulated macroscopic currents, giving potentiation at the peak.

3.3.7 Occupancy Probabilities and Agonist Concentration

The aim of examining occupancy probabilities was to determine how dFBr increased macroscopic desensitization, and if potentiation was equivalent at all concentrations. Figure 3.13 shows the occupancy probabilities for concentration jumps into 10 μM, 100 μM, and 1 mM ACh. At high concentrations (1mM) the open probability is approximated by P_{O2} for ACh and ACh + dFBr models, because P_{O1} is <0.005, as the simulated concentration decreases, P_{O1_ACh} increases to 0.032. At high concentrations, dFBr increased the peak response 1.6-fold (P_{O2_ACh} = 0.38, P_{O2_dFBr} = 0.601). For jumps into low concentration of ACh (10 μM) dFBr increased open probability by a factor of 2.3 (P_{O2_ACh} + P_{O1_ACh} = 0.1, P_{O2_dFBr} + P_{O1_dFBr} = 0.23).

For concentrations greater than 100 μM an increase in P_{O2} was the primary contributor to potentiation, whereas below 100 μM P_{O1} becomes a significant contributor. For all concentrations P_{D2} and P_{D3} both contributed to desensitization with P_{D3} contributing the most in ACh, whereas P_{D2} contributed the most in dFBr. In all case P_{D1} contributed very little to desensitization. For concentrations greater than 100 μM P_{D2_dFBR} was larger than P_{D2_ACh}, and is the primary cause for increased desensitization seen by dFBr in macroscopic simulations. P_{D3_dFBR} is < 0.1 compared to P_{D3_ACh} being

>0.65 at 0.500 ms. The lower probability of entering D3 leads to more entries into O2 contributing to initial potentiation.

3.3.8 Potentiation During a Pulse of High Agonist Concentration

We examined the macroscopic responses to an agonist concentration profile typical of fast synapses by driving models with an alpha function with an agonist concentration of 1mM. Peak open probability in ACh (P_{O2_ACh} = 0.35) was slightly lower compared to concentration jumps (P_{O2_ACh} = 0.38) of the same concentration. P_{open} was larger for dFBr when a similar comparison was made (P_{O2_dFBr} = 0.634) when driven with an alpha function versus (P_{O2_dFBr} = 0.601) when driven with a concentration jump. Overall, dFBr yielded a 1.8-fold increase in peak amplitude.

The development of desensitization following a pulse of agonist was faster with dFBr, while recovery from desensitization was significantly slower. The presence of dFBr decreased the time to peak of P_{D2} (P_{D2_ACh} = 41.2 ms, P_{D2_dFBr} = 27 ms) and P_{D3} (P_{D3_ACh} = 8.1 ms, P_{D3_dFBr} = 5.3 ms). P_{D2_dFBr} was lower with the alpha function versus the concentration jump, while P_{D3} maintained similar levels, despite having a longer decay time course in the presence of dFBr (P_{D3_ACh} τ=6.7 s, P_{D3_dFBr} τ=21.8 s).

123

3.4 Discussion

3.4.1 Fitted Models

We attempted to fit HS $\alpha 4\beta 2$ nAChR single channel data with 3 model types and their variants. The desensitization model types were just a subset of possible configurations that would be viable for describing the desensitization time course of the receptors. The classical mechanisms such as Katz and Thesleff and MWC have been successfully utilized in prior studies to describe nicotinic receptors (Edelstein et al., 1996; Colquhoun and Sakmann, 1985). In their simpler forms the primary classical mechanisms of Katz and Thesleff and MWC failed to describe the single-channel data that they were fitted to, even when the Katz and Thesleff contained a modification of an additional open state. Modifying the MWC to account for desensitization proved to the most successful. We found that a model containing 3 desensitized states gave the best overall fits, error values, and simulated currents. Some combinations gave simulated currents that demonstrated extremely long (>20s) desensitization time courses similar to or longer than those seen in previous whole cell experiments on oocytes, but these models contained the largest amount of error (Weltzin and Schulte, 2015). In our data we could not justify adding more than 3 desensitized states in an activation mechanism due to the lack of complexity in the closed time distribution and the possibility of more than one channel in our data. The likelihood that we are not capturing any activation information in our patches was also investigated This scenario is plausible given that 1 μM ACh is around the EC_{50} for these receptors and previous reports on nicotinic receptors have observed a lack of activation data at high concentrations (Elenes and Auerbach, 2002).

Several desensitization schemes were explored for all concentrations, but an additional open state was found to be needed to describe the open lifetime distribution. While the closed time distributions appear rather simple, they most likely contain several desensitized states that are difficult to resolve. This added with the instability at the end of the dFBr data adds additional complexity to result interpretation.

3.4.2 Scheme 2 Predictions

The MWC based mechanisms gave consistent activation rates across the two concentrations of 0.1 and 1 μM ACh. The MWC modified scheme 2 gave the most promising results in terms of errors, peak open probability and desensitization. We discounted any schemes that when simulated over long periods (>25s) gave high steady state currents and no visible desensitization. In order to test the effects dFBr would have on macroscopic currents we used models obtained from 1 μM ACh and the 1 μM ACh + 1 μM dFBr data. The primary finding was that dFBr potentiates peak currents of HS receptors across all concentrations. At higher concentrations ($\geq$5 μM) potentiation is offset by an increase in desensitization, resulting in overall lower charge transfer, while at very low concentrations ($\leq$ 3 μM) dFBr increases the desensitization time course, and charge transfer increases. Potentiation at high concentrations is brought about via an increase in the amount of diliganded openings, while increased desensitization occurs via an increase into the desensitized state D2. This increase directly affects the slow desensitization time course, while having little effect on the fast time component. At low concentrations, potentiation primarily occurs via an increase in

the mean open time of O1, as well as a decreased rate of entry into the desensitized

state off of the diliganded closed state. While the concentration is not high enough for

the change in desensitization to override potentiation, we do observe that receptors will

be 'pushed' into the long lived desensitized states by the increased rate into the

diliganded open state.

The potential implications our findings have for signaling will largely depend on

where HS receptors are expressed and in how they are exposed to agonist. For

signaling at classical fast synapses, dFBr could have significant consequences based

upon the agonist concentration profile HS receptors are exposed to. At synapses where

there are brief, high concentrations of ACh, dFBr will initially potentiate receptors before

pushing them into desensitization. Based on our simulations this would result in an

overall decrease in charge transfer. However, if the receptors are exposed to long

lasting ambient (low) levels of ACh concentration, such as in a 'volume transmission'

model (Ren et al., 2011; Descarries et al., 1997), then dFBr is capable of boosting

receptor responsiveness and increasing overall charge transfer for HS receptors.

3.4.3 Model Discrepancies

All of our dFBr data contained instability that arose near the end of the patch.

This instability is due to either multiple receptors dropping out as the patch ages or dFBr

having a greater effect on the open channel duration which becomes weaker as the

patch progresses. The instability could also be a product of both scenarios. Loss of

receptors is the more likely culprit as more than one observable channel is seen in the

126

first half of the records. The 0.1 and 1 μM ACh data is very stable, and we have very high confidence in the results for those patches. Of all of our data for the 10 μM ACh patches consistently had only one observable channel, but were unstable near the end of the records and the initial P_{open} obtained from stability plots is very low. It was noted that at 10 μM the open time distributions became shorter, and it is possible that block is involved even at concentrations this low. Another consistent discrepancy was in the 10 μM data all gave significantly lower activation rates compared to other concentrations. Whether this is due to open channel block on the single-channel level or another mechanism is currently unknown. Properties of potential block will have to be investigated further on a single-channel level with higher concentrations of agonist (25-100 μM ACh).

There were consistent discrepancies throughout all of the MWC models. The most notable of these was that the 0.1 μM ACh data gave higher P_{open} simulated currents compared to the 1 μM ACh. This larger P_{open} is due to the fact that the 0.1 μM data has a 20–fold larger rate of entry into the diliganded open state. In our 1 μM data we do begin to see short closings disappearing which would account for the discrepancy between the two concentrations. All of the 0.1 μM models had higher rates between the singly-liganded and diliganded open state, which did not appear to have a large effect on simulated currents. We were unable to determine the reason behind the 0.1 μM data having an increase in these rates. In future studies we will need to investigate lower concentrations of ACh (1-50 nM) with dFBr and see if we still see similar effects as we have observed with 1 μM data.

127

3.4.4 HEPES Effects on HS Single-Channel Data

In previous studies, HEPES appeared to be a PAM selective for the HS subtype compared to LS $\alpha4\beta2$ and $\alpha7$ nicotinic acetylcholine receptors (Weltzin et al., 2014). HEPES is thought to potentiate and inhibit by binding to the $\beta2+/\beta2-$ interface of the HS $\alpha4\beta2$ receptors. It was also found that, inhibition of HEPES potentiated responses occurs at concentrations greater than 100 mM HEPES. Due to the binding location of HEPES, the presence of the Good's buffer could be altering our HS dFBr data.

In oocyte preparations, the presence of a HEPES buffer altered the efficacy of dFBr for the HS $\alpha4\beta2$ receptors. The lower efficacy of dFBr in the HS subtype may be the result of competition between HEPES and dFBr (Weltzin et al., 2014). In our preparations we utilized 5 mM of HEPES buffer, as is common in a lot of electrophysiology recordings. We believe that the presence of HEPES on HS receptors gives the appearance of increased desensitization in dFBr. This is due to HEPES binding at the $\beta2+/\beta2-$ interface, offsetting dFBr's steady state potentiating effects by inhibiting the receptor. Therefore, it would be wise in future single molecule studies of HS $\alpha4\beta2$ receptors to not utilize HEPES as a buffer in order to eliminate any unnecessary alterations in the observed gating.

Overall, we have provided a larger picture of the kinetics on a single-channel level of the high sensitivity $\alpha4\beta2$ nAChR and give more insight into the potential effects of dFBr on these receptors. Our data supports dFBr exhibiting potentiation by increasing peak current at all concentrations, but an overall decrease in charge transfer is observed at higher concentrations potentially due to the presence of HEPES. The

128

effect this has on desensitization largely depends on the concentration profile of ACh, with increased desensitization existing at higher concentrations. Our model offers one possibility to what we observed on a single-channel level for the HS receptors, and provides a starting point for future analysis of dFBr analogues.

3.5 Acknowledgements
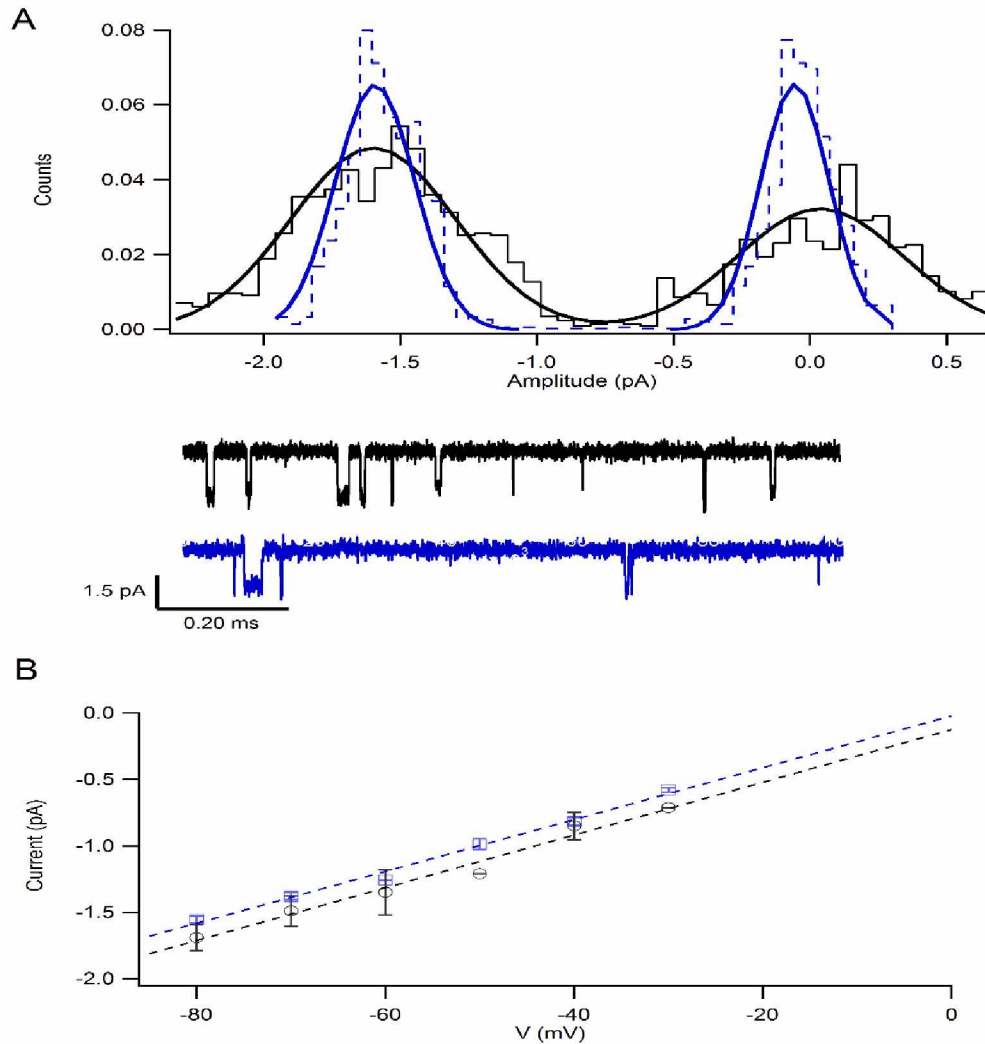
Figure 3.1: Unitary conductance's of $\alpha 4_2 \beta 2_3$ receptors. (A) Open point amplitude

distribution for high sensitivity (HS) conductance channels in the absence [19.5 pS ± 1.8

(mean±SD), black traces] and presence [19.9 pS ±0.34 (mean ±SD), blue traces] of

dFBr with respective traces underneath. Calibration: 200 ms and 1.5 pA. (B) I-V plot

shows mean value (± SD) for HS [19.9 ± 1.1 pS; n=7; black circles] recorded in 1 µM

ACh and HS receptors recorded in 1 µM ACh + 1 µM dFBr [19.8 ± 0.34 pS; n=4; blue

squares]. I/V data gave slopes of ~20 pS in the absence and presence of dFBr with

reversal potentials of 6.3 and 1.2 mV respectively.

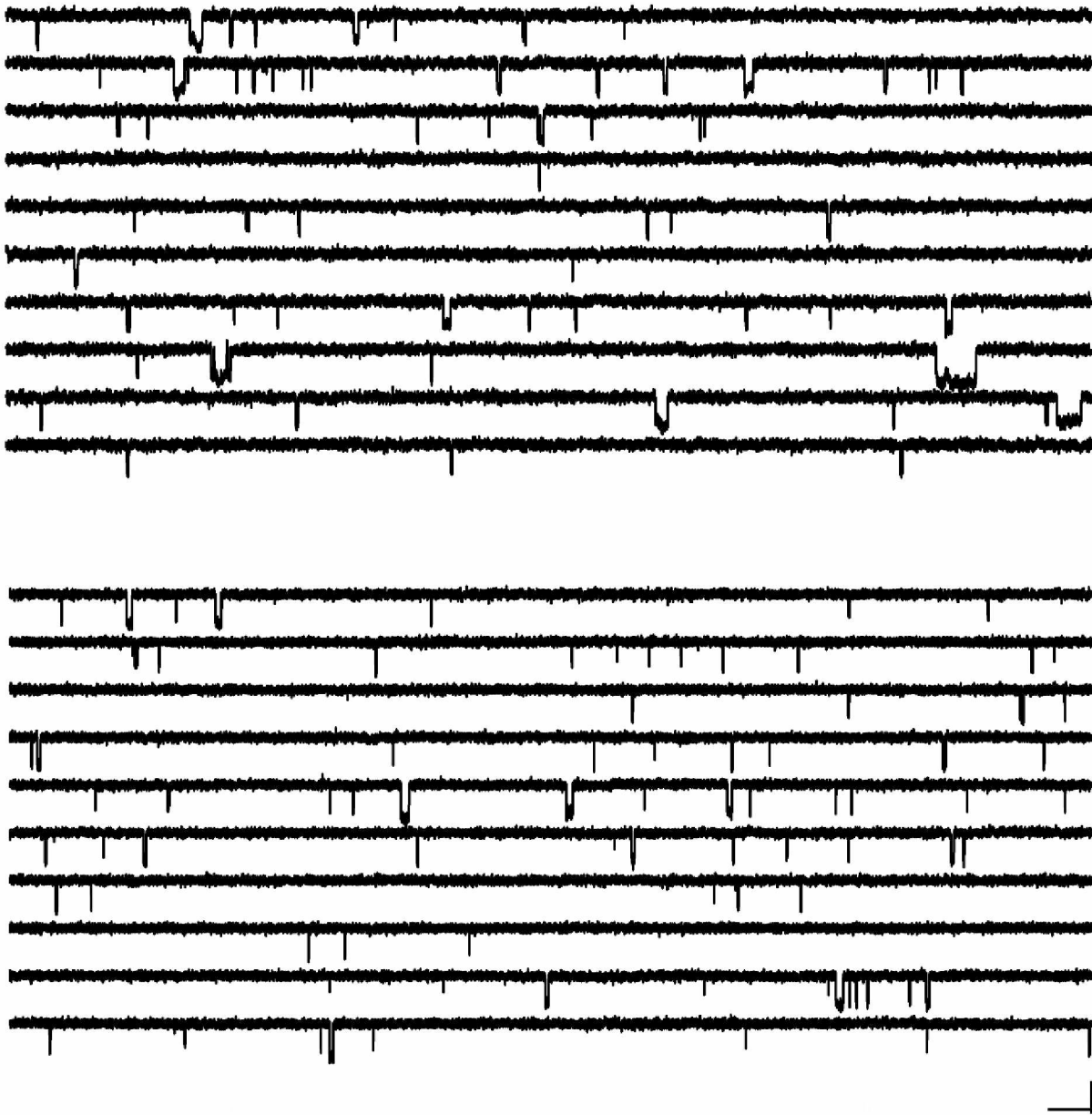Figure 3.2: Steady state recordings of $\alpha 4_2\beta 2_3$ receptors. Steady state recordings of HS in 1μM (top) and 1 μM ACh + 1 μM dFBr. Contiguous recordings of 50 s of data filtered at 1kHz (-3dB, 4-pole Bessel). Calibration: 100ms, 1.5 pA.
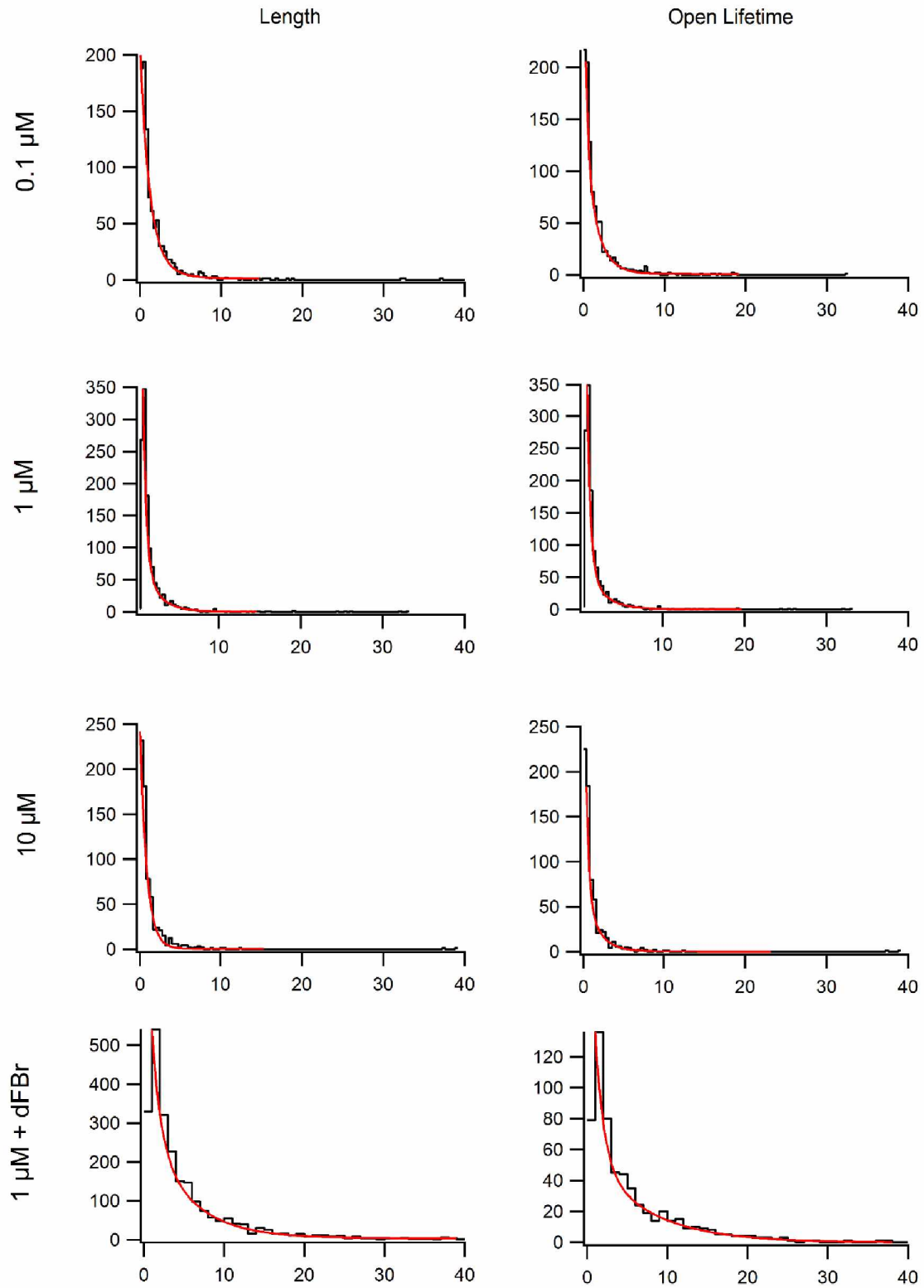
Figure 3.3: Burst characteristics of $\alpha 4_2 \beta 2_3$ receptors. See caption on next page

Figure 3.3: Burst characteristics of $\alpha4_2\beta2_3$ receptors. Distributions of burst length (left) and open lifetime (right). Distributions are fitted with two exponentials (red line) and are plotted up to 20 ms for comparison. Varied concentrations (0.1 μM, 1 μM, and 10 μM) of ACh are compared [t_{crit}: 1.13 ms, 1.65 ms, and 2.8 ms respectively] to 1 μM ACh + 1 μM dFBr (t_{crit}: 0.57 ms). Bursts usually contained single opening at concentrations greater than 0.1 μM and are defined in methods. Bursts length time constants slightly diminishes with increasing concentration [0.1 μM: τ_1= 1.2 ms, τ_2= 5.9 ms; 1 μM: τ_1= 3.12 ms, τ_2= 3.4 ms; 10 μM: τ_1= 0.96 ms, τ_2= 1.23 ms] with the presence of dFBr increasing τ_s [τ_1= 4.5 ms and τ_2= 5.04 ms]. A similar effect is observed with open lifetime [0.1 μM: τ_1= 1.1 ms, τ_2= 5.8 ms; 1 μM: τ_1= 2.9 ms, τ_2= 3.7 ms; 10 μM: τ_1= 0.9 ms, τ_2= 1.3 ms] with dFBr also increasing apparent open lifetime [τ_1=4.5 ms and τ_2= 10.7 ms].
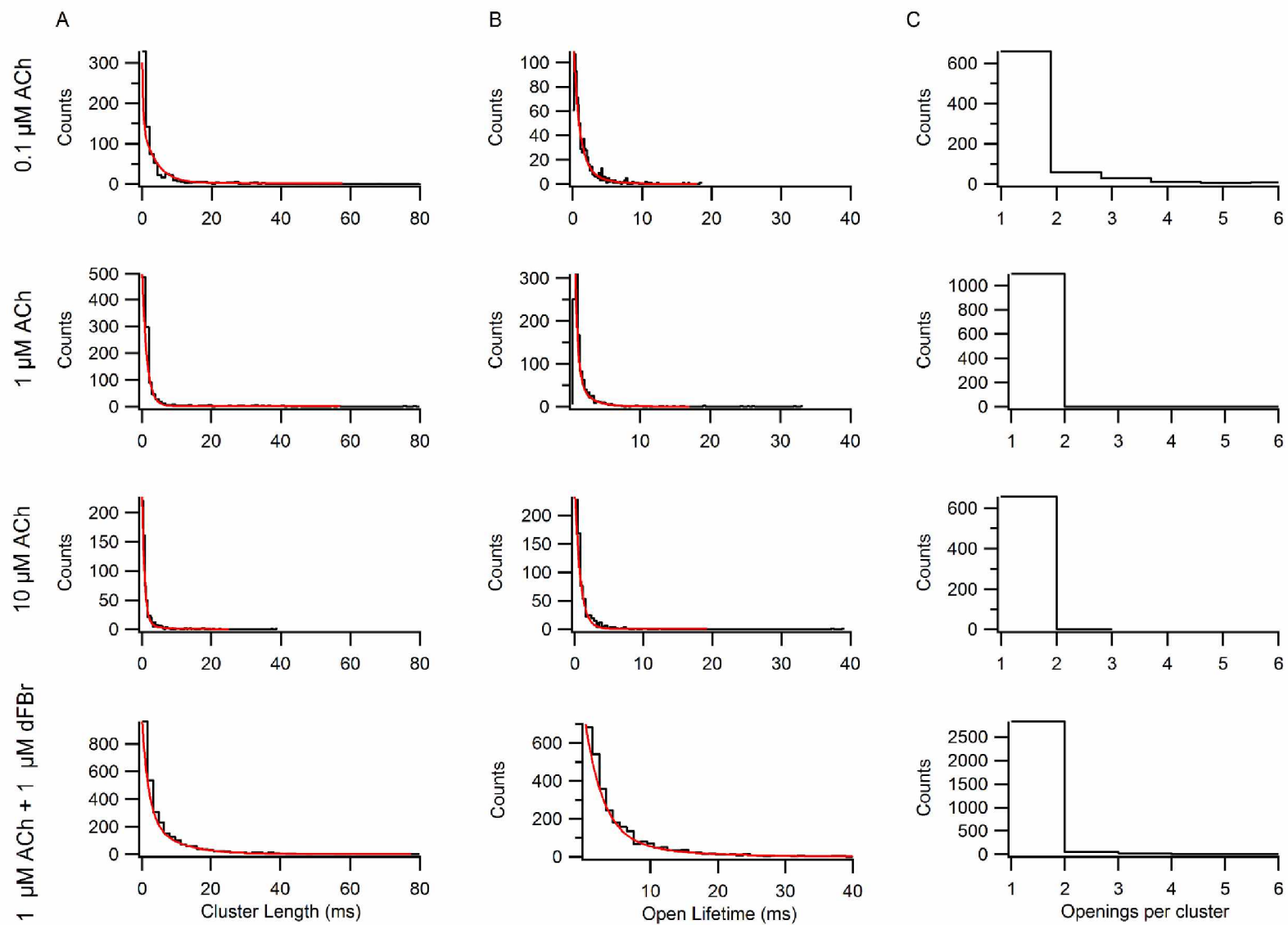
Figure 3.4: Cluster characteristics of $\alpha 4_2\beta 2_3$ receptors. See caption on next page

Figure 3.4: Cluster characteristics of $\alpha 4_2 \beta 2_3$ receptors. Distributions of cluster length

(left), open lifetime (middle), and openings per cluster (right). Distributions are fitted with

two exponentials (red line) for 0.1 μM (t_{crit}: 31.5 ms), 1 μM (t_{crit}: 42.2 ms) and 10 μM ACh

(t_{crit}: 20.4 ms) and 1 μM ACh + 1 μM dFBr (t_{crit}: 5.33 ms). The determination of critical

time is described in methods. (A) Cluster length for 0.1-10 μM ACh and 1 μM ACh + 1

μM dFBr. Distributions are plotted up to 80 ms for comparison between them. Cluster

length decreases with increasing ACh concentrations (0.1 μM: τ_1= 0.297 ms, τ_2= 4.01

ms; 1 μM: τ_1= 0.49 ms, τ_2= 2.43 ms; 10 μM: τ_1= 0.37 ms, τ_2= 1.83 ms). The presence

of dFBr increased the long time constant for cluster length (τ_1= 1.89 ms, τ_2= 8.48 ms).

(B) Distribution of open lifetime for 0.1 to 10 μM ACh and 1 μM ACh + 1 μM dFBr.

Distributions are plotted up to 40 ms for comparison. Open lifetimes decrease with

increasing concentration [0.1 μM: τ_1= 0.78 ms, τ_2= 2.1 ms; 1 μM: τ_1= 0.41 ms, τ_2= 1.9

ms; 10 μM: τ_1= 0.33 ms, τ_2= 1.6 ms]. (C) Histograms for openings per burst for 0.1-10

μM ACh and 1 μM ACh + 1 μM dFBr
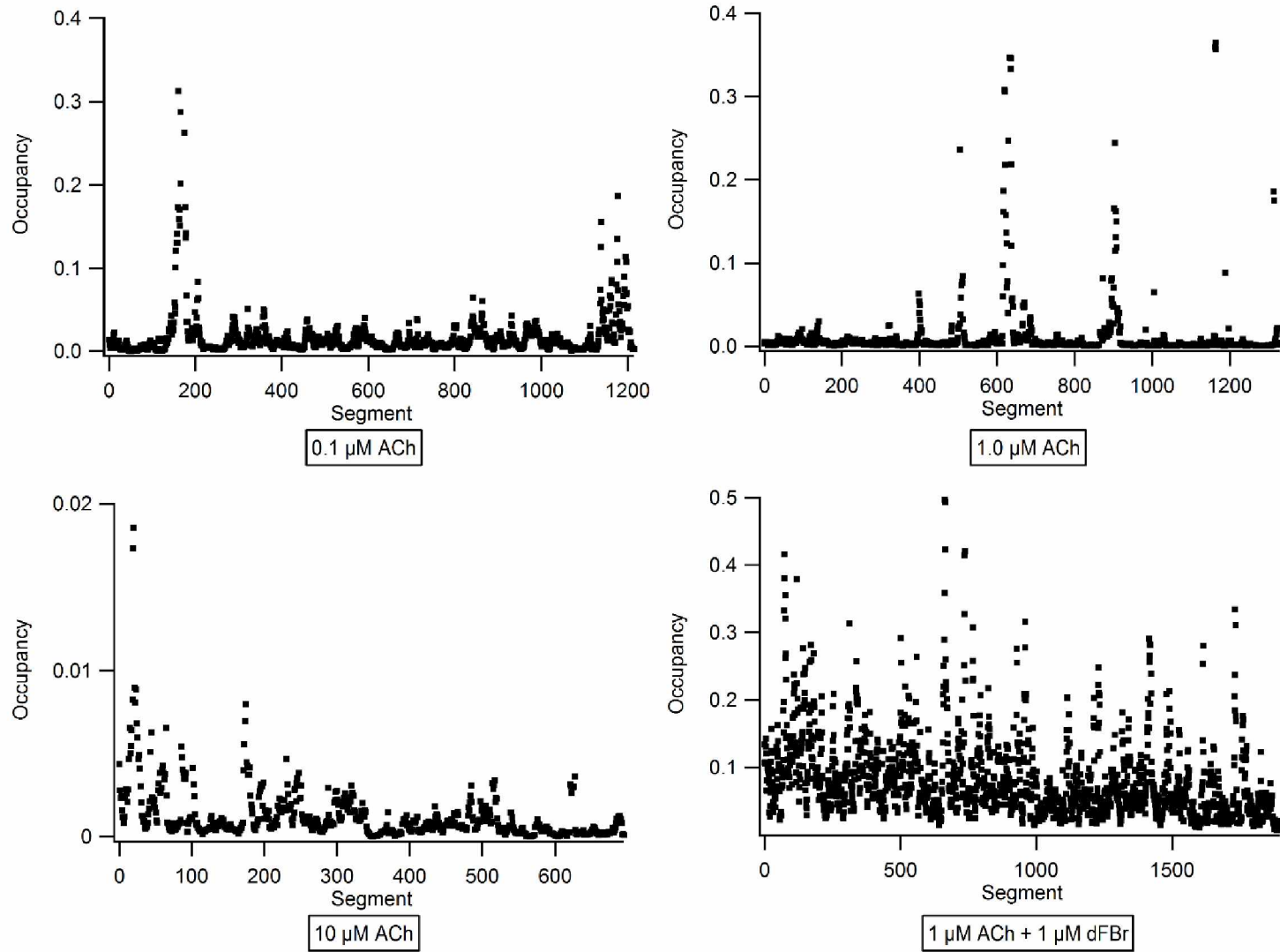
Figure 3.5: Stability plots for $\alpha4_2\beta2_3$ receptors. See caption on next page.

Figure 3.5: Stability plots for $\alpha 4_2 \beta 2_3$ receptors. Segments were plotted vs occupancy of the open state for 0.1-10 μM ACh and 1 μM ACh + 1 μM dFBr. 0.1 μM [top-left; 0.0067±0.014 (mean±SD)] and 1 μM ACh [top-right; 0.016±0.022 (mean±SD)], both contained one observable channel and were the most stable. 10 μM [bottom-left; 0.0011±0.0009 (mean±SD)] loses activity after ~500 segments and 1 μM ACh + 1 μM dFBr [bottom-right; 0.0502±0.04 (mean±SD)] loses activity after ~1200 segments, both contained more than one observable channel.
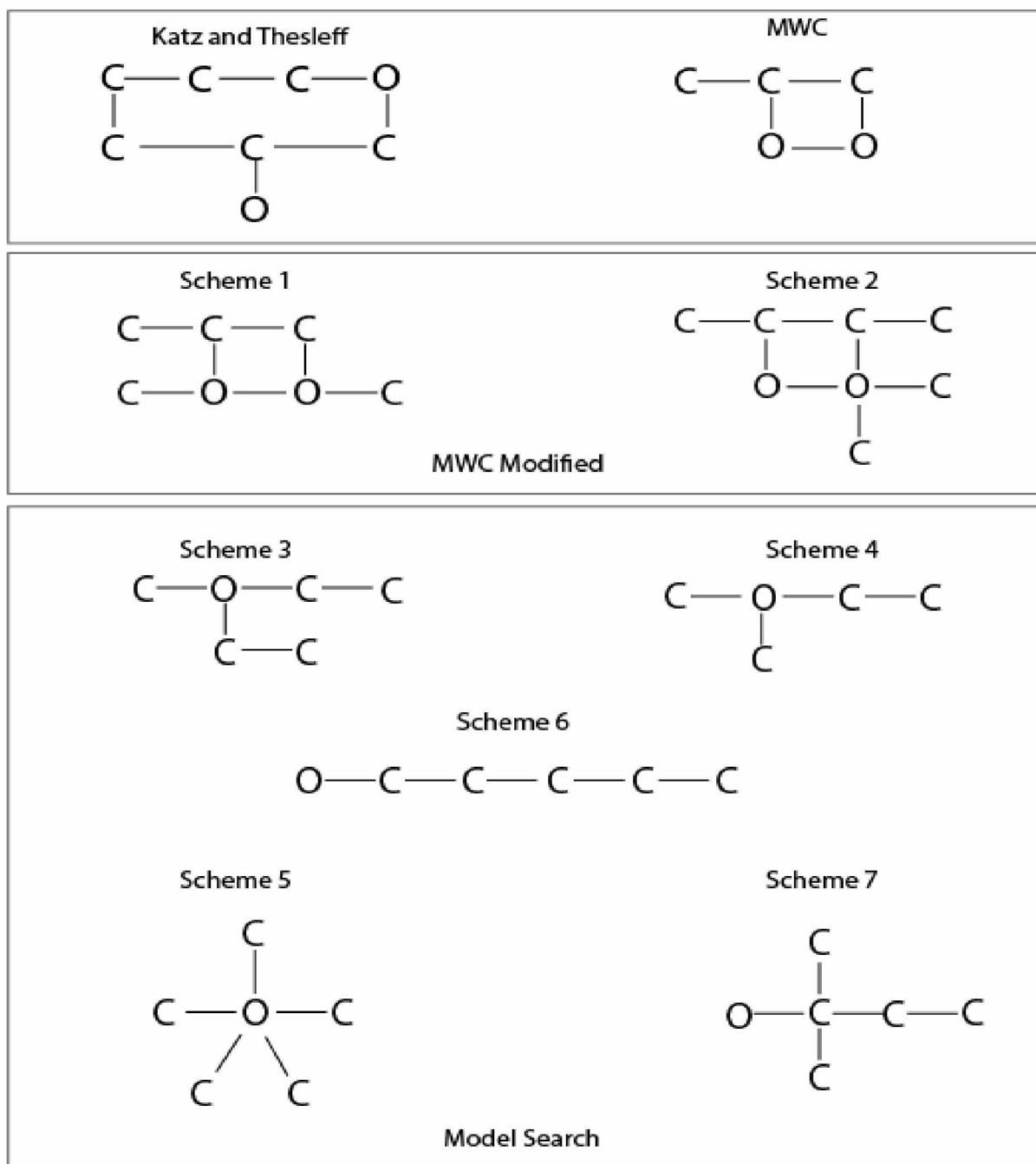
Figure 3.6: $\alpha 4_2 \beta 2_3$ receptor mechanisms. Mechanisms fitted to 0.1-10 μM ACh and 1 μM ACh + 1 μM dFBr data. Scheme 1-3 are mechanisms that include activation including classical Katz and Theslaff mechanisms. Scheme 3-7 are desensitization models based upon most common outcomes for QuB's model search.
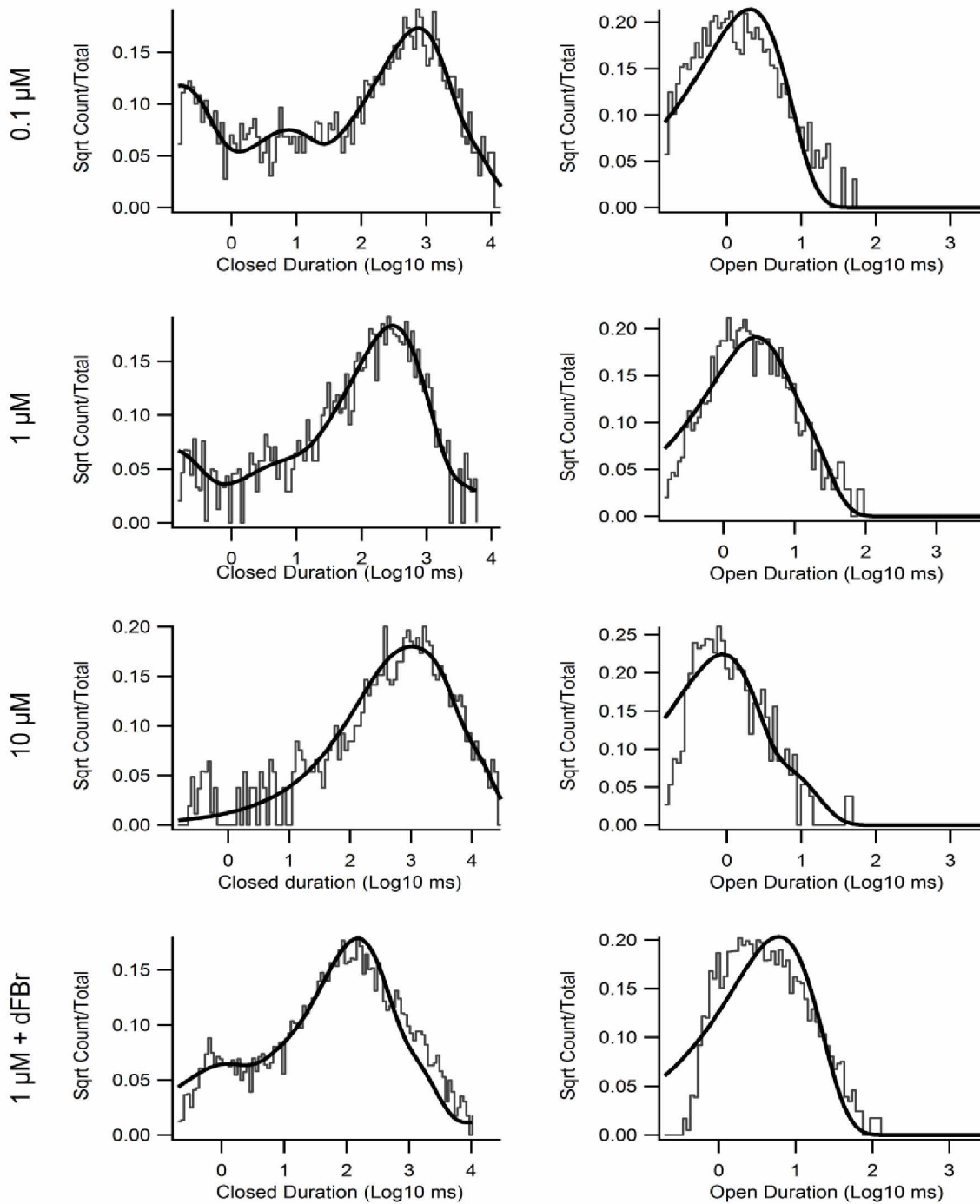
Figure 3.7: Katz and Thesleff model fits. Fits for the modified Katz and Thesleff shown

in Figure 3.6 for ACh concentrations 0.1 -10 µM and 1 µM ACh + 1 µM dFBr (bottom).
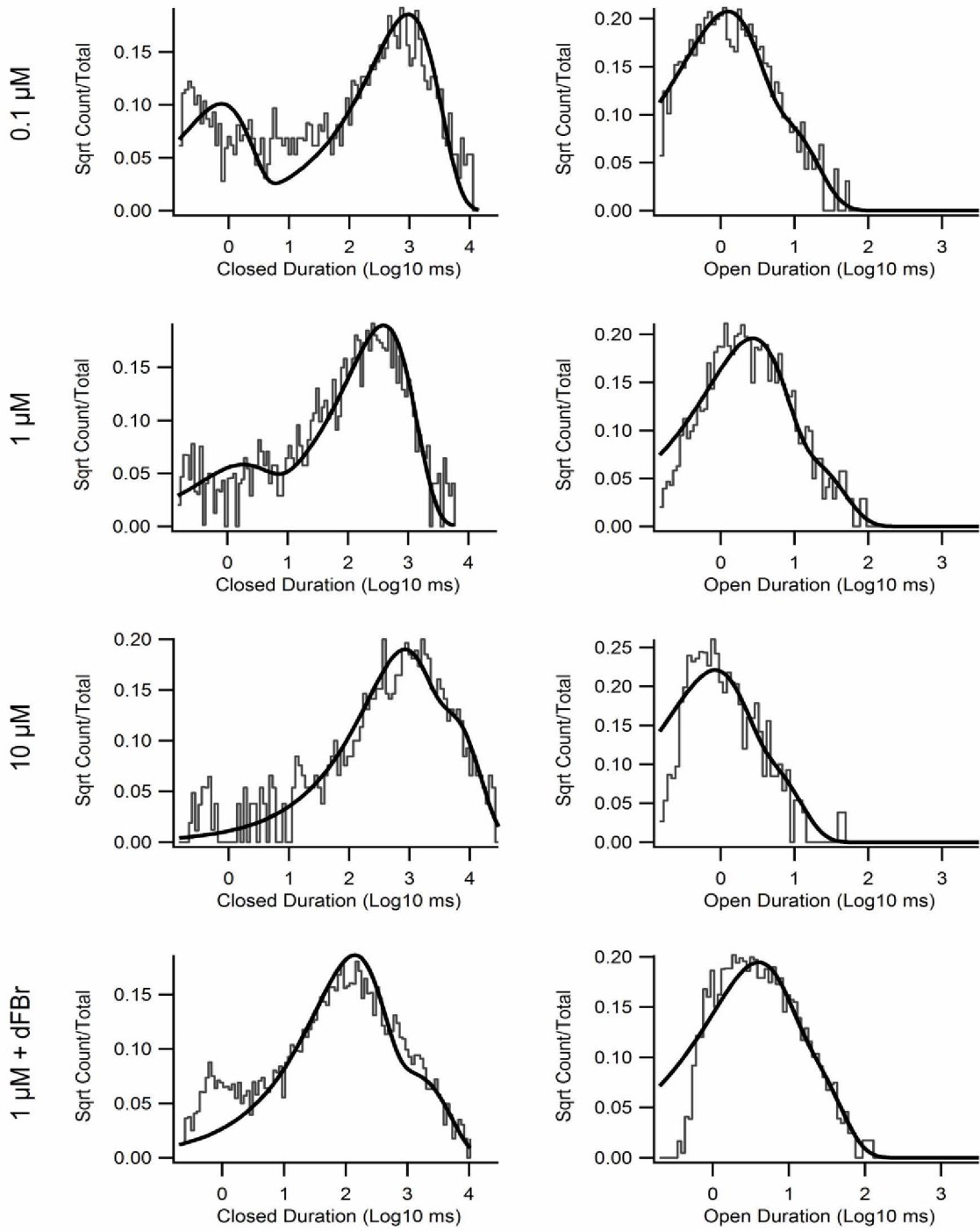
Figure 3.8: MWC model fits. Fits for the MWC shown in Figure 3.6 for ACh

concentrations 0.1 -10 μM and 1 μM ACh + 1 μM dFBr (bottom).
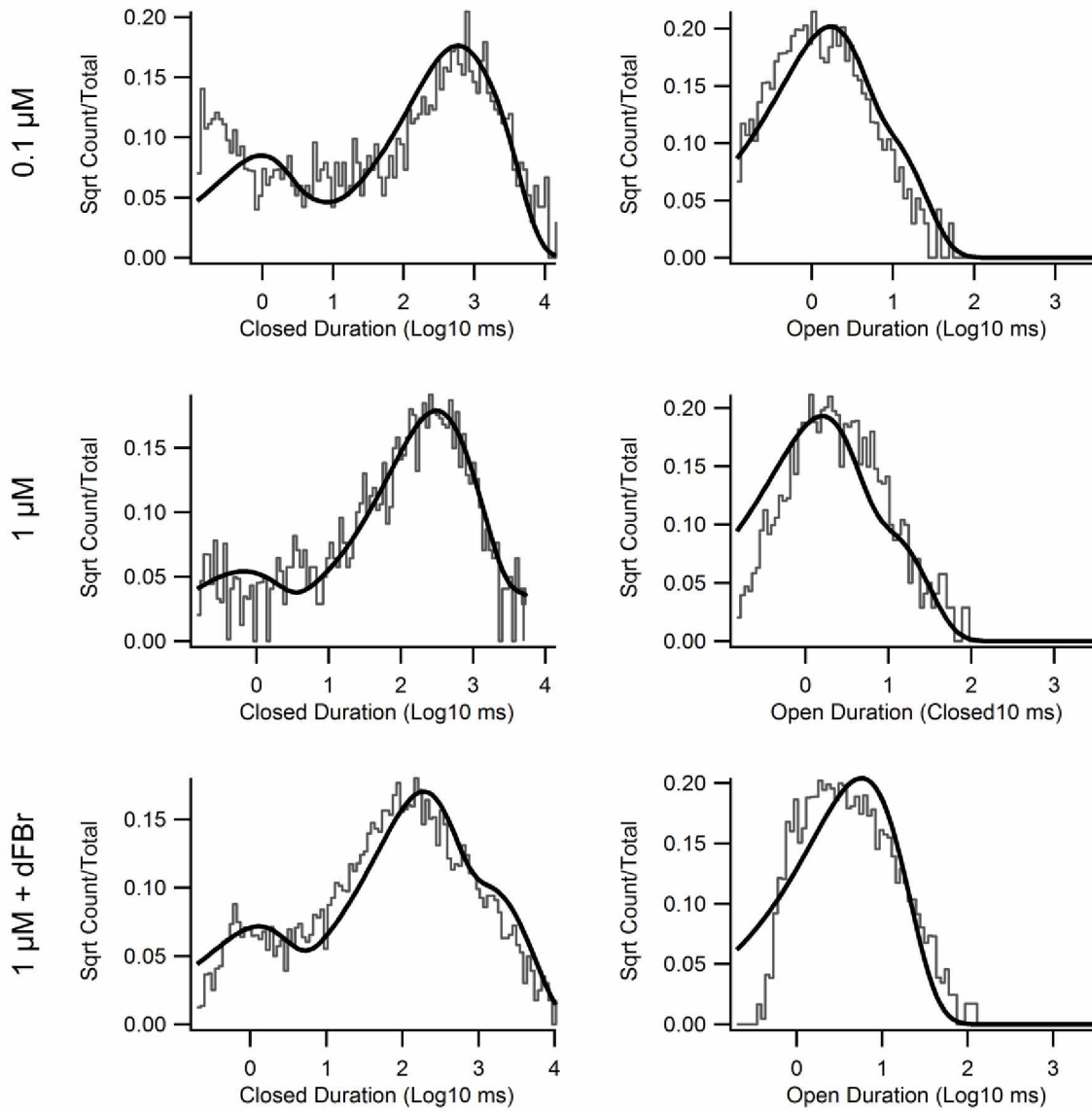
Figure 3.9: Scheme 1 model fits. Open and closed duration distributions from patches for 0.1 μM, 1 μM ACh and 1 μM ACh 1 μM dFBr (top, middle and bottom respectively) fitted with gating model scheme 1 shown in Figure 3.6. Scheme 1 is a modified version of the MWC model in Figure 3.4.
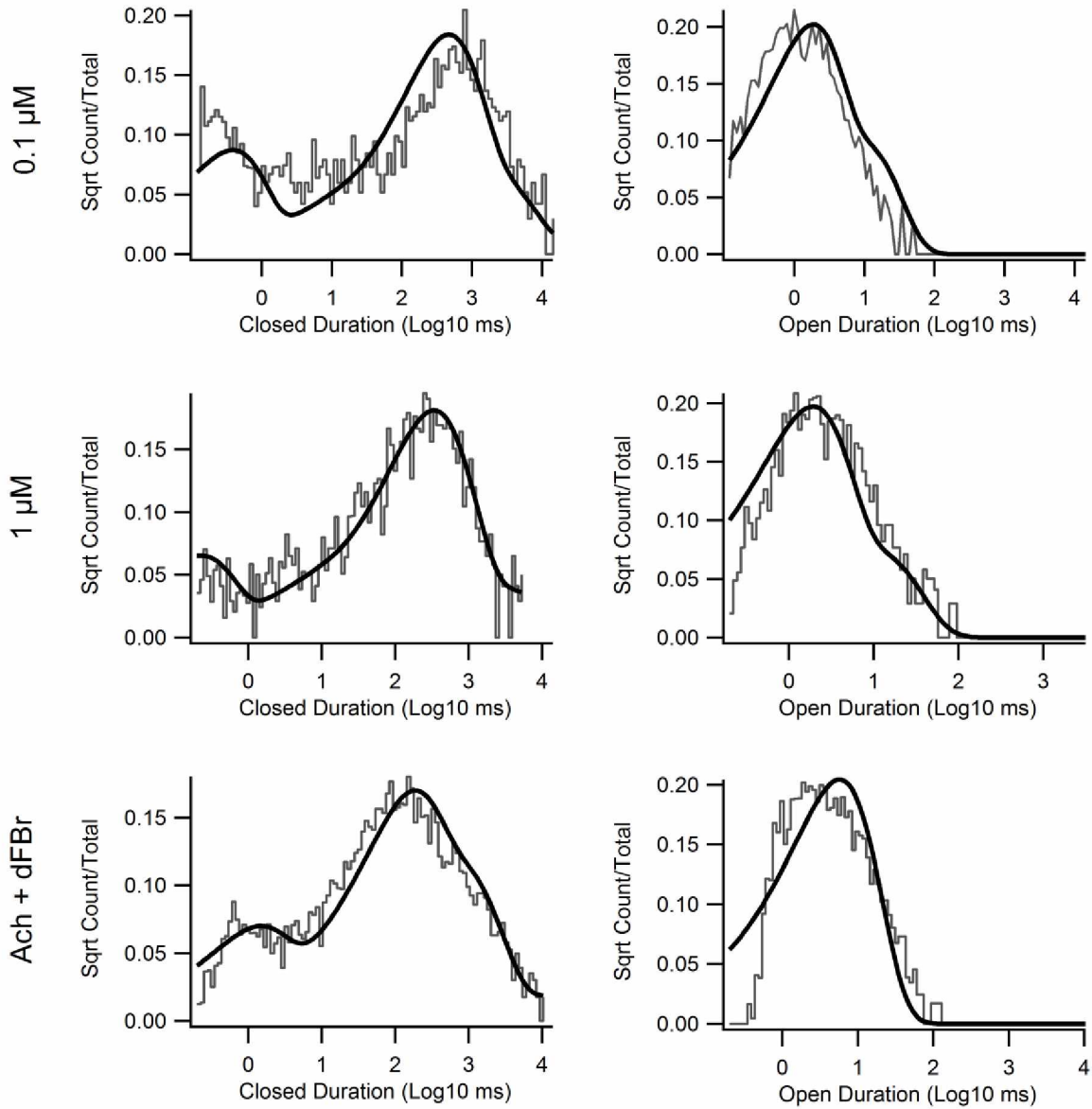
Figure 3.10: Scheme 2 model fits. Open and closed duration distributions from patches for 0.1 μM and 1 μM ACh (top, middle and bottom respectively) fitted with gating model scheme 2 shown in Figure 3.6. Scheme 2 is modified version of MWC models shown in Figure 3.4.

A
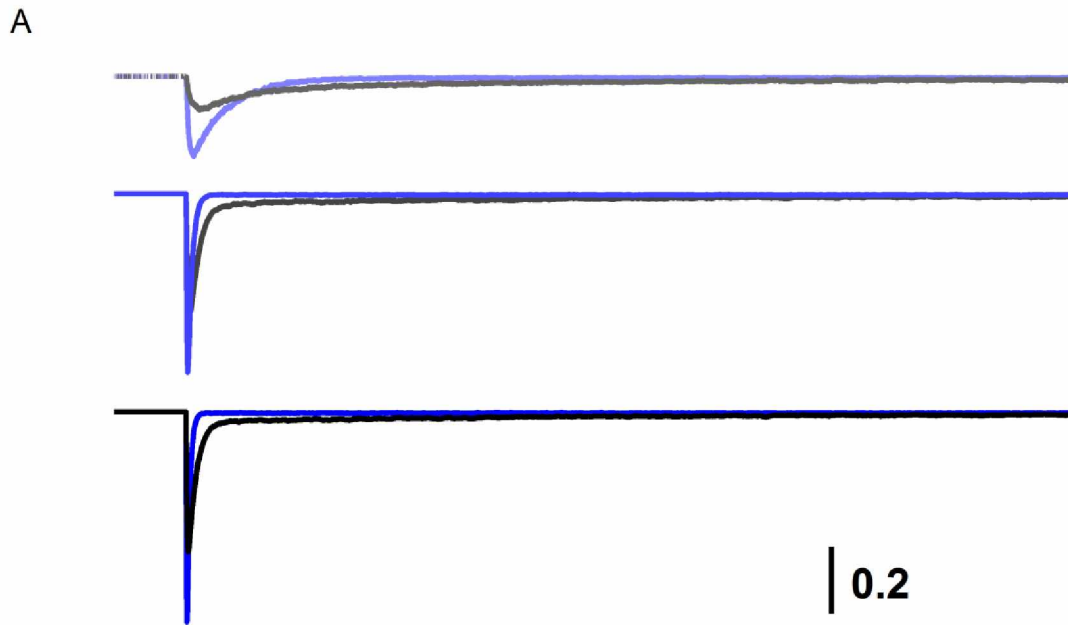
Figure 3.11A: Concentration dependence of peak and steady-state currents for scheme 2. (A) Simulated currents are shown for the ACh (black traces) and dFBr (blue traces) MWC based scheme 2 driven by 2.5 s jumps into 10 μM (top), 100 μM (middle), and 1 mM (bottom) ACh. Exponential functions were fitted to the decay phase of currents for all concentrations. For 1 mM ACh the exponential functions were ACh scheme 2: A_1= 0.37, τ_1= 17 ms, A_2=0.23, τ_2=794 ms, y_0= 0.008. dFBr scheme 2: A_1= 0.28, τ_f= 0.006 ms, A_2=0.32, τ_s=0.006 ms, y_0= 0.05. Rise times (10 – 90%) for ACh and dFBr models with 1 mM ACh were 5.4 ms and 2.1 ms, respectively. Calibration bar: units of open probability (P_{open}).

B
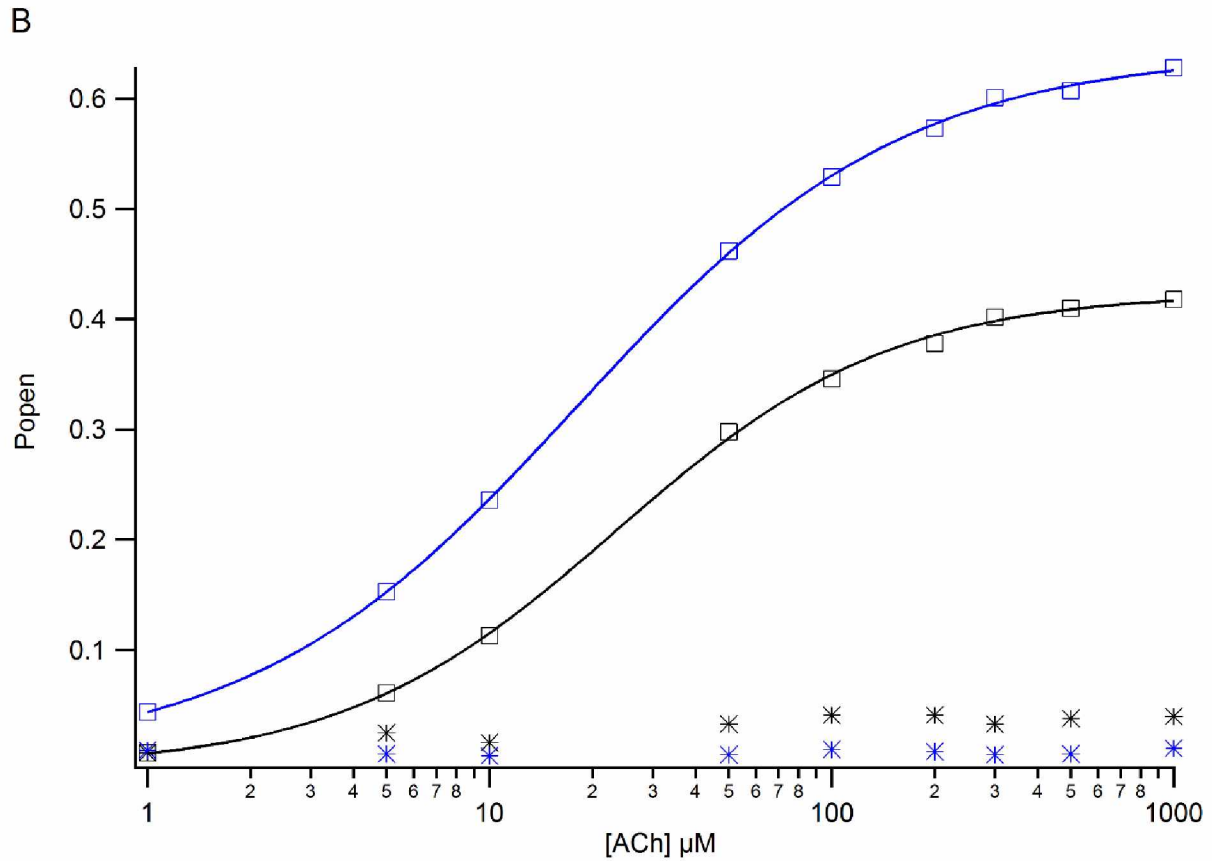
Figure 3.11B: Concentration dependence of peak and steady-state currents for scheme 2. (B) Open probability (P_{open}) of peak (squares) and steady-state (stars) responses are plotted for ACh (black) and dFBr (blue) scheme 2 models as a function of ACh concentration (1, 5, 10, 50, 100, 200, 300, 500, and 1000 μM). The P_{open} at the peak for saturating ACh concentration was ~ 0.42 for ACh and 0.63 for dFBr.

C
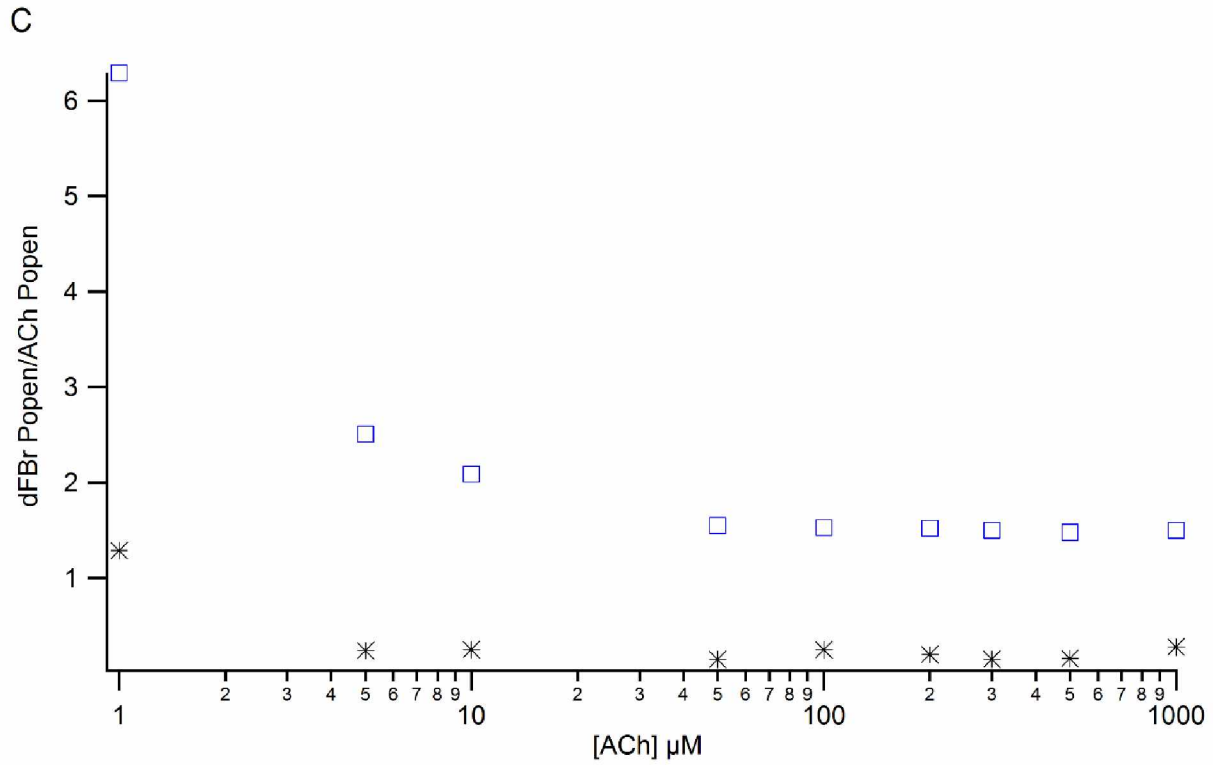
Figure 3.11C: Concentration dependence of peak and steady-state currents for scheme 2. (C) The ratio of dFBr to ACh scheme 2 P_{open} is shown as a function of ACh concentration. Potentiation of peak response (stars) was largest at very low ACh (600% increase for 1 μM ACh) and declined to a steady value of 150% increase at 50 μM ACh. Steady-state, desensitized responses (blue star) were diminished ~25% at concentrations above 1 μM ACh.

146

A
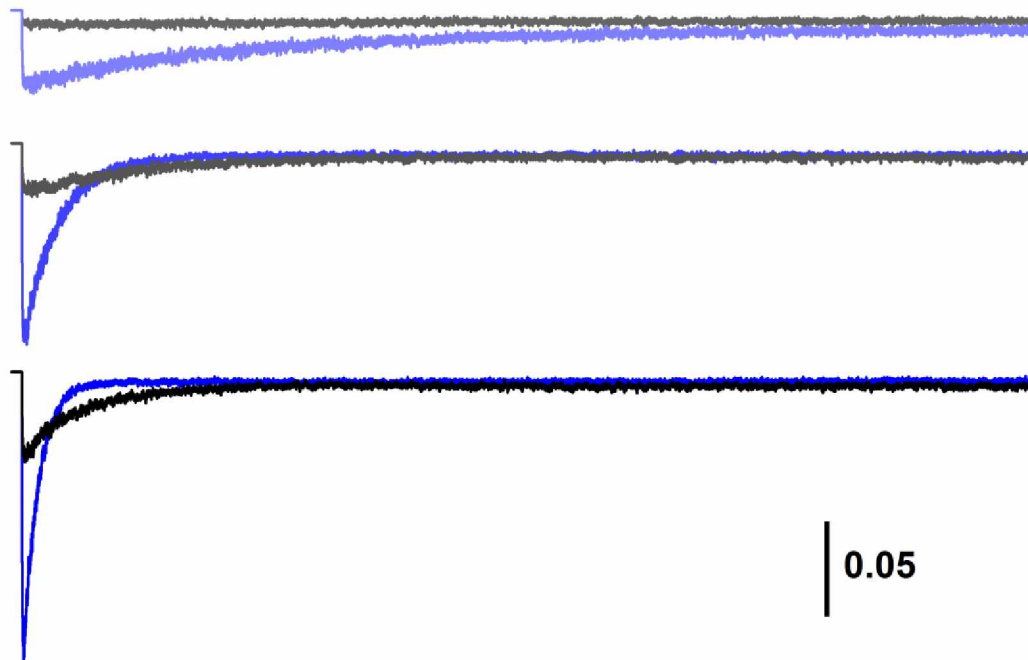
Figure 3.12A: Potentiation of peak and steady-state currents at low concentrations of

ACh. (A) Simulated currents at low concentrations are shown for the ACh (black

traces) and dFBr (blue traces) scheme 2 models driven by 15 s jumps into 1 μM (top), 3

μM (middle), and 5 μM (bottom) ACh. Calibration bar: units of open probability (P_{open}).

B
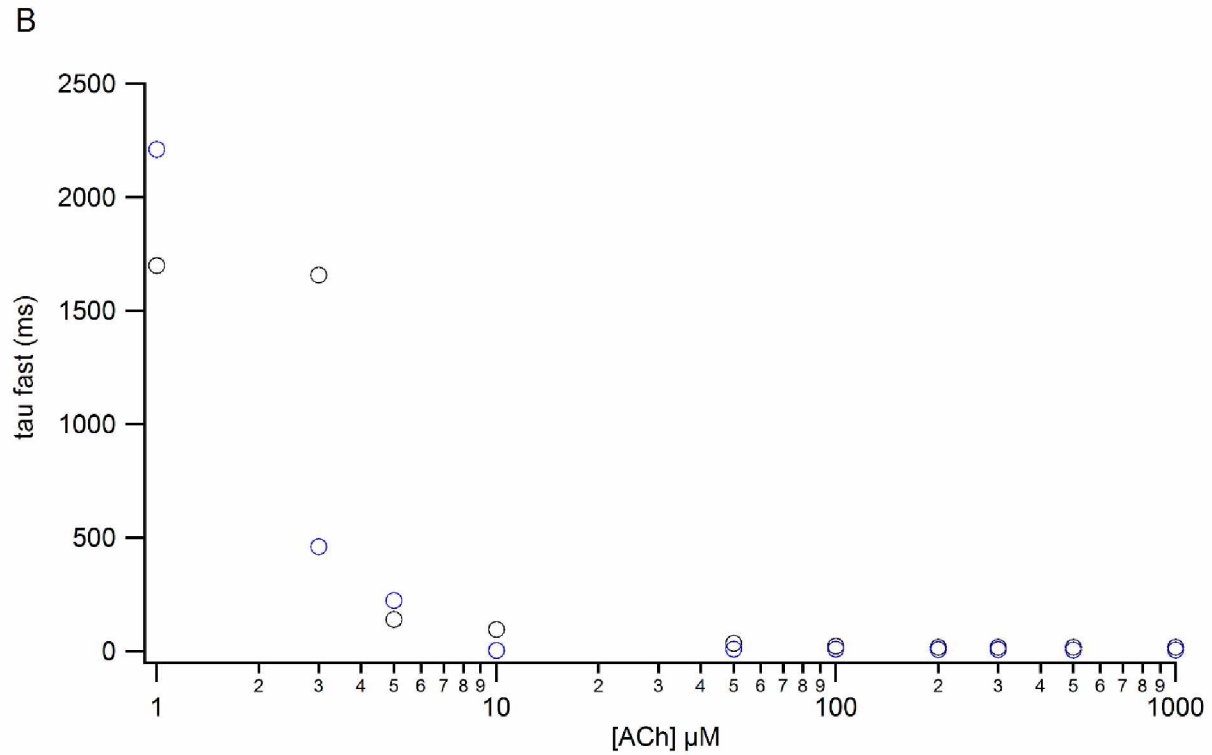
Figure 3.12B: Potentiation of peak and steady-state currents at low concentrations of ACh. (B) The fast time (τ_f) component are plotted for ACh (black) and dFBr (blue) scheme 2 models as a function of ACh concentration (1, 3, 5, 10, 50, 100, 200, 300, 500, 1000 μM). dFBr only showed slower τ_f at 1 μM ACh, higher concentrations yielded faster decay time courses.

C
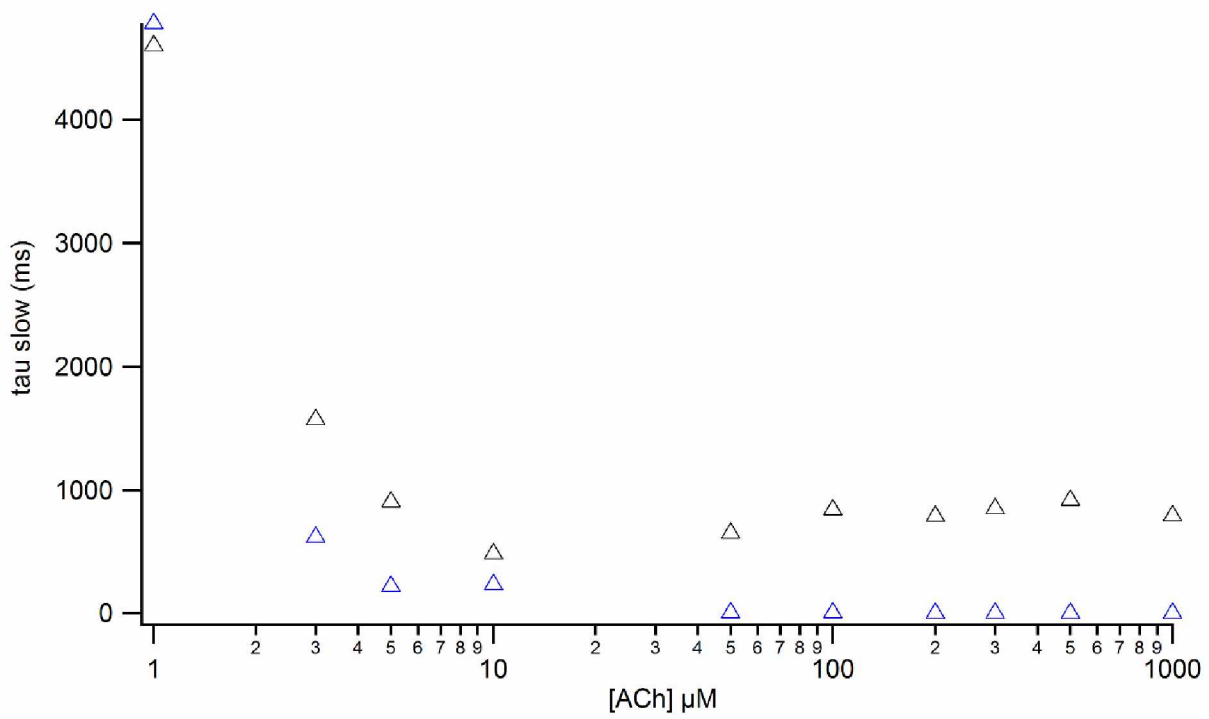
Figure 3.12C: Potentiation of peak and steady-state currents at low concentrations of ACh. (C) The slow time (τ_s) component are plotted for ACh and dFBr scheme 2 models as a function of ACh concentration. Slower time component at concentrations higher than 10 μM, almost completely disappears in the presence of dFBr.
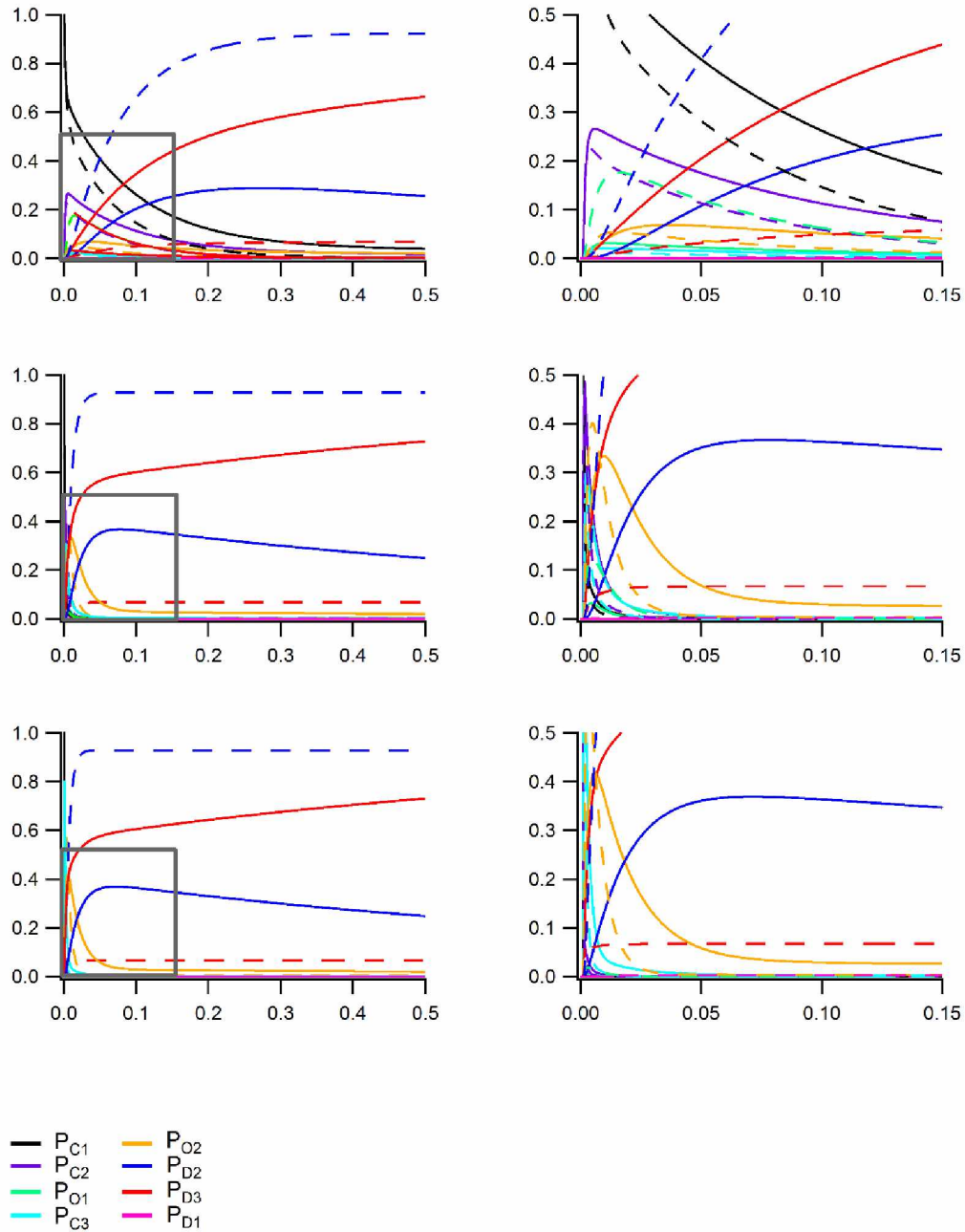
Figure 3.13: Occupancy probabilities of $\alpha 4_2 \beta 2_3$ receptors using a concentration jump profile. Left: Occupancy probabilities (y-axis) of channel states after a concentration jump are shown for 10, 100 and 1000 μM ACh (top to bottom) using either the scheme 2 for ACh (solid lines) or scheme 2 for dFBr (dashed lines). Right: enlarged portion (grey squares, y-axis: 0.5 and x-axis: 0.15).

150

A
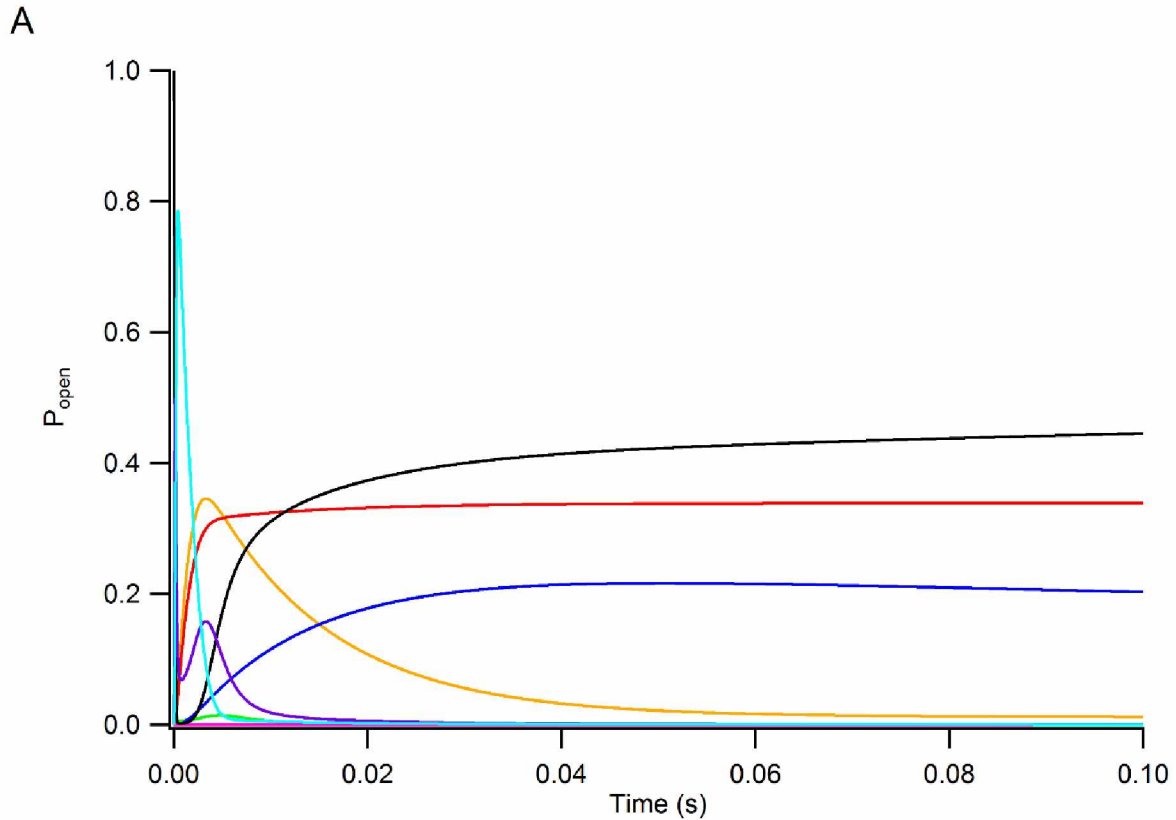
Figure 3.14A: Response to a pulse of a high concentration of agonist. Occupancy

probabilities are shown for models driven by an alpha function to mimic a synaptic

agonist concentration profile. (A) Responses shown for the ACh model. Peak open

probability (P_{O2}) was 0.352 at 3.4 ms compared with 0.634 at 2.1 ms for dFBr (shown in

B; 1.8-fold potentiation). The decay of P_{O2} was fitted with one exponential (τ=12.9 ms).

P_{D2} was fitted with two exponential components (A_1=0.60, τ_1=526 ms, A_2=0.40, τ_2=633

ms, y_0=0), and P_{D3} was fitted with one components (τ=6.7 s, y_0=0).

B
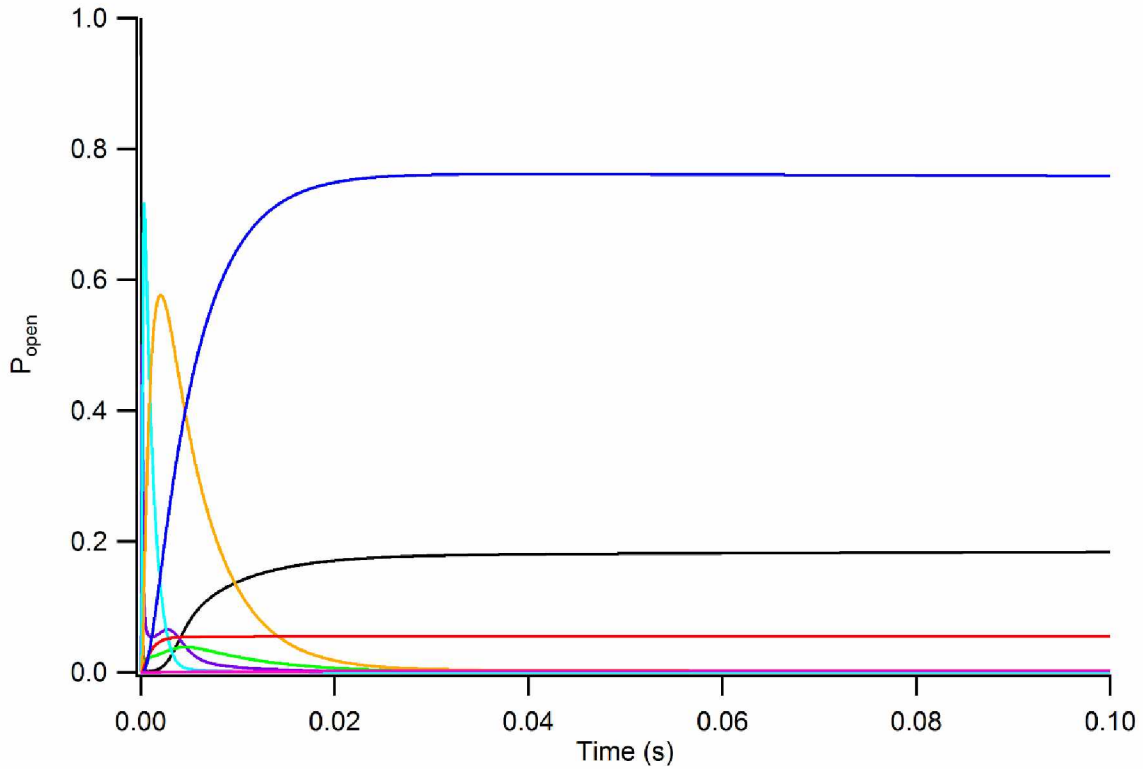
Figure 3.14B: Response to a pulse of a high concentration of agonist. (B) For the dFBr model the decay of P_{O2} was also fitted with one exponential component (τ=5 ms). P_{D2} was fitted with two components (A_1=0.54, τ_1=18.1 s, A_2=0.46, τ_2=15.2 s, y_0=0), and P_{D3} was fitted with a single exponential (τ=21.8 s, y_0=0).

Table 3.1: Rate constants for Katz and Thesleff mechanism
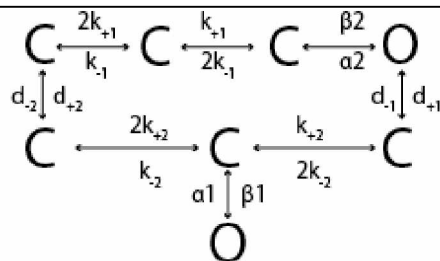
		Table 3.1			
Rate constants	*Unit*	*0.1 μM*	*1 μM*	*10 μM*	*+dFBr*
$2k_{+1}$	$M^{-1}s^{-1}$	7E9 ± 18%	1E9 ± 32%	2E6 ± 100%	5E9 ± 20%
k_{+1}	$M^{-1}s^{-1}$	3.5E9 ± 18%	5.5E8 ± 32%	9.6E5 ± 100%	2.5E9 ± 20%
$2k_{-1}$	s^{-1}	4803 ± 16%	6720 ± 21%	2.5 ± 84%	1189 ± 17%
k_{-1}	s^{-1}	2401 ± 16%	3360 ± 21%	1.3 ± 79%	595 ±
β_1	s^{-1}	0.5 ± 11%	2.3 ± 6%	1.7 ± 8%	1.1 ± 6%
α_1	s^{-1}	657 ± 11%	447 ± 5%	1250 ± 6%	225 ± 4%
β_2	s^{-1}	2206 ± 36%	3113 ± 46%	2E-6 ± 100%	146 ± 66%
α_2	s^{-1}	619 ± 34%	156 ± 41%	0.001 ± 100%	164 ± 37%
$2k_{+2}$	$M^{-1}s^{-1}$	2.2E5 ± 27%	6.5E5 ± 32%	1.2E6 ± 100%	8E5 ± 23%
k_{+2}	$M^{-1}s^{-1}$	1.1E5 ± 18%	3.2E4 ± 31%	9.6E5 ± 100%	4E5 ±23%
$2k_{-2}$	s^{-1}	0.07 ± 29%	0.03 ± 33%	2.2 ± 32%	0.04 ± 30%
k_{-2}	s^{-1}	0.035 ± 29%	0.02 ± 40%	1.1 ± 31%	0.02 ± 30%
d_{+1}	s^{-1}	170 ± 33%	288 ± 51%	602 ± 100%	183 ± 30%
d_{-1}	s^{-1}	11 ± 17%	18 ± 36%	5.5 ± 100%	111 ± 32%
d_{+2}	s^{-1}	4.1 ± 65%	24 ± 26%	240 ± 100%	0.2 ± 100%
d_{-2}	s^{-1}	0.2 ± 50%	0.18 ± 28%	0.78 ± 100%	0.005 ± 100%

Table 3.2: Rate constants for MWC mechanism.

$$C \underset{k_{-1}}{\overset{2k_{+1}}{\rightleftharpoons}} C \underset{2k_{-1}}{\overset{k_{+1}}{\rightleftharpoons}} C$$

$$\alpha 1 \Big| \beta 1 \qquad \alpha 2 \Big| \beta 2$$

$$O \underset{k_{-2}}{\overset{k_{+2}}{\rightleftharpoons}} O$$
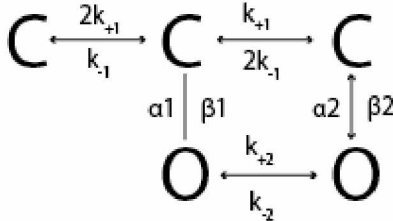
	Table 3.2				
Rate constants	Unit	0.1 μM	1 μM	10 μM	dFBr
$2k_{+1}$	$M^{-1}s^{-1}$	4.9E7 ± 10%	2.4E7 ± 24%	4E4 ± 100%	4E5 ± 300%
k_{+1}	$M^{-1}s^{-1}$	2.4E7 ± 10%	1.2E7 ± 24%	2E4 ± 100%	2E5 ± 300%
$2k_{-1}$	s^{-1}	1080 ± 16%	931 ± 20%	0.85 ± 21%	1.7 ± 12%
k_{-1}	s^{-1}	2167 ± 16%	466 ± 20%	0.42 ± 21%	0.85 ± 12%
$\beta 1$	s^{-1}	362 ± 24%	405 ± 24%	1.2 ± 100%	5.5 ± 100%
$\alpha 1$	s^{-1}	818 ± 10%	28 ± 33%	1385 ± 100%	246 ± 100%
$\beta 2$	s^{-1}	15 ± 21%	303 ± 49%	1.4 ± 100%	4E-5 ± 100%
$\alpha 1$	s^{-1}	0.1 ± 24%	85 ± 77%	329 ± 100%	6E-4 ± 100%
k_{+2}	$M^{-1}s^{-1}$	2.2E9 ± 17%	580 ± 100%	92 ± 100%	3.8E7 ± 100%
k_{-2}	s^{-1}	103 ± 26%	0.001 ± 100%	0.001 ± 100%	103 ± 100%

Table 3.3: Rate constants for scheme 1 fits.

$$C \xrightarrow[k_{-1}]{2k_{+1}} C \xrightarrow[2k_{-1}]{k_{+1}} C$$
$$\alpha1 \;\big|\; \beta1 \qquad \alpha2 \;\big|\; \beta2$$
$$C \xleftarrow[d_{+1}]{d_{-1}} O \xrightarrow[k_{-2}]{k_{+2}} O \xrightarrow[d_{-2}]{d_{+2}} C$$

Table 3.3				
Rate	Unit	0.1 μM	1 μM	+dFBr
$2k_{+1}$	$M^{-1}s^{-1}$	7.6E7 ± 98%	2.32E7 ± 26%	3.8E7 ± 100%
k_{+1}	$M^{-1}s^{-1}$	3.8E7 ± 98%	1.16E7 ± 26%	1.9E7 ± 100%
$2k_{-1}$	s^{-1}	1712 ± 35%	2455 ± 12%	1472 ± 8%
k_{-1}	s^{-1}	856 ± 35%	1227 ± 12%	736 ± 8%
$\beta1$	s^{-1}	396 ± 59%	114 ± 32%	137 ± 18%
$\alpha1$	s^{-1}	287 ± 28%	671 ± 30%	175 ± 18%
$\beta2$	s^{-1}	37 ± 22%	1543 ±59%	519 ± 100%
$\alpha2$	s^{-1}	0.1 ± 100%	29 ± 98%	22.4 ± 100%
k_{+2}	$M^{-1}s^{-1}$	9.1E8 ± 100%	1.1E6 ± 100%	0.0048 ± 0.01%
k_{-2}	s^{-1}	147 ± 32%	0.76 ± 100%	1.3E-8 ± 100%
d+1	s^{-1}	307 ± 60%	54 ± 11%	0.18 ± 53%
d-1	s^{-1}	0.49 ± 70%	0.14 ± 11%	8.6E-4 ± 11%
d+2	s^{-1}	33 ± 35%	99 ± 5%	99 ± 3.3%
d-2	s^{-1}	361 ± 58%	5.3 ± 8%	0.7 ± 3.7%

155

Table 3.4: Rate constants for scheme 2 fits.

$$C \underset{k_{-1}}{\overset{2k_{+1}}{\rightleftharpoons}} C \underset{2k_{-1}}{\overset{k_{+1}}{\rightleftharpoons}} C \underset{d_{-3}}{\overset{d_{+3}}{\rightleftharpoons}} C$$

$$\alpha_1 \updownarrow \beta_1 \qquad \alpha_2 \updownarrow \beta_2$$

$$O \underset{k_{-2}}{\overset{k_{+2}}{\rightleftharpoons}} O \underset{d_{-2}}{\overset{d_{+2}}{\rightleftharpoons}} C$$

$$d_{-1} \updownarrow d_{+1}$$

$$C$$

	Table 4.4			
Rate	*Unit*	*0.1 μM*	*1 μM*	*+dFBr*
$2k_{+1}$	$M^{-1}s^{-1}$	9 E7 ± 13%	2.8E7 ± 32%	3.5E7 ± 94%
k_{+1}	$M^{-1}s^{-1}$	4.5E7 ± 13%	1.4E7 ± 33%	1.7E7 ± 94%
$2k_{-1}$	s^{-1}	794 ± 12%	1261 ± 20%	1678 ± 7.8%
k_{-1}	s^{-1}	397 ± 12%	631 ± 20%	839 ± 7.8%
β_1	s^{-1}	82 ± 52%	52 ± 42%	178 ± 95%
α_1	s^{-1}	1090 ± 8.5%	417 ± 35%	181 ± 90%
β_2	s^{-1}	6370b ± 18.6%	323 ± 71%	1000 ± 24%
α_2	s^{-1}	300 ± 17%	40 ±95%	27 ± 98%
k_{+2}	$M^{-1}s^{-1}$	3.3E9 ± 25%	2E3 ± 99%	2.7 ±74%
k_{-2}	s^{-1}	214 ± 18%	0.003 ± 99%	7.2E-6 ± 99%
d_{+1}	s^{-1}	3 ± 99%	2.7E-4 ± 99%	0.39 ± 56%
d_{-1}	s^{-1}	0.35 ± 98%	0.023 ± 99%	3.7E-5 ± 99%
d_{+2}	s^{-1}	57 ± 29%	44 ± 23%	195 ± 3.5%
d_{-2}	s^{-1}	0.33 ± 18%	4.3 ± 35%	0.77 ± 4%
d_{+3}	s^{-1}	975 ± 25%	236 ± 55%	63 ± 55%
d_{-3}	s^{-1}	43 ± 50%	0.19 ± 31%	0.08 ± 41%

156

3.6 References

Buisson, B., and D. Bertrand. 2001. Chronic exposure to nicotine upregulates the human (alpha)4((beta)2 nicotinic acetylcholine receptor function. *J. Neurosci.* 21:1819–1829. doi:21/6/1819 [pii].

Buisson, B., M. Gopalakrishnan, S.P. Arneric, J.P. Sullivan, and D. Bertrand. 1996. Human alpha4beta2 neuronal nicotinic acetylcholine receptor in HEK 293 cells: A patch-clamp study. *J. Neurosci.* 16:7880–7891.

Changeux, J.-P. 2010. Nicotine addiction and nicotinic receptors: lessons from genetically modified mice. *Nat. Rev. Neurosci.* 11:389–401. doi:10.1038/nrn2849.

Colquhoun, D., and B. Sakmann. 1985. Fast events in single-channel currents activated by acetylcholine and its analogues at the frog muscle end-plate. *J. Physiol.* 369:501–57. doi:10.1113/jphysiol.1985.sp015912.

Descarries, L., V. Gisiger, and M. Steriade. 1997. Diffuse transmission by acetylcholine in the CNS. *Prog. Neurobiol.* 53:603–625. doi:10.1016/S0301-0082(97)00050-6.

Edelstein, S.J., O. Schaad, E. Henry, D. Bertrand, and J.P. Changeux. 1996. A kinetic mechanism for nicotinic acetylcholine receptors based on multiple allosteric transitions. *Biol. Cybern.* 75:361–79. doi:10.1007/s004220050302.

Elenes, S., and A. Auerbach. 2002. Desensitization of diliganded mouse muscle nicotinic acetylcholine receptor channels. *J. Physiol.* 541:367–383. doi:10.1113/jphysiol.2001.016022.

Khiroug, S.S., L. Khiroug, and J.L. Yakel. 2004. Rat nicotinic acetylcholine receptor alpha2beta2 channels: comparison of functional properties with alpha4beta2 channels in Xenopus oocytes. *Neuroscience.* 124:817–22. doi:10.1016/j.neuroscience.2004.01.017.

Kim, J.S., A. Padnya, M. Weltzin, B.W. Edmonds, M.K. Schulte, and R.A. Glennon. 2007. Synthesis of desformylflustrabromine and its evaluation as an $\alpha 4 \beta 2$ and $\alpha 7$ nACh receptor modulator. *Bioorganic Med. Chem. Lett.* 17:4855–4860. doi:10.1016/j.bmcl.2007.06.047.

Nelson, M.E., A. Kuryatov, C.H. Choi, Y. Zhou, and J. Lindstrom. 2003. Alternate Stoichiometries of alpha 4beta 2 Nicotinic Acetylcholine Receptors. *Mol Pharmacol.* 63:332–341. doi:10.1124/mol.63.2.332.

Nicolai, C., and F. Sachs. 2013. Solving Ion Channel Kinetics with the QuB Software. *Biophys. Rev. Lett.* 8:191–211. doi:10.1142/S1793048013300053.

Qin, F. 2004. Restoration of single-channel currents using the segmental k-means method based on hidden Markov modeling. *Biophys. J.* 86:1488–1501. doi:10.1016/S0006-3495(04)74217-4.

Qin, F., A. Auerbach, and F. Sachs. 1996. Estimating Single-Channel Kinetic Parameters from Idealized Patch-Clamp Data Containing Missed Events. *Biophys. J.* 70:264–280.

Qin, F., A. Auerbach, and F. Sachs. 1997. Maximum likelihood estimation of aggregated Markov processes. *Proc. R. Soc. London B.* 264:375–383.

Ren, J., C. Qin, F. Hu, J. Tan, L. Qiu, S. Zhao, G. Feng, and M. Luo. 2011. Habenula "

Cholinergic" Neurons Corelease Glutamate and Acetylcholine and Activate

Postsynaptic Neurons via Distinct Transmission Modes. *Neuron*. 69:445–452.

doi:10.1016/j.neuron.2010.12.038.

Sala, F., J. Mulet, K.P. Reddy, J.A. Bernal, P. Wikman, L.M. Valor, L. Peters, G.M.

König, M. Criado, and S. Sala. 2005. Potentiation of human α4β2 neuronal nicotinic

receptors by a Flustra foliacea metabolite. *Neurosci. Lett.* 373:144–149.

doi:10.1016/j.neulet.2004.10.002.

Weltzin, M.M., Y. Huang, and M.K. Schulte. 2014. Allosteric modulation of alpha4beta2

nicotinic acetylcholine receptors by HEPES. *Eur. J. Pharmacol.* 732:159–168.

doi:10.1016/j.ejphar.2012.06.001.

Weltzin, M.M., and M.K. Schulte. 2010. Pharmacological Characterization of the

Allosteric Modulator Desformylflustrabromine and Its Interaction with a4b2

Neuronal Nicotinic Acetylcholine Receptor Orthosteric Ligands. *Am. Soc.

Pharmacol. Exp. Ther.* 334:917–926. doi:10.1124/jpet.110.167684.2006.

Weltzin, M.M., and M.K. Schulte. 2015. Desformylflustrabromine Modulates

alpha4beta2 Neuronal Nicotinic Acetylcholine Receptor High- and Low-Sensitivity

Isoforms at Allosteric Clefts Containing the beta2 Subunit. *J. Pharmacol. Exp. Ther.*

354:184–194. doi:10.1124/jpet.115.223933.

Appendix
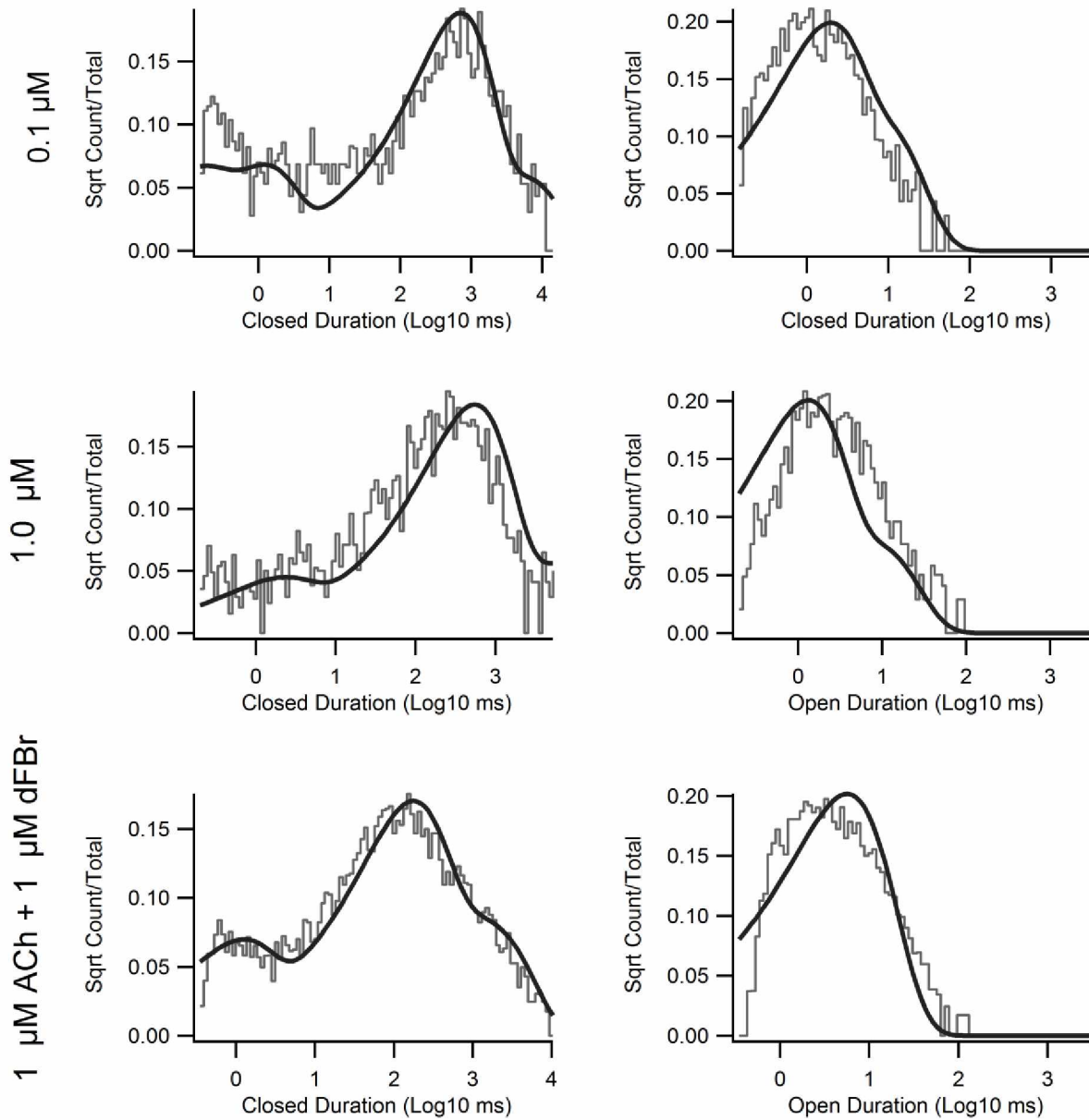
Figure A.3.1: Model based off LS receptor mechanism. Open and closed duration distributions from patches for 0.1 μM, 1 μM and 1 μM ACh + 1 μM dFBr (top, middle and bottom respectively) group fitted with the LS gating model shown in Figure 2.6.

Figure A.3.2: Scheme 3 model fits. Open and closed duration distributions from patches for 0.1 μM, 1 μM and 10 μM ACh (top, middle and bottom respectively) group fitted with gating model scheme 3 shown in Figure 3.6. Scheme 3 contains no activation steps.

Figure A.3.3: Scheme 4 model fits. Open and closed duration distributions from patches for 0.1 μM, 1 μM and 10 μM ACh (top, middle and bottom respectively) group fitted with gating model scheme 4 shown in Figure 3.6.
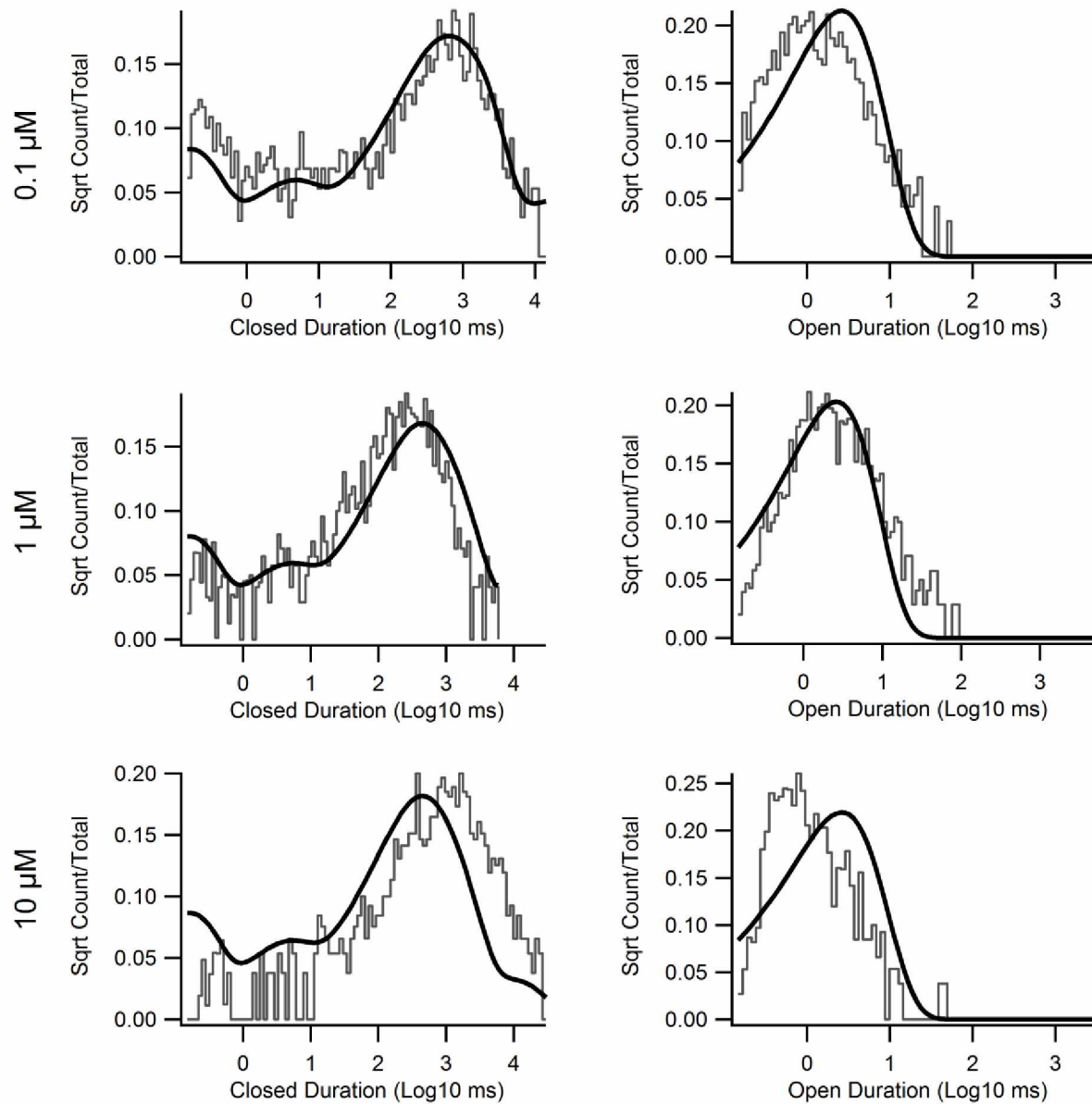
Figure A.3.4: Scheme 5 model fits. Open and closed duration distributions from patches for 0.1 μM, 1 μM and 10 μM ACh (top, middle and bottom respectively) group fitted with gating model scheme 5 (star) shown in Figure 3.6.
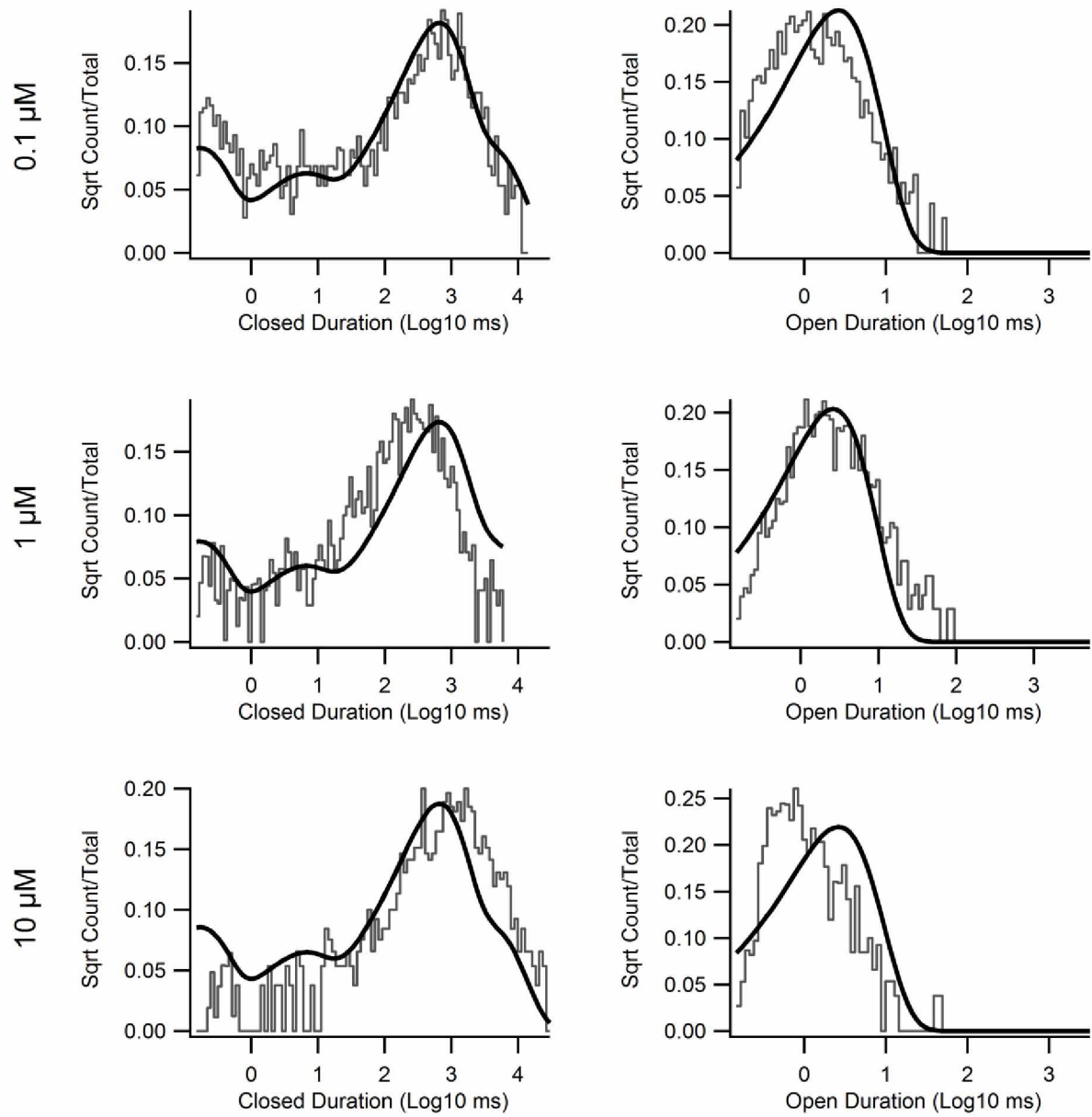
Figure A.3.5: Scheme 6 model fits. Open and closed duration distributions from patches for 0.1 μM, 1 μM and 10 μM ACh (top, middle and bottom respectively) group fitted with gating model scheme 6 (linear) shown in Figure 3.6.
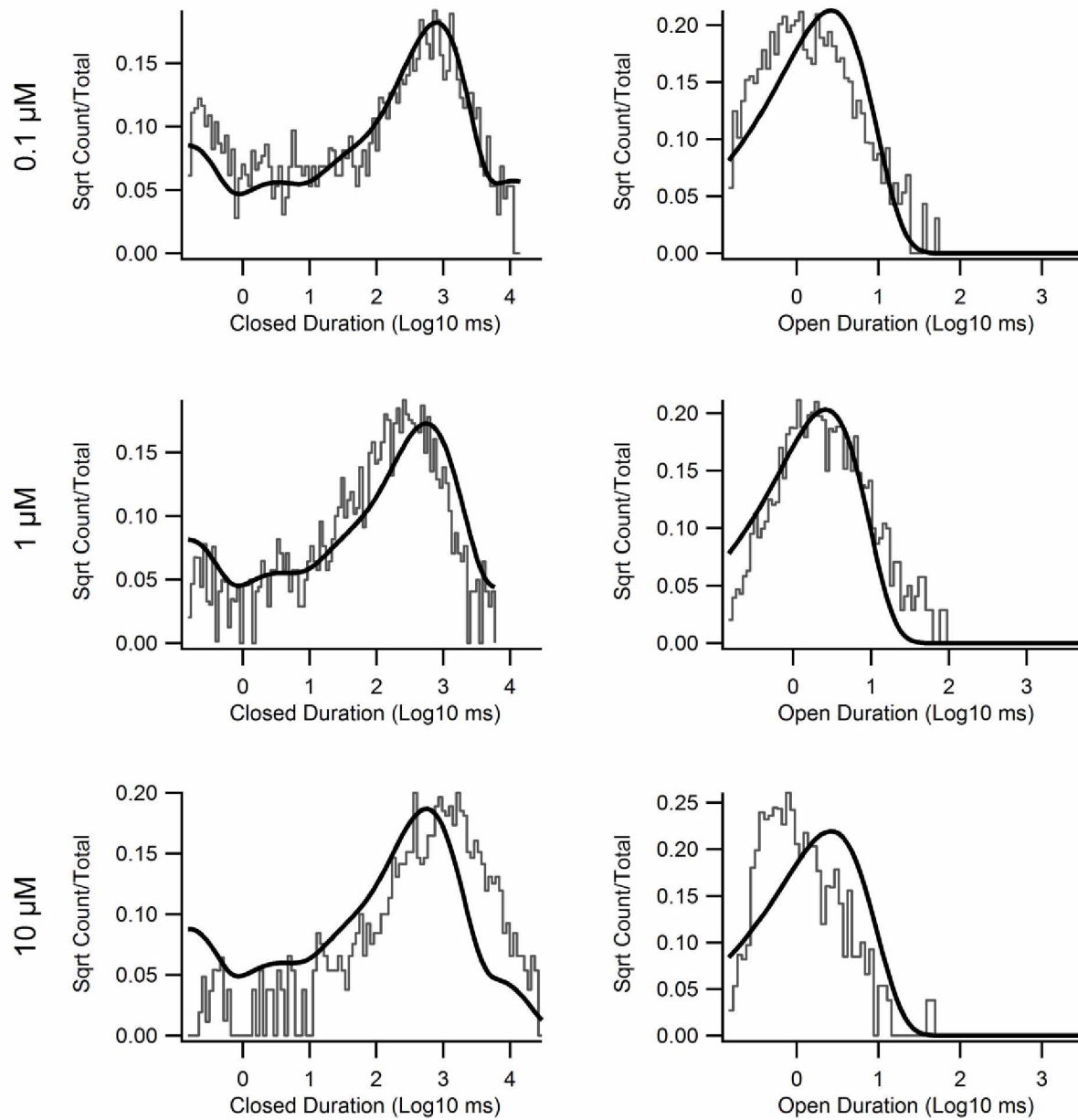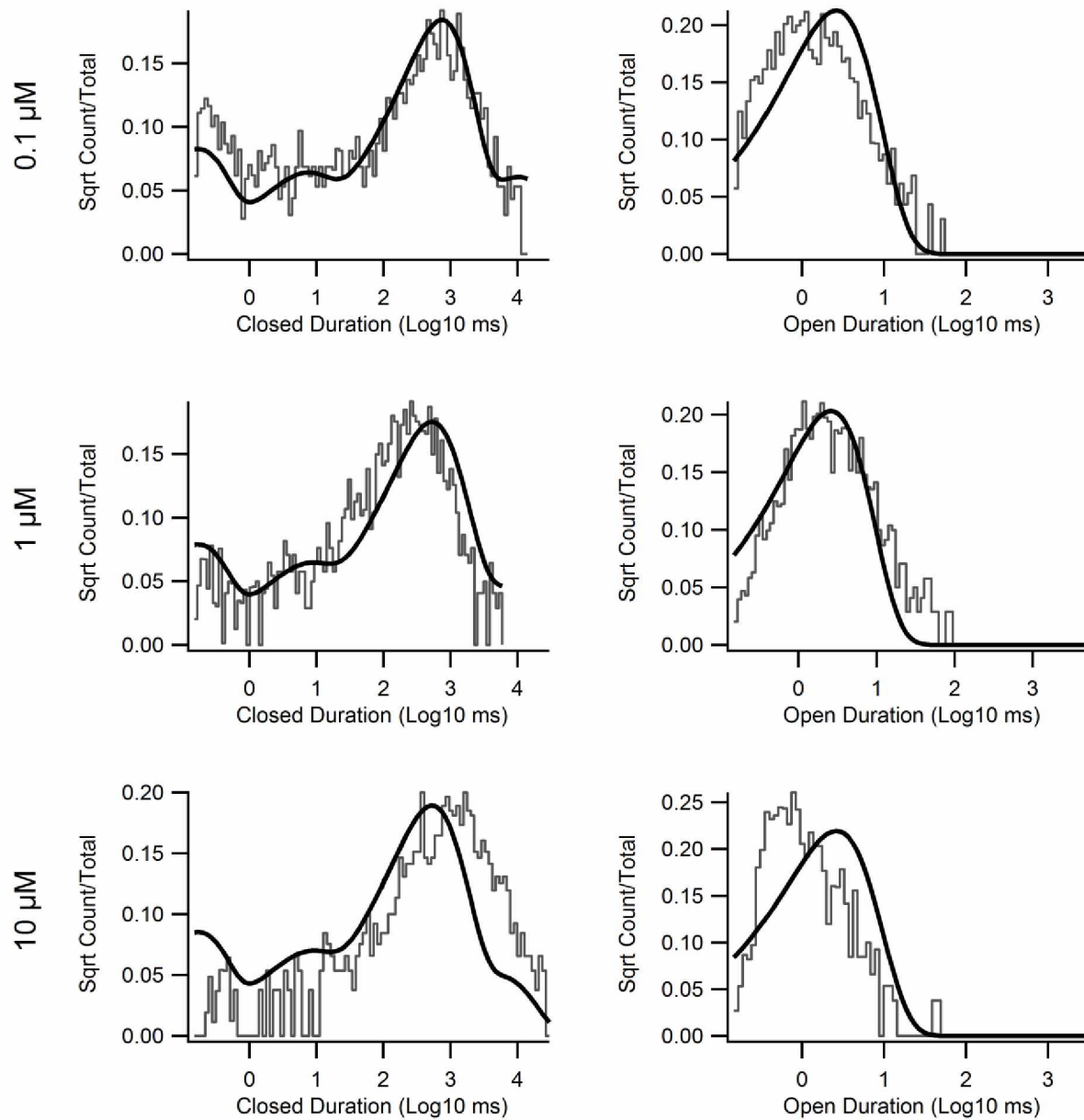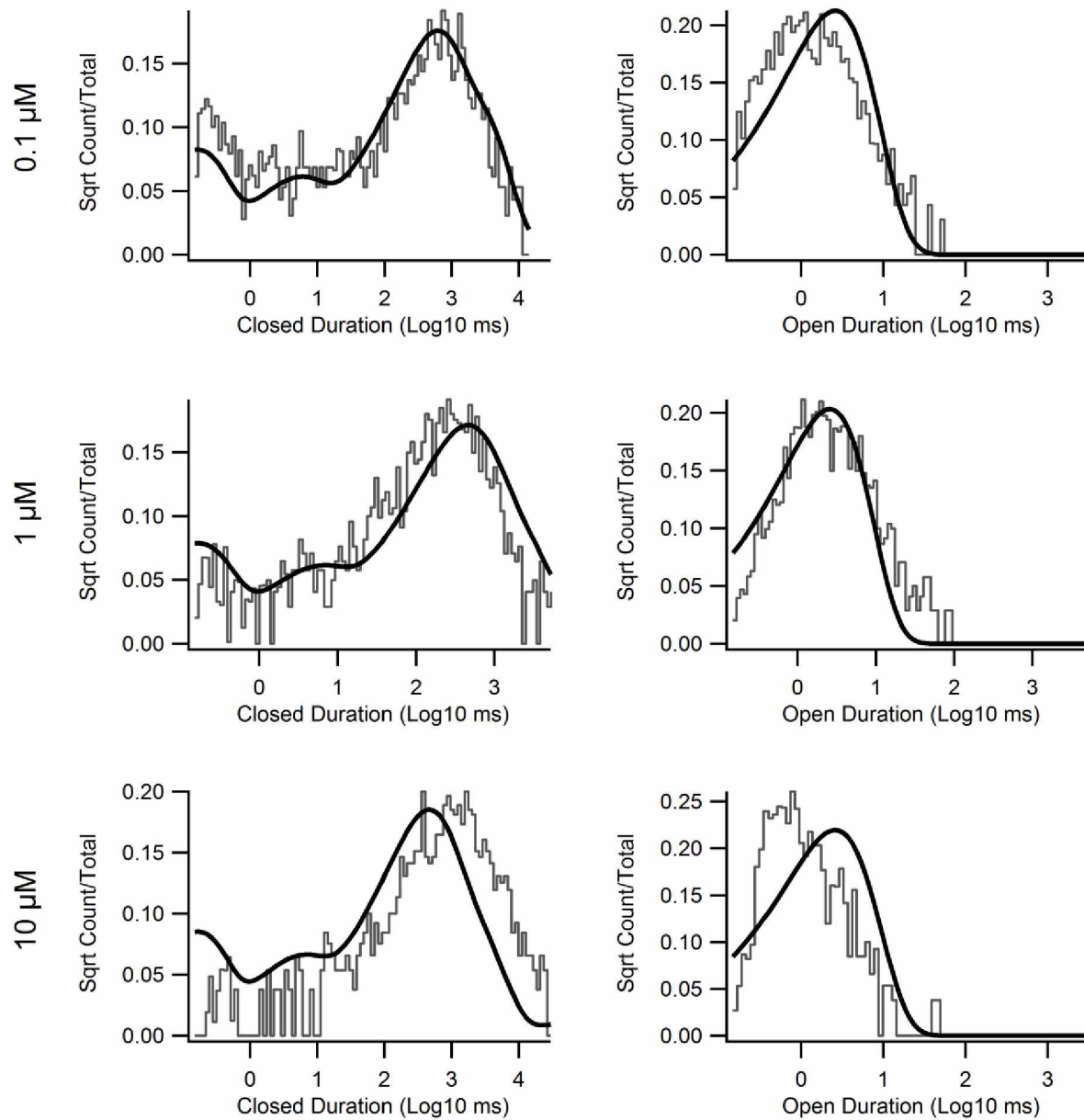
Figure A.3.6: Scheme 7 model fits. Open and closed duration distributions from patches for 0.1 µM, 1 µM and 10 µM ACh (top, middle and bottom respectively) group fitted with gating model scheme 7 shown in Figure 3.6.

Table A.3.1 LS based mechanism rate constants.

$$C \underset{k_{-1}}{\overset{2k_{+1}}{\rightleftharpoons}} C \underset{2k_{-1}}{\overset{k_{+1}}{\rightleftharpoons}} C \underset{d_{-1}}{\overset{d_{+1}}{\rightleftharpoons}} C$$

$$\alpha 1 \Big| \beta 1 \qquad \alpha 2 \Big| \beta 2$$

$$O \underset{k_{-2}}{\overset{k_{+2}}{\rightleftharpoons}} O \underset{d_{-2}}{\overset{d_{+2}}{\rightleftharpoons}} C$$

Table A.3.1

Rate	Unit	0.1 μM	1 μM	+dFBr
$2k_{+1}$	$M^{-1}s^{-1}$	1.3E8 ± 10%	2.32E7 ± 26%	3.8E7 ± 100%
k_{+1}	$M^{-1}s^{-1}$	6.7E7 ± 10%	1.16E7 ± 26%	1.9E7 ± 100%
$2k_{-1}$	s^{-1}	1571 ± 8%	2455 ± 12%	1563 ± 8%
k_{-1}	s^{-1}	785 ± 8%	1227 ± 12%	781 ± 8%
$\beta 1$	s^{-1}	106 ± 9%	114 ± 32%	139 ± 99%
$\alpha 1$	s^{-1}	539 ± 5%	671 ± 30%	185 ± 99%
$\beta 2$	s^{-1}	4100 ± 14%	1543 ± 59%	221 ± 100%
$\alpha 2$	s^{-1}	101 ± 13%	29 ± 98%	16 ± 100%
k_{+2}	$M^{-1}s^{-1}$	7.1E8 ± 12%	1.1E6 ± 100%	7.6E-7 ± 100%
k_{-2}	s^{-1}	82 ± 9%	0.76 ± 100%	3.5E-6 ± 100%
d_{+1}	s^{-1}	2863 ± 18%	51 ± 11%	993 ± 33%
d_{-1}	s^{-1}	0.3 ± 10%	0.2 ± 11%	2.5 ± 23%
d_{+2}	s^{-1}	2E-7 ± 100%	0.5 ± 5%	196 ± 4%
d_{-2}	s^{-1}	6E-9 ± 100%	2.6E-10 ± 8%	0.33 ± 4%

Table A.3.2: Rate constants for scheme 3 and scheme 4.

Rate constants	Scheme 3	+dFBr	Scheme 4	+dFBr
kO1	67 ± 14%	122 ± 3.5%	66 ± 12%	17 ± 7%
k1O	6580 ± 13%	6.6 ± 5%	6457 ± 11%	961 ± 11%
kO2	193 ± 57%	47 ± 9%	345 ± 2.4%	46.2 ± 8.9%
k2O	2.4 ± 27%	0.98 ± 6%	18 ± 16%	7.5 ± 7.7%
k23	0.4 ± 156%	0.002 ± 80%	147 ± 21%	0.002 ± 90%
k32	0.3 ± 42%	43500 ± 100%	15 ± 11%	0.002 ± 90%
kO4	185 ± 59%	22.2 ± 8%	32.4 ± 13%	117 ± 3.7%
k4O	41 ± 52%	1308 ± 12%	0.1 ± 10%	6.3 ± 5.5%
k45	208 ± 30%	6.8 ± 57%	-	-
k54	6 ± 116%	0.002 ± 600%	-	-

Table A.3.3: Rate constants for scheme 5.
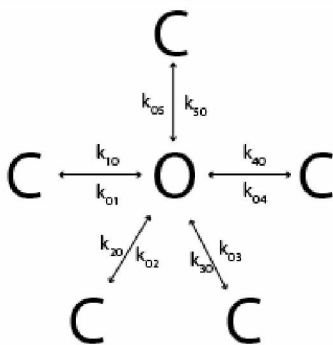
Table A.3.3

Rate constants	Scheme 5	+dFBr
k1O	6955 ± 12%	13.8 ± 38%
kO1	67.5 ± 13%	45 ± 65%
k2O	279 ± 21%	0.002 ± 90%
kO2	28 ± 10%	0.11 ± 68%
k3O	3.5 ± 13%	1316 ± 13%
kO3	117 ± 11%	20 ± 8%
k4O	0.06 ± 13%	5 ± 21%
kO4	17 ± 17%	81 ± 35%
k5O	1 ± 0.01%	1 ± 0.01%
kO5	217 ± 6%	40 ± 6%

Table A.3.4: Rate constants for scheme 6 and scheme 7.

$O \xrightarrow[k_{1O}]{k_{O1}} C \xrightarrow[k_{21}]{k_{12}} C \xleftarrow[k_{32}]{k_{23}} C \xleftarrow[k_{43}]{k_{34}} C \xrightarrow[k_{54}]{k_{45}} C$

$O \xrightarrow[k_{1O}]{k_{O1}} C \xrightarrow[k_{21}]{k_{12}} C \xrightarrow[k_{32}]{k_{23}} C$ with $C \; \uparrow k_{14} \downarrow k_{41}$ above and $C \; \uparrow k_{51} \downarrow k_{15}$ below the central C.

Rate constants	Scheme 6	+dFBr	Scheme 7	+dFBr
k1O	1001 ± 690%	143 ± 15%	6428 ± 13%	1429 ± 13%
kO1	444 ± 610%	186 ± 2%	65 ± 13%	22 ± 9%
k12	5496 ± 861%	1088 ± 13%	-	-
k21	114 ± 473%	54 ± 9%	-	-
k23	173 ± 492%	2.5 ± 22%	7.9 ± 39%	2.2 ± 65%
k32	18 ± 292%	3 ± 26%	0.007 ± 42%	8 ± 54%
k34	0.23 ± 148%	0.43 ± 61%	-	-
k43	0.34 ± 109%	0.89 ± 26%	-	-
k45	5.7e-12 ± 2600%	0.008 ± 0.06%	-	-
k54	1.8e-9 ± 2056%	0.002 ± 0.01%	-	-
kO2	-	-	31 ± 10%	127 ± 3%
k2O	-	-	208 ± 20%	7.5 ± 8%
kO4	-	-	185 ± 59%	1 ± 0.001%
k4O	-	-	1.95 ± 7%	0.008 ± 50%
kO5	-	-		
k5O	-	-		

Chapter 4: Conclusions and Future Directions

4.1 General Overview

We have used single molecule methods to investigate the action of a positive allosteric modulator, dFBr. We have provided the first step in developing a model that describes the gating of the human $\alpha4\beta2$ nicotinic receptors. Full gating models that give a fairly accurate representation of function allows naïve and modulated receptors to be simulated under a range of agonist profiles and concentrations. By determining the mechanism of modulation for HS and LS $\alpha4\beta2$ receptors on a single-channel level, we have greatly enhanced the understanding of the potential therapeutic benefit dFBr has on $\alpha4\beta2$ receptors at cholinergic synapses. How dFBr modulates would be determined by the agonist concentration profile at a synapse. The concentration differences would be dependent upon the spatial differences between receptors and local neurotransmitter release sites.

4.1.1 dFBr Destabilizes Desensitized States of $\alpha4_3\beta2_2$ Receptors

Models were constructed for the LS subtype of the $\alpha4\beta2$ nAChR. It was found that a 7 state model based off of an MWC mechanism described our data well and yielded unique rate constants for naïve and modulated receptors. The model contained two open states; a monoliganded open state off of C2 (O1) and a diliganded open state off of C3 (O2), as well as 5 closed states: two ligand binding steps (C1- C2 and C2 to

C3) and two desensitized states, one distal to C3 (D1) and the other distal to O2 (D2). For the LS subtype ($\alpha 4_3 \beta 2_2$) nAChRs the primary finding was that dFBr destabilized the two desensitized states D1 and D2 by decreasing their mean lifetimes. The lifetime of D1 was decreased from 77 ms to 7.6 ms, and D2 decreased from 1.7 s to 490 ms.

Macroscopic simulations provided insight into the contribution destabilization of desensitized states has on modulation. State occupancy probabilities were investigated by driving the model with various profiles of ACh concentration. Potentiation at peak current exhibited by dFBr was primarily due to the destabilization of D1, which slowed the initial fast rate of macroscopic desensitization. Whereas, potentiation of steady state currents arose from a lower probability of occupying D2. The simulated dose response curves did not have a biphasic quality to them as seen in previous reports for LS receptors. The biphasic quality seen in LS receptors is due to the unique $\alpha 4$-$\alpha 4$ binding site, which allows for the binding of one additional agonist. Unlike the LS which contains two unique binding sites, the HS variant of the receptor only contains one type of agonist binding site, and therefore does not display a biphasic dose response curve (Harpsøe et al., 2011). Our model does not contain 3 activation steps, but still has an EC_{50} (74 μM) close to the reported values for LS receptors (75 μM) (Nelson et al., 2003). While an additional activation step was tested, we found that the presence of a 3rd activation step did not give an accurate representation of the data. It may be that our concentration of ACh is too low to observe activation of the low sensitivity component of the receptor. However, this does not account for why our simulated dose response curves give EC_{50} values similar to reported values.

We investigated previous reports that dFBr increases peak current 3-fold under high agonist concentrations. Our models using single-channel data predicted less than 1.1-fold potentiation at EC_{75} (300 μM), compared to the 3-fold potentiation observed in previous studies (Weltzin and Schulte, 2010). When occupancy probabilities were calculated, we found that a slow rise in ACh concentration yields a lower peak P_{open} for naïve receptors and a larger increase in response when dFBr was applied. Our results do not support a large increase in peak current when high ACh concentrations are applied as seen in oocyte experiments. This discrepancy is likely in part due to slow solution exchange, which allows for desensitization to develop resulting in a lower peak amplitude in oocyte experiments.

The effects that dFBr would have on $\alpha 4_3\beta 2_2$ receptors would largely be dependent on the agonist concentration profile at the synapse. Under simulated agonist concentration profiles similar to that at fast synapses, dFBr increased the open response amplitude. If the nicotinic receptors at fast cholinergic synapses become saturated with agonist, then dFBr's ability to increase peak amplitude responses would be relatively ineffective at increasing postsynaptic signals. For LS receptors dFBr may be more suited for stimuli arising from a volume transmission scenario, where increasing the recovery from desensitization would have the greatest impact.

4.1.2 Synchronization of $\alpha 4_2 \beta 2_3$ Receptors

For the HS $\alpha 4\beta 2$ nAChR mechanisms were constructed and their viability as an accurate representation of channel gating was determined. It was found that an 8 state mechanism, based off of a simple MWC mechanism, best described our experimental single-channel HS data. The mechanism was composed of two activation steps (C1-> C2 and C2 ->C3), two open states: a monoliganded open state off of C2 (O1) and a diliganded open state off of C3 (O2). The open states contained transitions between one another. The HS model that best described our data and contained the best overall fits, error values and simulated currents contained 3 desensitized states. One distal to C3, with an additional two desensitized states off of O2.

For the HS nAChr subtype the primary finding was that dFBr synchronizes receptor openings at high concentrations by increasing the opening rate. dFBr potentiates peak currents across all concentrations, but charge transfer is reduced at simulated macroscopic responses with a concentration greater than or equal to 5 μM. The decrease in charge transfer at concentrations greater than 5 μM is at due to an increase in desensitization. For concentrations lower than 3 μM, the presence of dFBr resulted in an increase in charge transfer, reflective of a decrease in the likelihood of entering the desensitized state D2. The potentiation observed at low concentrations is brought on by the increase in the mean open lifetime of O1. While at higher concentrations, the increase into O2 has a larger effect on potentiation and the receptors desensitize more quickly.

174

With regards to signaling, the effects dFBr would have is dependent upon the synapse and the concentration of ACh in the synaptic cleft. dFBr has the ability to potentiate peak amplitude responses of HS receptors at low and high concentrations, but an increase in charge transfer is only observed at low concentrations. When in the presence of dFBr an overall decrease in charge transfer occurs, and postsynaptic signals generated from low frequency inputs may not benefit even though an increase in peak amplitude is observed over a wide range of agonist concentrations. However, dFBr would be the most beneficial if the receptors are exposed to low concentrations of agonist.

4.1.3 Implications for Nicotine Addiction

The pleasurable effects of nicotine occur due to the desensitization of high affinity nAChRs in the VTA. One of the most prominent types, $\alpha 4\beta 2$ receptors, is mostly expressed on GABAergic neurons and dopaminergic inputs. These receptors desensitize rapidly when they are exposed to nicotine with the reinforcing nature of nicotine due to upregulation of $\alpha 4$ containing nAChRs on VTA GABAergic neurons (Nashmi et al., 2007). Receptor upregulation of $\alpha 4\beta 2$ is directly related to desensitization, and receptors become hypersensitive after chronic exposure to nicotine leading to increased inhibition of dopaminergic activity (Hilario et al., 2012; Ngolab et al., 2015).

Our findings demonstrate that dFBr has the potential to be useful for the treatment of nicotine addiction. It is well known that the $\alpha 4\beta 2$ receptors are upregulated

175

when chronically exposed to nicotine and there is some evidence that the high

sensitivity form may be most affected. The effect that dFBr would have on HS receptors

is unclear in our data as we observe increased desensitization due to the presence of

channel block or HEPES, but we find that dFBr would increase receptors

responsiveness when exposed to ambient concentrations of ACh. In the VTA $\alpha 4 \beta 2$

receptors are largely expressed on presynaptic inputs into dopaminergic neurons, and

limiting the receptors ability to desensitize would be beneficial in reducing upregulation

of the receptors. For LS receptors, the application of dFBr could lift receptors out of

desensitization by destabilizing of desensitized states. This would give increased

activity from inputs into dopaminergic neurons and could potentially lead to

downregulation of $\alpha 4 \beta 2$ receptors back to normal levels, since receptor desensitization

and upregulation have been shown to be linked (Fenster et al., 1999). The increase in

activity within the VTA without the presence of nicotine would aid in eliminating

symptoms of withdrawal that accompanies smoking cessation, which is one of the

factors that prevents success in quitting (West et al., 1989).

4.1.4 Implications for the Treatment of Alzheimer's Disease

One possible therapeutic approach for the treatment of Alzheimer's disease is

through the use of compounds that interfere with nAChR-Aβ interactions. Previous

studies have looked at the interactions of dFBr and Aβ on $\alpha 4 \beta 2$ receptors and found

that dFBr dissociates Aβ from the receptors. In our studies we found that dFBr

increases responses for both $\alpha 4 \beta 2$ subtypes, making it a potential candidate for

Alzheimer's disease if used in conjunction with other drugs. dFBr may be best paired

with compounds that demonstrate the ability to dissociate Aβ from α7 nAChRs,

antibodies that target Aβ, or both of these options. Compounds such as 2-[2- (4-

bromophenyl)-2-oxoethyl]-1-methyl pyridinium (S 24795), a partial α7 nAChR agonist,

have been found to dissociate Aβ in a concentration dependent manner (Wang et al.,

2009, 2010). Combining dFBr with compounds like S-24795 will combat the negative

effects Aβ binding has on α4β2 and α7 nAChRs, thereby potentially preventing further

progression of the disease. The use of immunotherapy is still in its infancy (Goure et

al., 2014), but the presence of compounds such as S-24795 and dFBr coupled with

immunotherapy could potentially drastically reduce the concentration of Aβ in the brain.

dFBr's ability to increase responses by destabilizing desensitized states for LS

receptors and increasing open time for HS receptors could help enhance cognitive

ability, while simultaneously dissociating Aβ from receptors. Combating Alzheimer's

disease would require a therapy that combats the disease from many angles potentially

utilizing multiple compounds such as dFBr.

4.2 Future Work

The investigation of dFBr on a single molecule level focused on characterizing

the mechanisms of modulation for the α4β2 LS and HS nicotinic receptors. The goal

was to provide a comprehensive gating model for both stoichiometric forms of the α4β2

receptors and determine the mechanism of action for the PAM dFBr. Determining how

allosteric modulators would behave under different forms of synaptic transmission is

crucial to understanding the effect potentiation has on cholinergic synapses. Further investigation is needed into the effect structural changes have on receptors and allosteric modulators, and how these changes would change the mechanism of modulation. Understanding the structure-function relationship between dFBr analogs and nAChRs will help determine whether these changes increase dFBr's viability as a therapeutic agent, aiding in rational drug design.

4.2.1 Effect of Linked Subunits on $\alpha 4\beta 2$ Gating Models

One of the primary difficulties of doing whole cell and single-channel studies on receptors that contain more than one subtype, is receptor heterogeneity. While single-channel helps circumvent heterogeneity, more than one subtype can still be present in a patch adding complexity to data analysis. Many attempts have been made to address this problem and express $\alpha 4_3\beta 2_2$ (LS) and $\alpha 4_2\beta 2_3$ (HS) receptors separately. Strategies include using a 1:4 or 4:1 (or larger) ratio of $\alpha 4{:}\beta 2$ subunit cDNAs for injecting or transfecting into the appropriate cell line. This technique gives monophasic concentration profiles, which suggests that there are homologous population of either $\alpha 4_3\beta 2_2$ or $\alpha 4_2\beta 2_3$ subtype (Moroni et al., 2006; Nelson et al., 2003), but it is currently unknown if this technique abolishes the unwanted stoichiometric form of the receptor. Alternatively, constructs with two units attached via synthetic linkers can be used to constrain the stoichiometry of $\alpha 4\beta 2$ receptors (Zhou et al., 2003). These studies would be done on two linker configurations $\alpha 4\text{-}6\text{-}\beta 2$ and $\beta 2\text{-}6\text{-}\alpha 4$ in order to determine if the position of the linker has any noticeable effect on the desensitization or bursting characteristics of the receptor. With these studies the linker would have to be added to

178

the transfection medium in a 2:1 ratio of α4-6-β2/ β2-6-α4 to α4/β2 cDNAs, depending on the subtype being studied. Linkers also have the advantage of being able to be combined with mutated subunits, allowing for greater insight into the effects of mutations on gating. Conducting single molecule studies on receptors that contain mutations would increase understanding of the structure function relationship for the receptors, and determine if mutations affect activation, burst, and desensitization kinetics. Preliminary work for this project involved introducing the linked subunit cDNA into a mammalian vector. Investigation into whether the naive receptors kinetics differ from that of linked receptors would also be beneficial for future studies utilizing linked subunits.

4.2.2 Investigation of dFBr Analogues

The compound being studied, dFBr, has potential drawbacks in its use as an effective therapeutic agent. Being a natural product, dFBr could have poor transit across the blood brain barrier, selectivity, and efficacy. A nicotine self-administration study conducted with rats administered with dFBr demonstrated that dFBr is present in cerebral fluid. This finding indicates that dFBr crosses the blood-brain barrier, but is available only at one-third the concentration compared to blood. There is room for improvement with dFBr's qualities, including the compounds ability to transit across the blood brain barrier (Liu, 2013). In order for dFBr to be considered an effective therapeutic treatment dFBr needs to be improved and made more selective in its therapeutic target. To accomplish this, analogues can be tested to determine what

structural aspects of dFBr are important for modulation. Single-channel analysis would help in determining if a change in structure affected dFBr's mechanism of modulation and therefore which components are most important. These studies would be done using five dFBr analogues with EC_{50}s ranging from 1 to 6.3 μM and IC_{50}s from 8 to 90 μM, with some analogues only displaying inhibition. An optimal ligand for both receptor subtypes would destabilize desensitized states as well as increase peak current across a wide range of concentrations. Determining the structural components that exhibit potentiation via destabilization of desensitized states versus potentiation of peak current would allow for a therapeutic agent that has more specificity. Currently, at high concentrations of agonist dFBr only destabilizes desensitized states on the LS subtype, while increasing desensitization on the HS subtype. Peak current at high concentrations of agonist for the HS subtype is still modulated by dFBr, whereas the LS subtype is not. Analogues would help elucidate if dFBr can become more selective in its actions for the HS versus LS subtype, enhancing its potential as a therapeutic agent. Studies investigating the effects structural modifications have on a single-channel level furthers the drug design process and leads to more rational drug design.

4.2.3 Investigation of the Mechanisms of Action of NS206 and NS9283

The positive allosteric modulator dFBr displays two types of modulation, affecting desensitization as well as peak currents. Unlike dFBr, NS206 and NS9283 compounds each display a single type of modulation via different mechanisms. The compounds differ in their structure as well as their binding sites, and thus behave very differently.

NS206 potentiates both stoichiometric forms of the receptor displaying higher efficacy on HS receptors increasing ACh evoked currents 3-4fold and potentiates LS receptors 1.5 fold. While NS206 potentiates both stoichiometric forms of the receptor, NS9283 potentiates only the LS form of the $\alpha4\beta2$ receptor (Grupe et al., 2013). Further comparison on the differences between the two compounds, it is found that NS9283 increases potency and gives monophasic properties. Whereas NS206 displays no change in ACh potency and for the LS subtype continues to have biphasic properties (Olsen et al., 2013). Both compounds do not affect receptor desensitization for either stoichiometry and when co-applied, work additively. It would be worthwhile investigating how the mechanisms of modulation differ between these two compounds, whether there is an additive effect on the single-channel level, and if the mechanisms are similar in form to dFBr's mechanism. Conducting single-channel analysis on two compounds that give rise to individual types of modulation, differ in structure, and mechanism would help increase understanding on what aspects of the $\alpha4\beta2$ nAChR kinetic mechanism the compounds affect the most and if all PAMs display similar modes of action. Developing an understanding of the relationship between compound structure, kinetic mechanisms and binding sites is an important aspect of intelligent and efficient drug development.

4.3 References

Fenster, C.P., T.L. Whitworth, E.B. Sheffield, M.W. Quick, and R.A.J. Lester. 1999. Upregulation of Surface α4β2 Nicotinic Receptors Is Initiated by Receptor Desensitization after Chronic Exposure to Nicotine. *J. Neurosci.* 19:4804–14.

Goure, W.F., G.A. Krafft, J. Jerecic, and F. Hefti. 2014. Targeting the proper amyloid-beta neuronal toxins: a path forward for Alzheimer's disease immunotherapeutics. *Alzheimers. Res. Ther.* 6:42. doi:10.1186/alzrt272.

Grupe, M., A.A. Jensen, P.K. Ahring, J.K. Christensen, and M. Grunnet. 2013. Unravelling the mechanism of action of NS9283, a positive allosteric modulator of (??4)3(??2)2 nicotinic ACh receptors. *Br. J. Pharmacol.* 168:2000–2010. doi:10.1111/bph.12095.

Harpsøe, K., P.K. Ahring, J.K. Christensen, M.L. Jensen, D. Peters, and T. Balle. 2011. Unraveling the high- and low-sensitivity agonist responses of nicotinic acetylcholine receptors. *J. Neurosci.* 31:10759–66. doi:10.1523/JNEUROSCI.1509-11.2011.

Hilario, M.R.F., J.R. Turner, and J. a Blendy. 2012. Reward Sensitization: Effects of Repeated Nicotine Exposure and Withdrawal in Mice. *Neuropsychopharmacology.* 37:2661–2670. doi:10.1038/npp.2012.130.

Liu, X. 2013. Positive allosteric modulation of ??4??2 nicotinic acetylcholine receptors as a new approach to smoking reduction: Evidence from a rat model of nicotine self-administration. *Psychopharmacology (Berl).* 230:203–213. doi:10.1007/s00213-013-3145-2.

Moroni, M., R. Zwart, E. Sher, B. Cassels, and I. Bermudez. 2006. Alpha4 Beta2

Nicotinic Receptors With High and Low Acetylcholine Sensitivity:

Pharmacology,Stoichiometry, and Sensitivity To Long-Term Exposure To Nicotine.

Mol Pharmacol. 70:755–768. doi:10.1124/mol.106.023044.not.

Nashmi, R., C. Xiao, P. Deshpande, S. McKinney, S.R. Grady, P. Whiteaker, Q. Huang,

T. McClure-Begley, J.M. Lindstrom, C. Labarca, A.C. Collins, M.J. Marks, and H.A.

Lester. 2007. Chronic Nicotine Cell Specifically Upregulates Functional 4* Nicotinic

Receptors: Basis for Both Tolerance in Midbrain and Enhanced Long-Term

Potentiation in Perforant Path. *J. Neurosci.* 27:8202–8218.

doi:10.1523/JNEUROSCI.2199-07.2007.

Nelson, M.E., A. Kuryatov, C.H. Choi, Y. Zhou, and J. Lindstrom. 2003. Alternate

Stoichiometries of alpha 4beta 2 Nicotinic Acetylcholine Receptors. *Mol Pharmacol.*

63:332–341. doi:10.1124/mol.63.2.332.

Ngolab, J., L. Liu, R. Zhao-Shea, G. Gao, P.D. Gardner, and A.R. Tapper. 2015.

Functional Upregulation of α4* Nicotinic Acetylcholine Receptors in VTA

GABAergic Neurons Increases Sensitivity to Nicotine Reward. *J. Neurosci.*

35:8570–8. doi:10.1523/JNEUROSCI.4453-14.2015.

Olsen, J.A., J.S. Kastrup, D. Peters, M. Gajhede, T. Balle, and P.K. Ahring. 2013. Two

distinct allosteric binding sites at ??4??2 nicotinic acetylcholine receptors revealed

by NS206 and NS9283 give unique insights to binding activity-associated linkage at

cys-loop receptors. *J. Biol. Chem.* 288:35997–36006.

doi:10.1074/jbc.M113.498618.

Wang, H.-Y., K. Bakshi, C. Shen, M. Frankfurt, C. Trocmé-Thibierge, and P. Morain. 2010. S 24795 Limits β-Amyloid–α7 Nicotinic Receptor Interaction and Reduces Alzheimer's Disease-Like Pathologies. *Biol. Psychiatry.* 67:522–530. doi:10.1016/j.biopsych.2009.09.031.

Wang, H.-Y., A. Stucky, J. Liu, C. Shen, C. Trocme-Thibierge, and P. Morain. 2009. Dissociating beta-amyloid from alpha 7 nicotinic acetylcholine receptor by a novel therapeutic agent, S 24795, normalizes alpha 7 nicotinic acetylcholine and NMDA receptor function in Alzheimer's disease brain. *J. Neurosci.* 29:10961–73. doi:10.1523/JNEUROSCI.6088-08.2009.

Weltzin, M.M., and M.K. Schulte. 2010. Pharmacological Characterization of the Allosteric Modulator Desformylflustrabromine and Its Interaction with a4b2 Neuronal Nicotinic Acetylcholine Receptor Orthosteric Ligands. *Am. Soc. Pharmacol. Exp. Ther.* 334:917–926. doi:10.1124/jpet.110.167684.2006.

West, R., P. Hajek, and M. Belcher. 1989. Time course of cigarette widhdrawal symptoms while using nicotine gum. *Psychopharmacology (Berl).* 99:143–145. doi:10.1007/BF00634470.

Zhou, Y., M.E. Nelson, A. Kuryatov, C. Choi, J. Cooper, and J. Lindstrom. 2003. Human alpha4beta2 acetylcholine receptors formed from linked subunits. *J. Neurosci.* 23:9004–9015.